NACA RM L51F26

NACA

RESEARCH MEMORANDUM

EFFECTS OF PROPELLER-SHANK GEOMETRY AND PROPELLER-SPINNER-JUNCTURE CONFIGURATION ON CHARACTERISTICS OF AN NACA 1-SERIES COWLING-SPINNER COMBINATION WITH AN EIGHT-BLADE DUAL-ROTATION PROPELLER.

By Arvid L. Keith, Jr., Gene J. Bingham, and
Arnold J. Rubin

Langley Aeronautical Laboratory
Langley Field, Va.

NATIONAL ADVISORY COMMITTEE
FOR AERONAUTICS

WASHINGTON
September 25, 1951

ERRATUM

NACA RM L51F26

EFFECTS OF PROPELLER-SHANK GEOMETRY AND
PROPELLER-SPINNER-JUNCTURE CONFIGURATION ON CHARACTERISTICS
OF AN NACA 1-SERIES COWLING-SPINNER COMBINATION WITH
AN EIGHT-BLADE DUAL-ROTATION PROPELLER

By Arvid L. Keith, Jr., Gene J. Bingham, and
Arnold J. Rubin

September 25, 1951

Page 65, figure 18, upper right plot: the inlet average total pressure curve (solid-line curve) for the 24-percent-thick shank propeller with ideal juncture at the climb blade angle ($\beta_F = 47.4^\circ$; $\beta_R = 46.6$) is in error. The necessary correction is made in the figure below.

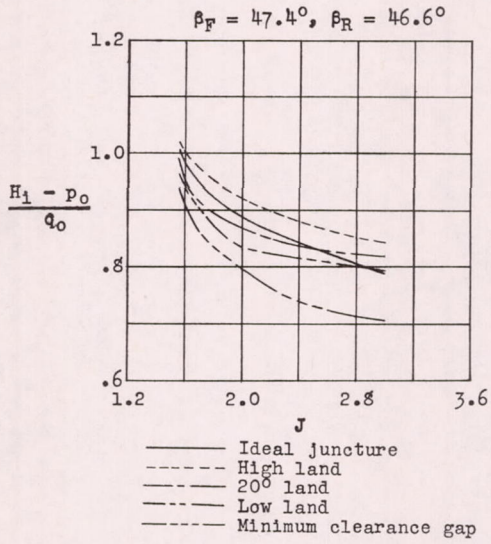

NATIONAL ADVISORY COMMITTEE FOR AERONAUTICS

RESEARCH MEMORANDUM

EFFECTS OF PROPELLER-SHANK GEOMETRY AND PROPELLER-SPINNER-JUNCTURE CONFIGURATION ON CHARACTERISTICS OF AN NACA 1-SERIES COWLING-SPINNER COMBINATION WITH AN EIGHT-BLADE DUAL-ROTATION PROPELLER

By Arvid L. Keith, Jr., Gene J. Bingham, and
Arnold J. Rubin

SUMMARY

An investigation has been conducted at low speed in the Langley low-turbulence tunnel to study the effects of variations in propeller-shank geometry and propeller-spinner-juncture configuration on the aerodynamic characteristics of an NACA 1-series cowling-spinner combination equipped with an eight-blade dual-rotation propeller. Several propellers, which had maximum shank thicknesses varying from 12 to 100 percent (round shank) of the blade chord, were investigated with "ideal" sealed and faired propeller-spinner junctures over ranges of blade angles and advance ratios covering high-speed, cruising, and climbing flight. A representative propeller was investigated with several propeller-spinner-juncture arrangements that permitted blade rotation. Blowing and suction slots on the spinner were investigated in attempts to reduce the inlet-velocity ratio required to avoid flow separation ahead of the inlet.

The addition of any of the propellers to the basic cowling-spinner combination did not increase the minimum inlet-velocity ratio required to avoid boundary-layer separation from the spinner surface and did not decrease the predicted critical Mach number of the cowling. Propeller operation also delayed separation from the inner cowling-lip surface at high inlet-velocity ratios.

At the simulated design-cruise condition, the propeller with 12-percent-thick shanks and "ideal" propeller-spinner juncture produced average total pressure coefficients at the cowling inlet and diffuser nearly equal to those obtained with propeller removed. Increases in propeller-shank thickness causes significant reductions in these coefficients; the round-shank propellers caused much greater losses than the airfoil-shank propellers of the same thickness. The incorporation of

propeller-spinner-juncture arrangements that permitted blade rotation also reduced the total pressure coefficients as long as the juncture was located inside the spinner boundary layer. An airfoil-land-type juncture which had the land-shank gap located well above the spinner surface gave total pressure coefficients approximately equal to those for the "ideal" juncture in the simulated high-speed and cruise conditions and was superior in the climb condition. Of the two boundary-layer-control methods investigated only the suction scoop provided any improvement over the basic configuration with propeller operating.

INTRODUCTION

The power and economy of gas-turbine engines are markedly dependent on the efficiency of the air-induction system (reference 1). In the case of the turbopropeller engine equipped with a conventional cowling-spinner combination (D-type cowling), the problem of obtaining low intake losses is complicated by the presence of an initial boundary layer on the spinner ahead of the inlet and by interference effects introduced by the propeller.

General procedures and charts for the selection of high-critical Mach number cowling-spinner combinations of high intake efficiency are presented in reference 2. The application of these design procedures and data for determining optimum cowling and spinner proportions for a given installation necessarily requires a knowledge of the effects of propeller operation on the stability of the spinner boundary layer and on the flow in the vicinity of the cowling. Reference 2 presented some information on this subject for the case of the thick-shanked single-rotation propeller and pointed out the need for similar information for other types of propellers. In each case, information is needed relative to the loss characteristics and design requirements of efficient propeller-spinner-juncture arrangements.

The present investigation was undertaken in the Langley low-turbulence tunnel to study the effects of propeller-shank geometry and propeller-spinner-juncture shape on the aerodynamic characteristics of a cowling-spinner combination equipped with a high-solidity, high-advance-ratio, dual-rotation propeller. This configuration is of great interest at the present time for high-subsonic-speed turbopropeller-powered aircraft and presents a particularly difficult design problem, from the viewpoint of obtaining low intake losses, because of the large size of the spinner, the number of blades, the large size of the blade-root sections, and the counter-rotation of the propeller elements. The investigation is preliminary in the sense that it was conducted at low speeds so that additional tests at high speeds are required to establish

the effects of compressibility. It was believed that a preliminary investigation of this nature was justifiable in order to determine whether low losses are possible and to define the configurations of greatest interest for the necessary future investigation at high speeds.

For the main part of the investigation, the basic cowling-spinner combination was tested with no-propeller and with five propeller configurations with varying shank shapes and thicknesses. Each of the propellers was tested with an aerodynamically "ideal" propeller-spinner juncture; that is, the shank was extended to the spinner surface and sealed. Four juncture configurations that permitted blade rotation were tested with one of the airfoil-shank propellers. Attempts to reduce the minimum inlet-velocity ratio for avoidance of spinner boundary-layer separation by boundary-layer control were also made by using a blowing slot between spinner components and a suction scoop at various positions ahead of the inlet. The internal- and external-flow characteristics of the several configurations were evaluated from total-pressure surveys at the cowling inlet, in the ducting, and behind the propeller and static-pressure surveys over the spinner and cowling surface.

SYMBOLS

A	area
b	blade chord
d	inlet diameter
D	maximum diameter
F	frontal area of cowling
h	normal distance from central body
h'	blade thickness
H	total pressure
M	Mach number
n	revolutions per second
p	static pressure
P	static pressure coefficient $\left(\frac{p - p_o}{q_o}\right)$

q	dynamic pressure
Q	volume rate of flow
r	radius from cowling center line unless otherwise specified
R	maximum radius measured from cowling center line
V	velocity
J	propeller advance ratio $\left(V_o/nD_p\right)$
x	distance from nose of cowling, basic spinner, open-nose spinner, suction scoop, or propeller land
X	maximum length of component
y	ordinate measured from axis of rotation or cowling reference line
Y	maximum ordinate of component
Z	land height above spinner surface normal to axis
α	angle of attack of center line of model
β	angle of attack of propeller blades from plane of rotation (blade angle values given herein at $(r/R)_p = 0.75$)
δ	nominal boundary-layer thickness $\left(\text{defined as normal distance from surface to point where } \frac{H - p_o}{q_o} = 0.95\right)$

Subscripts:

av	average value weighted according to area at measuring station
b	blowing slot or suction scoop
c	cowling
cr	critical
d	diffuser

F	front blade
i	inlet
o	free stream
p	propeller or condition in flow behind propeller
R	rear blade
s	spinner

MODEL

An isometric sketch of the general model arrangement is presented in figure 1 and photographs of the several test configurations are presented in figure 2. The test model consisted of a 12-inch maximum-diameter nacelle mounted in the midposition on a two-dimensional NACA 65_3-018 wing. The NACA 1-series nondimensional ordinates (reference 2) were used in the design of the cowlings and spinner of the present investigation. These ordinates are presented in table I.

Spinners.- The NACA 1-46.5-085 spinner $\left(\frac{D_s}{D_c} = 0.465, \frac{X_s}{D_c} = 0.85\right)$ selected for the basic cowling-spinner combination was considered the smallest-diameter shortest-length NACA 1-series spinner that would enclose a blade-angle-change mechanism required for a large-diameter eight-blade dual-rotation propeller. The division between the front and rear spinner halves occurred at station $\frac{x_s}{X_s} = 0.609$; the gap between spinner components was 0.03 inch.

Two attempts were made to reduce the value of inlet-velocity ratio required to avoid flow separation ahead of the cowling inlet by application of boundary-layer control. In the first case, the nose section of the basic spinner was removed (fig. 2(c)) and refaired as shown in table II. Air at free-stream total pressure was ducted through the hollow front section and ejected into the spinner boundary layer through a slot formed between the front- and rear-spinner halves. In the second case, an annular suction scoop was installed at the base of the spinner in several longitudinal positions, 3.00, 1.50, and 0 inches ahead of the inlet (table III). The scoop flow exited from the model nacelle through three streamline tubes located 120° apart (table III and fig. 2(d)). The exits were located in a low-pressure region on the cowling to induce the scoop flow.

Cowlings.- The NACA 1-62.8-070 cowling $\left(\frac{d}{D_c} = 0.628; \frac{X_c}{D_c} = 0.70\right)$ was selected as the basic cowling. (See tables I, II and fig. 2.) An NACA 1-series inner liner ($Y = 0.01D_c$; $X = 0.04D_c$; see table II) was incorporated at the inner lip as recommended in reference 2 to delay the formation of bubbles of separation from the lower inner-lip surface to high values of inlet-velocity ratio as required for the take-off and climb conditions. The internal ducting included a 9° equivalent conical diffuser (area ratio, 1.82 to 1.0). The inlet-annulus area, $\frac{A_i}{F} = 0.164$, for the basic cowling-spinner combination was considered sufficient for the air-flow requirements of a high-powered turbopropeller engine when operating in the cruise condition at a Mach number of 0.8 and inlet-velocity ratio of 0.5 at an altitude of 35,000 feet.

For the tests with the spinner boundary-layer suction scoops installed, the basic cowling was replaced by an NACA 1-70-070 cowling with $0.01D_c$ inner liner (table III and fig. 2(d)). The resulting inlet-annulus area, $\frac{A_i}{F} = 0.222$, for this cowling-scoop combination will intake the same mass flow of air as the basic cowling at an inlet-velocity ratio of 0.36 at the assumed operating conditions. The internal ducting for this configuration was also changed to a 6.48° equivalent conical diffuser (area ratio, 1.40 to 1.0). The inlet and diffuser area ratios, $\frac{A_i}{F}$ and $\frac{A_d}{A_i}$, for the combination of the NACA 1-70-070 cowling with an NACA 1-46.5-085 spinner with scoop removed were 0.256 and 1.345, respectively.

Propellers and propeller-spinner junctures.- Plan-form and blade-form curves of the several eight-blade dual-rotation propellers are presented in figure 3. Each propeller was composed of NACA 16-series sections and was designed to operate at an advance ratio of 4.2 at the assumed cruise condition. Three airfoil-type shank propellers with root thicknesses of 12, 24, and 40 percent (figs. 3(a), 3(b), and 3(c)) were designed with the same section lift coefficients and blade twist distributions and were identical in geometry with exception of the distribution of section thickness inboard of the 55-percent-radius station. Two round-shank propellers which had shank diameters equal to the maximum thickness of the 24- and 40-percent airfoil-type shank propellers were also investigated (figs. 3(d) and 3(e)). These two round-shank propellers also had the same section lift coefficients and twist distributions as the airfoil shank propellers, but the distribution of blade-width ratio and thickness ratio differed inboard of the 25-percent- and 55-percent-radius stations, respectively.

Each propeller was tested with an aerodynamically "ideal" propeller-spinner juncture; that is, the propeller shank extended to the spinner surface and was sealed. In addition, the 24-percent-thick shank propeller was tested with four "practical" juncture configurations with which the propeller could be rotated through 120° of blade-angle change; this change is representative of the range from full feather to reverse thrust. For the first juncture a section of the blade root just high enough to allow this blade-angle change was removed (fig. 2(h) and table IV). The second juncture consisted of a low airfoil-type land which was installed under the front sections of the front and rear propeller components and filled the minimum-height opening, except for a gap large enough to allow blade-angle changes (fig. 2(i) and table IV). A second airfoil-type land (fig. 2(j) and table IV) extending farther from the spinner surface was also investigated. In this case the land height was selected such that the gap between the propeller blade and the land would be out of the spinner boundary layer. The land shape and angle for both these configurations were the same as that for the propeller-shank at comparable radius stations; for propeller blade angles other than the design value, the blade shank and land were no longer alined (fig. 2(k)). The fourth juncture was a land designed to cover the base of the blade for a blade-angle range from the assumed-climb propeller-blade angle of 47.4° front and 46.6° rear $\left(\text{at } \frac{r}{R} = 0.75\right)$ to the assumed high-speed blade angle of 67.4° front and 66.6° rear (see fig. 2(l) and table V). In each of the three land configurations tested, the land-shank gap was 0.010 inch.

APPARATUS AND TESTS

The model was mounted in the middle of the tunnel with the support wing spanning the 3- by $7\frac{1}{2}$-foot rectangular test section of the Langley low-turbulence tunnel. Internal flow was induced and controlled by a variable-speed centrifugal blower and the flow quantity was measured by a calibrated orifice meter. The flow exited from the model diffuser into a small plenum chamber and then was conducted to the blower through auxiliary ducts on the top and bottom of the support wing (fig. 1). The eight-blade dual-rotation propellers were driven by a 20-horsepower variable-speed electric motor through a 3 to 1 reduction, right-angle gear drive; the driving motor and gear drive were both mounted internally in the support wing. Because of the limited power of the driving motor and the small width of the tunnel test section, each propeller was cut off at the 64.4-percent-radius station (fig. 3) and the tips were rounded; the advance ratios presented, however, are based on the full-model scale diameter of 3.09 feet.

Surface pressure distributions over the top of the spinner, top of the cowling, and inside lip of the cowling were measured by means of 5, 8, and 4 flush orifices, respectively. With propeller removed, pressure surveys at a station 0.75 inch inside the inlet were made by using a rake of eight total-pressure tubes extending across the annulus at the top of the inlet and two total-pressure tubes located 0.06 and 0.12 inch from the cowling inner surface at the bottom of the inlet. Pressure surveys were also conducted at the end of the 1.82-area-ratio diffuser of the basic 0.628 d/D_c cowling and at the end of the 1.40- and 1.345-area-ratio diffusers of the 0.70 d/D_c cowling by means of eleven total-pressure tubes extending across the annulus at the top section. The diffuser total-pressure rake was offset so as to be out of the wake of the inlet rake. The spinner boundary-layer thickness δ was determined from the inlet total pressure distributions.

With propeller installed, the total-pressure-tube instrumentation was replaced by shielded total-pressure tubes. A seven-tube rake of shielded total-pressure tubes was also installed just behind the propeller and extended from the cowling surface to the propeller tip (see fig. 2(b)). The quantity flow through the open-nose-spinner configuration was determined for the propeller-removed case by means of measurements of a total- and static-pressure tube located in each side of the exit in the horizontal plane. Suction flows for the boundary-layer scoop configurations were determined from measurements of a total- and static-pressure tube in each of the three exits.

The pressure measurements of the model were recorded by photographing a multitube manometer. Differential orifice meter pressures were read visually from a second multitube manometer.

Total- and static-pressure surveys were conducted for inlet-velocity ratios ranging from 0.3 to 1.6 and angles of attack ranging from 0 to 10° for both the propeller removed and installed conditions. The assumed propeller operating conditions are tabulated below:

Flight Condition	Blade angle (deg)		Advance ratio, J
	Front	Rear	
High-speed	67.4	66.6	5.25
Cruise (design)	63.1	62.3	4.20
Climb	47.4	46.6	1.56

A range of advance ratio was investigated for each of the propeller blade angles. All tests were conducted at a tunnel airspeed of 100 miles per hour which corresponds to a Mach number of 0.13 and a Reynolds number of approximately 0.94×10^6 based on the 12-inch-maximum cowling diameter of the model.

RESULTS AND DISCUSSION

Internal Flow

Basic cowling-spinner combination, propeller removed.- Total pressure distributions across the annulus at the top of the inlet and diffuser of the basic cowling-spinner combination are presented in figure 4. At the higher inlet-velocity ratios, total pressure coefficients near unity were obtained over a large part of the inlet and diffuser; the localized losses which occurred in the inner and outer sections of the diffuser at the highest inlet-velocity ratios were probably due to increased skin friction at the duct walls. As the inlet-velocity ratio was reduced from the higher values, small total-pressure losses began to occur at the inner section of the inlet annulus because of increases in boundary-layer thickness over the spinner. With further reductions in inlet-velocity ratio to values below 0.50, the spinner boundary layer thickened rapidly under the influence of the increasingly adverse pressure rise ahead of the inlet (fig. 5) and soon separated; this separation caused significant losses in total pressure. Increases in angle of attack also increased the magnitude of the pressure rise ahead of the inlet (fig. 5) and required higher values of inlet-velocity ratio to avoid the large losses due to separation. These effects are clearly shown in figure 6 which presents the boundary-layer thickness on top of the spinner and 0.75 inch inside the inlet as a function of inlet-velocity ratio and angle of attack; the spinner boundary-layer thickness δ, plotted in figure 6, has been arbitrarily defined as the distance normal from the central body to the point where the inlet total pressure coefficient $\frac{H_i - p_o}{q_o}$ equaled 0.95. The pronounced "knees" at the lower values of inlet-velocity ratio are indicative of the onset of separation. The small "knees" occurring in the δ curves of figure 6 at the higher inlet-velocity ratios may be associated with a forward movement in transition from laminar to turbulent flow as the inlet-velocity ratio was decreased.

The effects of roughness and spinner rotation on the spinner boundary-layer-thickness characteristics are presented in figures 7 and 8. Installation of varying degrees of roughness around the spinner at

approximately the minimum-pressure station $\left(\frac{x_s}{X_s} = 0.54\right)$ caused only small increases in the boundary-layer thickness (fig. 7) and did not affect significantly the inlet-velocity ratio at which the boundary layer began thickening rapidly. Similarly, rotation of the spinner with surfaces smooth both as a single- and a dual-rotation unit (fig. 8) did not cause significant changes in the inlet-velocity ratio required to avoid the rapid increase in thickness characteristics of the onset of separation. It is noted that the small "knee" which occurred at the high inlet-velocity ratios with the smooth nonrotating spinner was not obtained with the largest roughness particles installed or with the dual-rotation spinner. This result further points out the possibility of the "knee" being associated with a movement of transition.

In addition to total-pressure losses caused by thickening and separation of the spinner boundary layer at low inlet-velocity ratios, losses might also be expected to occur at the high-inlet-velocity ratio, high-angle-of-attack flight conditions (take-off and climb) because of separation from the inner surface of the lip at the bottom of the cowling. Such indications were determined from measurements of total-pressure tubes located 0.06 and 0.12 inch from the lower inner-lip surface of the cowling 0.75 inch inside the inlet (fig. 9). Low loss coefficients were maintained to the highest test inlet-velocity ratio at angles of attack up to 5° and also were maintained to an inlet-velocity ratio of about 1.0 at an angle of attack of 10°. At this high angle of attack, the losses measured by the tube nearest the surface (0.06 inch) increased rapidly with increases in inlet-velocity ratios above 1.0; this increase indicated the formation of bubbles of separation. These bubbles, however, were confined to a region very near the inner surface; no losses were indicated to occur at the tube 0.12 inch from the surface for any angle of attack and inlet-velocity-ratio condition. It appears, therefore, from this data and that presented in reference 2, that $0.01D_c$ height inner-lip fairing is probably sufficient to avoid significant losses over a large part of the range of flight conditions. The effect of propeller operation on the lower inner-lip separation characteristics will be discussed in a later section.

Average total pressure coefficients at the top of the inlet of the basic cowling-spinner combination weighted with respect to area are presented in figure 10. For the inlet-velocity-ratio range of 0.45 and greater, the coefficients closely approached unity for the case for an angle of attack of 0°. Below this value of inlet-velocity ratio, the total pressure decreased rapidly because of the thickening and subsequent separation of the spinner boundary layer ahead of the inlet. For angles of attack greater than 0°, the inlet-velocity ratio required to avoid spinner separation and the attending large losses in total pressure at the top of the inlet was increased considerably. It should be noted,

however, that the entering flow would be assymmetrical at angles of attack greater than 0° and that the spinner boundary layer would have the most detrimental effects on the average total pressures in the top section of the inlet. The total pressure coefficients of figure 10 (except for $\alpha = 0^{\circ}$), therefore, are considered conservative as average values for the entire inlet. The curves do indicate, however, that the assumed design inlet-velocity ratio of 0.50, which was obtained from reference 2, is sufficiently high to insure high inlet total pressures in the low angle-of-attack range likely to be encountered in the design cruise condition.

The average total pressure coefficients at the end of the 1.82-area-ratio diffuser are compared with those at the inlet in figure 11. At an angle of attack of 0°, the total-pressure losses between the inlet and diffuser remained nearly constant $\left(\text{about } 0.02q_o\right)$ from the minimum test inlet-velocity ratio to a value of about 0.80. For the inlet-velocity-ratio range above 0.80, the diffuser losses gradually increased to $0.08q_o$ at $\frac{V_i}{V_o} = 1.60$. Examination of these data in terms of the nominal inlet dynamic pressure show that the losses first decreased continuously for the inlet-velocity-ratio range 0.3 to 0.80 $\left(\frac{\Delta H}{q_i}\right.$ from 0.28 to $\left.0.03\right)$ and then remained approximately constant to the highest test inlet-velocity ratio. This result indicates that the separation had moved completely through the diffuser at $\frac{V_i}{V_o} = 0.80$ and the diffuser losses for the range of inlet-velocity ratio 0.80 and above were due simply to skin friction. At an angle of attack of 5°, average total pressure coefficients at the top of the diffuser station were considerably greater than those measured at the inlet for the range of inlet-velocity ratio below 0.80. It is apparent from these measurements that the assymetrical flow existing at the inlet for angles of attack other than zero was further distorted in the internal ducting so that total pressure coefficients determined from a single position in the diffuser cannot be considered as average values. Average total pressure coefficients in the internal ducting, therefore, will be discussed hereafter only at 0° angle of attack.

Basic cowling-spinner combination with "ideal" propeller-spinner juncture.- Total pressure distributions at the top of the inlet and diffuser with the propellers operating at the cruise condition are presented in figure 12. Comparison of these results shows that increases in thickness of the propeller shanks brought about reductions in total pressure at both the inlet and diffuser. The reductions in total pressure at the inner section of the inlet annulus might be expected to encourage boundary-layer separation at the low inlet-velocity ratios. Separation, however, did not occur above the propeller removed value of inlet-velocity

ratio except in the case of the thin (12 percent thick) shank propeller and, in this case, the separation inlet-velocity ratio was still below the design value of 0.50.

The effect of reducing the advance ratio was to increase the total pressures at the inlet and diffuser for each propeller configuration at inlet-velocity ratios high enough to avoid separation. (For example, see figs. 13(a) and 13(b)). Increases in angle of attack caused considerable increases in boundary-layer thickness on top of the spinner (compare figs. 13(a) and 13(c)) and, as in the propeller-removed case, required higher values of inlet-velocity ratio to avoid flow separation ahead of the inlet. These effects were generally the same over the entire range of propeller conditions investigated.

For the propeller-removed case, the formation of bubbles of separation from the lower cowling inner lip was indicated to occur at an inlet-velocity ratio just over 1.0 for high angles of attack (see fig. 9). With propeller installed, no such separation was observed. For the simulated cruise (low positive thrust) condition (fig. 14), loss coefficients measured by the reference total-pressure tube near the inner-cowling surface (0.06 inch) were small over the entire test range of inlet-velocity ratio and angle of attack. The effect of reducing the propeller-blade angle and advance ratio (simulating the climb condition) was to further reduce the already low loss coefficients. It appears, therefore, that, as indicated in reference 2, separation from the lower cowling inner lip is not likely to occur for the full range of flight conditions with the $0.01D_c$-height inner-lip fairing installed.

Average total pressure coefficients at the top of the inlet and diffuser with no propeller and with the several propellers operating at the design cruise condition $\left(\beta_F = 63.1^\circ;\ \beta_R = 62.3^\circ;\ \text{and } J = 4.2\right)$ are compared in the following table at 0° angle of attack and the design inlet-velocity ratio of 0.50:

Type of propeller	$\left(\frac{H_i - p_o}{q_o}\right)_{av}$	$\left(\frac{H_d - p_o}{q_o}\right)_{av}$
No propeller	0.96	0.94
12-percent-thick shank	.95	.90
24-percent-thick shank	.93	.87
40-percent-thick shank	.88	.84
Small round shank	.78	.72
Large round shank	.65	.55

These results demonstrate the superiority of the thin (12 percent thick) shank propeller for the selected design cruise condition and show that the coefficients obtained with the thin propeller were nearly equal to those for the propeller-removed case. Comparisons of the total pressure coefficients obtained with the 24- and 40-percent-thick airfoil-shank propellers with those for the small round and large round shank propellers which had the same maximum thickness, $0.022D_p$ and $0.035D_p$, respectively, also show that substantial gains are obtained through use of airfoil-type shanks. It is noted that the thin-shank propeller may have a much greater margin of superiority at the actual cruise Mach number than indicated previously, inasmuch as the thicker shank sections of the other propellers would operate at supercritical speeds so that shock-boundary-layer interaction effects could reduce the total pressure coefficients obtained with these propellers substantially below the low-speed values.

The effects of variations in blade angle and advance ratio on the average total pressure coefficients at the inlet and diffuser for the design inlet-velocity ratio are presented in figure 15. These results show that, over the range of advance ratio and β covering propeller operation from high speed to climb, the relative merits of the different propellers were essentially the same as that indicated for the design cruise condition in the preceding table.

Average total pressure coefficients at the inlet and diffuser are shown in figure 16 as a function of inlet-velocity ratio for several blade angle and values of advance ratio; the three blade angles and advance ratios which correspond approximately to the high-speed, cruise, and climb conditions are indicated on the figure. These results show that changes in inlet velocity above the design value of 0.50 also do not affect the order of merit of the several propellers. It is noted that total pressure coefficients substantially greater than those for the propeller-removed case were obtained with the thin shank propeller when operated at low advance ratio. The low total pressure coefficients obtained with the airfoil-shank propellers at the climb blade angle $\left(\beta_F = 47.4^\circ;\ \beta_R = 46.6^\circ\right)$ and advance ratio of 2.5 are attributed to reverse thrust.

Basic cowling-spinner combination with "practical" propeller-spinner junctures.- Average total pressure coefficients obtained with the several "practical" propeller-spinner junctures tested in conjunction with the 24-percent-thick shank propeller are presented in figures 17 and 18. The configuration with the gap under the forward part of the blades just large enough to permit adequate spinner clearance for the propeller through 120° of blade-angle change (table IV and fig. 2(h), low land removed) gave total pressure coefficients from 0.02 to 0.12 less than those for the "ideal" juncture over the test range of inlet-velocity ratio and propeller operating conditions. The greatest losses occurred

in the low inlet-velocity range for each propeller condition and are attributed to earlier separation of the spinner boundary layer. This earlier separation is believed to have been caused by losses due to flow through the gap between blade and spinner crosswise to the direction of the undisturbed stream; this flow was initiated by rotation and by differences in pressure on the thrust and suction faces of the propeller blades.

Installation of the low airfoil lands under the front sections of the propeller blades (see table IV and fig. 2(i)) caused significant reductions in the crosswise spinner flow and consequently effected reductions in the minimum inlet-velocity ratio required to avoid spinner separation. Substantial improvements in the average total pressure coefficients at the inlet and diffuser were obtained at low inlet-velocity ratios with this land compared to those for the case with the low land removed (figs. 17 and 18). At the cruise blade angle the coefficients were only 0.02 to 0.05 less than for the "ideal" juncture over the test ranges of inlet-velocity ratio and advance ratio. Increases in total pressure compared to the land-removed case were also realized at the simulated high-speed and climb blade angles and advance ratios. For these blade angles, the land was not alined with the blade root because the land angle was fixed at the design cruise blade angle.

The configuration with the broad land (20° land), which allowed a constant land-blade gap for the range of propeller blade angles simulating climb to high speed (see table V and fig. 2(l)), provided small increases in total pressure coefficient when compared to the low-airfoil land for both the climb and high-speed blade angles in the low inlet-velocity-ratio range (figs. 17 and 18). For the larger part of the inlet-velocity-ratio range, however, the total pressures for the high-speed blade angle as well as the cruise were from $0.02q_0$ to $0.05q_0$ less than those obtained with the low land (fig. 17) possibly because of the greater land drag.

It was believed that the internal flow characteristics of the configurations discussed were inferior to those for the "ideal" juncture configuration because of the detrimental effects of the juncture on the spinner boundary-layer characteristics. A second airfoil-type land, therefore, was investigated which had the opening between the land and the propeller blade end located high enough above the spinner surface to be well out of the spinner boundary layer (see table IV and fig. 2(j)). This land has been designated the "high-airfoil land".

Installation of the high land effected substantial increases in the average total pressure coefficients at the inlet and diffuser compared to the other "practical" juncture configurations (figs. 17 and 18). At the design cruise blade angle, the total pressures were everywhere

within $0.02q_o$ of those for the "ideal" juncture over the test range of inlet-velocity ratio and advance ratio and indicated that flow through the clearance gap between the land and the propeller blade end had no significant effects. When the blade angle was increased to the high-speed value $\left(\beta_F = 67.4^\circ;\ \beta_R = 66.6^\circ\right)$, small reductions in total pressure occurred compared to the "ideal" propeller for corresponding inlet-velocity ratios and advance ratios. It will be noted, however, that the reductions were substantially less than for the other "practical" juncture configurations in the low inlet-velocity-ratio range.

Operation of the high land at the simulated climb blade angle produced greater total pressure coefficients than any other propeller configuration over the test range of inlet-velocity ratio and advance ratio, including that for the "ideal" juncture. In the low range of inlet-velocity ratio where spinner boundary-layer separation occurred with the "ideal" juncture, the high land effected small reductions in the minimum inlet-velocity ratio for which such separation was avoided. These increases in total pressure coefficient and reductions in minimum inlet-velocity ratio are believed to be caused by the combination of the effects of a greater angle of attack of the land (see fig. 2(k)), which produced greater thrust at the inboard sections of the propeller, and a vortex type of flow (such as described in reference 3) generated at the gap between the propeller blade end and the land. Such a vortex type of flow, originating because of the pressure differences on the thrust and suction faces of the blade and high land, would tend to sweep the spinner boundary layer from the spinner surface into the stream; thereby, separation at lower inlet-velocity ratios would be delayed. A similar vortex type of flow is also thought to have existed in the case of the low airfoil land for the off design propeller conditions; the vortex strength, however, probably was insufficient to sweep the boundary layer into the higher-energy stream. Reference 3 points out that the vortex-generator height must be greater than the boundary-layer thickness in order to retard separation.

The fact that total pressure coefficients obtained with the high land were greater than with the "ideal" juncture for the climb case also indicates that some increases in the total pressure of the internal flow may be possible with small increases in the propeller-shank twist distribution as suggested in reference 4. The effect of the greater inboard loading on the propeller efficiency, however, must be considered. It will be noted that the high-land configuration would not be expected to cause any important changes in the external drag relative to the drag with the "ideal" juncture installed because all or most of the flow passing over the land entered the inlet.

Open-nose spinner.- The effects of installation of the open-nose boundary-layer control spinner on the internal flow characteristics of the model are presented in figures 19 and 20. The propeller-removed results will be discussed in this paragraph and compared with the results for the basic spinner. At an angle of attack of 0°, the inlet-velocity ratio of the open-nose spinner was about 0.63, which corresponds to approximately 8 percent of the cowling inlet flow at the design inlet-velocity ratio of 0.50, and the total pressure at the slot exit was about $0.85q_o$. In the low inlet-velocity-ratio range, where separation occurred with the basic spinner installed, injection of this high-energy flow into the spinner boundary layer through the annular exit between spinner components (see table II) caused substantial reductions in the boundary-layer thickness measured at the top of the inlet for the several test angles of attack and reduced the minimum inlet-velocity ratio for avoiding flow separation (fig. 19). As shown in figure 20, the minimum inlet-velocity ratio was reduced by about 0.08 and the average total pressure coefficient at the lowest test inlet-velocity ratio was increased by about 0.20. Gains in total pressure were also realized in the internal ducting at the lowest flow rates. These gains, however, were somewhat less than at the inlet because of the more extensive separation in the diffuser and, for the range of inlet-velocity ratio above approximately 0.43, the average total pressure after diffusion was lower than that obtained with the basic spinner. The average total pressure at the end of the diffuser was only $0.82q_o$ compared to $0.92q_o$ for the basic spinner at the highest test inlet-velocity ratio.

Installation of the propeller caused large reductions in the boundary-layer-control effectiveness of the open-nose spinner. In fact, with the 24-percent-thick shank propeller operating at the cruise condition, the total pressures measured at the inlet and diffuser never exceeded those obtained with the basic spinner over the entire test range of inlet-velocity ratio (fig. 20). The reasons for the loss of the effectiveness of the open-nose spinner with propellers installed are not readily apparent. Results from test with the open-nose spinner rotating alone (no propeller) have indicated, however, that the reduction in effectiveness of the open-nose spinner was not caused by any increase in spinner ducting loss due to rotation. It may be possible, therefore, to avoid the adverse effects of the propeller and at the same time to improve the boundary-layer-control effectiveness of this arrangement by relocating and redesigning the exit.

Suction-scoop configurations.- Boundary-layer thickness at the inlet of the NACA 1-70-070 cowling with the several boundary-layer suctions scoops installed at the base of the spinner, propeller removed, are compared with those for the combination of the basic spinner with an NACA 1-70-070 cowling in figure 21. The suction quantity for each scoop

was approximately constant over the test range of inlet-velocity ratio and equal to about 9 percent of the cowling inlet flow at $\frac{V_i}{V_o} = 0.50$. When the scoop was located 3 inches ahead of the cowling inlet (see table III), suction did not reduce the minimum inlet-velocity ratio required to avoid separation with the basic spinner and did not reduce the boundary-layer thickness for the entire test range of inlet-velocity ratio. When the scoop was installed at positions 1.5 inches ahead of the inlet and flush with the inlet, however, reductions of approximately 0.10 in minimum inlet-velocity ratio were obtained. For the case where the scoop was located at the inlet the boundary-layer thickness was reduced below that of the basic spinner over the entire test range of inlet-velocity ratio.

Average total pressure coefficients at the inlet and diffuser of the NACA 1-70-070 cowling with the suction scoop located at the inlet, the more practical case for a propeller directly ahead of the cowling inlet, are compared in figure 22 with those obtained with the basic spinner. The effect of suction, propeller removed, was to reduce the minimum inlet-velocity ratio for avoidance of high losses from about 0.45 to 0.35 and to increase substantially the total pressures everywhere in the low inlet-velocity-ratio range; at the minimum test inlet-velocity ratio of 0.30, the minimum total pressure obtained was $0.92q_o$ at the diffuser station compared to $0.70q_o$ for the basic spinner. Small increases in total pressure also were obtained in the higher range of inlet-velocity ratio.

As in the case of the basic configuration, the effect of installation of the 24-percent-thick shank propeller was to reduce the inlet and diffuser total pressure coefficients over most of the test inlet-velocity-ratio range. The maximum reduction at the cruise propeller condition was 0.09 and occurred at an inlet-velocity ratio of 0.35 (fig. 22). The coefficients obtained, however, were 0.02 to 0.05 higher in the low inlet-velocity-ratio range than those obtained without suction (compare figs. 16 and 22). Reductions in minimum inlet-velocity ratio to obtain equal coefficients was from 0.06 to 0.10 at the inlet and 0.12 to 0.25 at the diffuser. Some gains, therefore, appear possible through the use of boundary-layer control by suction. The significance of the gains, with regard to over-all airplane performance must, of course, include consideration of the suction-pumping-power requirements.

External Flow

Pressure distributions over cowling.- Static pressure distributions over the top surface of the basic NACA 1-62.8-070 cowling are presented

in figure 23. The phenomena (propeller removed) were generally similar to those for the NACA 1-series inlets discussed in reference 2. At an angle of attack of 0°, no sharp negative pressure peaks occurred in the distributions even at the lowest test inlet-velocity ratio of 0.28. The effect of increasing the inlet-velocity ratio was to increase the pressures in the vicinity of the nose because of the outward displacement of the stagnation region; the distribution over the rear section of the cowling and the minimum pressures, however, were essentially unaffected by inlet-velocity-ratio variations. As the angle of attack was increased, small localized negative pressure peaks occurred over the nose section at the lower inlet-velocity ratios, and increases in inlet-velocity ratio were required to produce peak-free distributions. Angle of attack increases also caused small reductions in the pressures over the rear section of the cowling.

Propeller operation at the design cruise condition $\left(\beta_F = 63.1^{\circ};\ \beta_R = 62.3^{\circ};\ J = 4.2\right)$ caused only small changes in the distribution and in the magnitude of the pressures over the cowling (fig. 23(b)). The total pressure just outside the cowling boundary layer was also reduced below the stream value for this condition (see fig. 24). Hence, there was no net increase in flow velocity over the cowling surface. As the propeller advance ratio was reduced, small increases occurred in both the total and static pressures in the region of the cowling surface (figs. 23(b) and 24). The increases in static pressure were greatest near the nose. Because the increases in total pressure were slightly greater than the static pressure increases, a small net increase occurred in the flow velocity over the surface compared to the propeller-removed and low-positive-thrust cases.

The total-pressure surveys behind the 24-percent-thick shank propeller, which was representative of all propellers at sections outboard of the cowling inlet, showed that a radial total-pressure gradient existed behind the propeller (fig. 24). The magnitude of this gradient increased with reductions in both blade angle and advance ratio. The maximum total-pressure rise for the range of propeller test conditions occurred at the outboard sections and was of the order of $0.47q_o$ (compare the advance ratio for the highest blade angle with the advance ratio for the lowest blade angle); whereas the maximum rise in the inboard sections (at the plane of the cowling inlet) never exceeded $0.18q_o$ for any propeller. This fact again illustrates the possibility of obtaining higher inlet total pressures through slight increases in the inboard propeller twist distribution. As noted previously, however, the effect of additional inboard loading on the propeller efficiency must be considered.

Predicted critical Mach number.- Critical Mach numbers predicted from low-speed pressure coefficients by the von Kármán extrapolation (reference 5) have been shown in previous papers (for example, reference 2) to be valid for test Mach numbers as low as 0.13 provided sharp negative pressure peaks do not occur in the pressure distributions. Mach numbers thus obtained, however, are unnecessarily conservative for design purposes inasmuch as they define only the lower limiting Mach number range within which force changes due to shock can occur. Reference 6 indicates that a margin of from 0.05 to 0.075 may exist between the critical and force-break Mach numbers. In the selection of the basic cowling-spinner design from the charts of reference 2, therefore, the critical Mach number for the present design was taken to be 0.05 less than the design cruise Mach number of 0.80 in order to obtain the shortest possible cowling.

Predicted critical Mach numbers for the combination of the basic NACA 1-62.8-070 cowling with the NACA 1-46.5-085 spinner (propeller removed) are presented in figure 25 as a function of inlet-velocity ratio. At an angle of attack of 0° and for the design inlet-velocity ratio of 0.50 the critical Mach number was 0.75, the value given for this cowling in the selection charts of reference 2. The effect of increasing the angle of attack was to reduce slightly the critical Mach numbers in the higher range of inlet-velocity ratios; in the lower range, where sharp local negative pressure peaks occurred in the surface pressure distributions, the critical Mach number decreased rapidly. The "knees" of the curves for angles of attack up to 5°, however, always occurred at inlet-velocity ratios below the design value of 0.50.

It has been shown previously that propeller operation did not produce increases in the flow velocity over the cowling (just outside the cowling boundary layer) at the higher values of advance ratio which correspond to high-speed flight. It is evident, therefore, that operation of propellers of the type investigated did not decrease the critical Mach number of the installation below the propeller-removed value. It is possible, of course, that some increase in flow velocity might be obtained if the propeller shanks were retwisted to increase the inboard loading. Only a small increase in loading is possible, however, so that any adverse effect of the propeller on the critical Mach number of the installation would be small enough to neglect in the design process.

SUMMARY OF RESULTS

The more important conclusions from an investigation of propeller-shank effects on the internal flow characteristics of a cowling-spinner

combination equipped with an eight-blade dual-rotation propeller are summarized as follows:

1. The addition of any of the propellers studied to the basic cowling-spinner combination did not increase the minimum inlet-velocity ratio required to avoid boundary-layer separation from the spinner surface and did not decrease the predicted critical Mach number of the cowling. Propeller operation also delayed separation from the inner-cowling-lip surface at high inlet-velocity ratios.

2. The propeller with 12-percent-thick shanks and with "ideal" sealed and faired propeller-spinner junctures produced total pressure coefficients at the cowling inlet and diffuser nearly equal to those with propeller removed at the design cruise operating condition. Total pressure coefficients substantially greater than those for the propeller-removed case were obtained at the propeller operating condition corresponding to climbing flight.

3. Increases in propeller-shank thickness caused significant reductions in the total pressure coefficients at the inlet and diffuser; coefficients for the round-shank propeller were as much as 0.30 less than those of the comparable-thickness airfoil-shank propeller.

4. The incorporation of propeller-spinner-juncture arrangements that permitted blade rotation reduced the total pressure coefficients at the inlet and diffuser as long as the juncture was located inside the spinner boundary layer.

5. An airfoil-land-type juncture which had the land-shank gap located well above the spinner surface gave total pressure coefficients nearly equal to those for the "ideal" juncture in the simulated high-speed and cruise conditions and was superior in the climb condition.

6. Of the two boundary-layer control methods investigated only the suction scoop provided any improvement over the basic configuration with propellers operating.

Langley Aeronautical Laboratory
National Advisory Committee for Aeronautics
Langley Field, Va.

REFERENCES

1. Hansen, Frederick H., Jr., and Mossman, Emmet A.: Effect of Pressure Recovery on the Performance of a Jet-Propelled Airplane. NACA TN 1695, 1948.

2. Nichols, Mark R., and Keith, Arvid L., Jr.: Investigation of a Systematic Group of NACA 1-Series Cowlings with and without Spinners. NACA Rep. 950, 1949. (Formerly NACA RM L8A15.)

3. Taylor, H. D.: Summary Report on Vortex Generators. U.A.C. Rep. R-05280-9, United Aircraft Corp. Res. Div., March 7, 1950.

4. Prince, Clifford H.: The Effects of Three Types of Propeller Shanks on Pressure Recovery of a Conical-Spinner-Turbine Intake at Mach Numbers of 0.4 and 0.7. U.A.C. Rep. R-14018-2, United Aircraft Corp. Res. Dept., June 29, 1948.

5. Von Kármán, Th.: Compressibility Effects in Aerodynamics. Jour. Aero. Sci., vol. 8, no. 9, July 1941, pp. 337-356.

6. Pendley, Robert E., and Robinson, Harold L.: An Investigation of Several NACA 1-Series Nose Inlets with and without Protruding Central Bodies at High-Subsonic Mach Numbers and at a Mach Number of 1.2. NACA RM L9L23a, 1950.

TABLE I

NACA 1-SERIES NOSE-INLET ORDINATES AS APPLIED TO COWLINGS AND SPINNERS

[Ordinates in percent. (See reference 2.)]

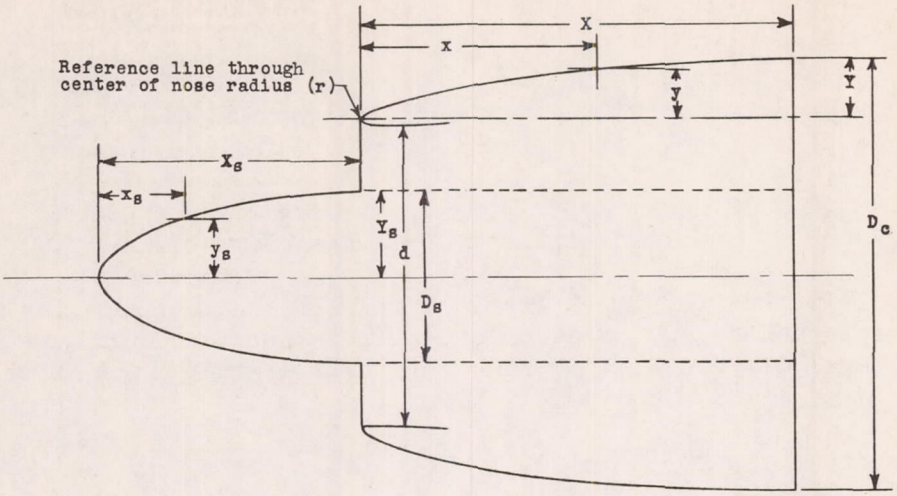

$$X = \left(\frac{X}{D_c}\right) D_c \qquad X_s = \left(\frac{X_s}{D_c}\right) D_c$$

$$Y = \frac{D_c - d}{2} - r \qquad Y_s = \frac{D_s}{2} = \frac{\left(\frac{D_s}{D_c}\right) D_c}{2}$$

$$\text{For } r = 0.025Y: \quad Y = \frac{D_c - d}{2.05} = \frac{D_c\left(1 - \frac{d}{D_c}\right)}{2.05}$$

x/X or x_s/X_s	y/Y or y_s/Y_s	x/X or x_s/X_s	y/Y or y_s/Y_s	x/X or x_s/X_s	y/Y or y_s/Y_s	x/X or x_s/X_s	y/Y or y_s/Y_s
0	0	13.0	41.94	34.0	69.08	60.0	89.11
.2	4.80	14.0	43.66	35.0	70.08	62.0	90.20
.4	6.63	15.0	45.30	36.0	71.05	64.0	91.23
.6	8.12	16.0	46.88	37.0	72.00	66.0	92.20
.8	9.33	17.0	48.40	38.0	72.94	68.0	93.11
1.0	10.38	18.0	49.88	39.0	73.85	70.0	93.95
1.5	12.72	19.0	51.31	40.0	74.75	72.0	94.75
2.0	14.72	20.0	52.70	41.0	75.63	74.0	95.48
2.5	16.57	21.0	54.05	42.0	76.48	76.0	96.16
3.0	18.31	22.0	55.37	43.0	77.32	78.0	96.79
3.5	19.94	23.0	56.66	44.0	78.15	80.0	97.35
4.0	21.48	24.0	57.92	45.0	78.95	82.0	97.87
4.5	22.96	25.0	59.15	46.0	79.74	84.0	98.33
5.0	24.36	26.0	60.35	47.0	80.50	86.0	98.74
6.0	27.01	27.0	61.52	48.0	81.25	88.0	99.09
7.0	29.47	28.0	62.67	49.0	81.99	90.0	99.40
8.0	31.81	29.0	63.79	50.0	82.69	92.0	99.65
9.0	34.03	30.0	64.89	52.0	84.10	94.0	99.85
10.0	36.13	31.0	65.97	54.0	85.45	96.0	99.93
11.0	38.15	32.0	67.03	56.0	86.73	98.0	99.98
12.0	40.09	33.0	68.07	58.0	87.95	100.0	100.00
Cowling nose radius: 0.025Y							

TABLE II.- OPEN-NOSE-SPINNER CONFIGURATION

[All dimensions are in inches]

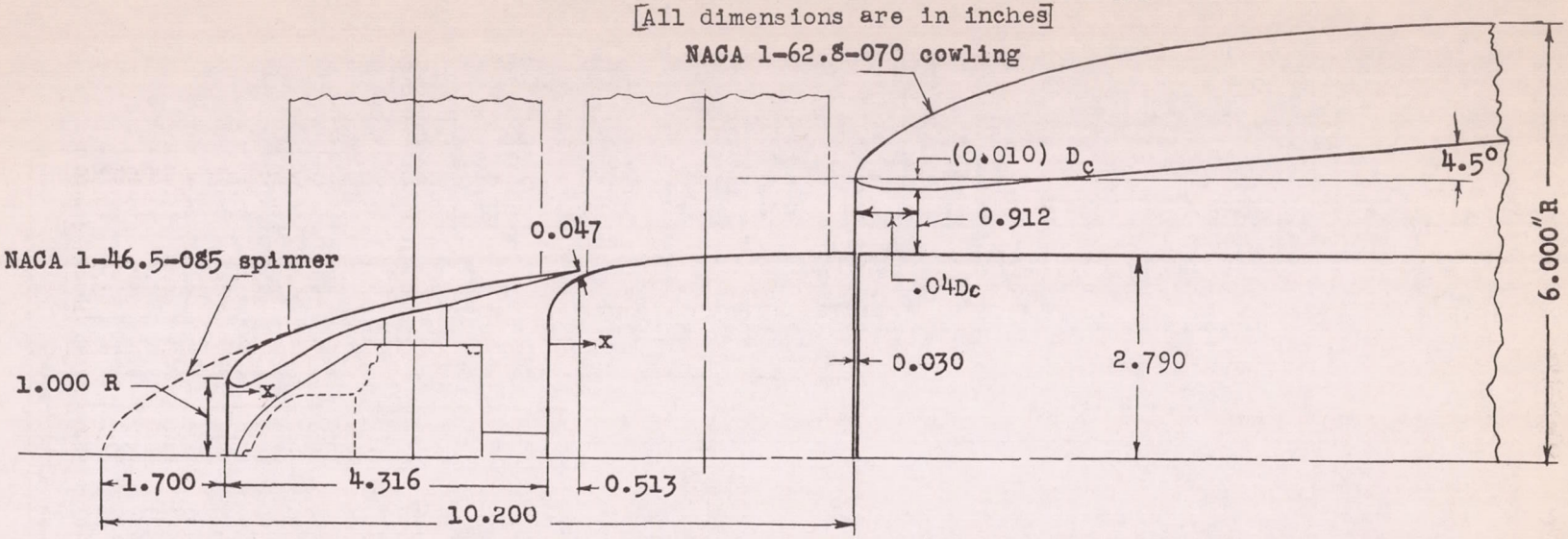

Open-Nose Spinner

x	R_{outer}	R_{inner}	x	R_{outer}
0	1.000	1.000	1.972	1.982
.04	1.125		2.176	2.034
.075	1.175	.925	2.380	2.086
.150	1.250	.940	2.580	2.134
.250	1.325	.975	2.788	2.180
.400	1.420	1.040	2.992	2.225
.600	1.530	1.155	3.196	2.267
.900	1.650	1.350	3.400	2.307
1.100	1.725	1.510	3.808	2.384
1.300	1.785	1.670	4.216	2.454
1.400	1.820	1.760	4.624	2.517
1.564	1.870		4.829	2.555
1.768	1.527			
L.E. Radius: 0.075				

Rear Section of Open-Nose Spinner

x	R	x	R
0	1.980	1.00	2.595
.05	2.180	1.30	2.640
.10	2.245	1.60	2.675
.15	2.295	1.90	2.705
.25	2.365	2.20	2.735
.35	2.415	2.50	2.750
.45	2.450	2.80	2.770
.60	2.505	3.35	2.785
.80	2.550	3.955	2.790
		4.184	2.792

NACA

TABLE III.- SUCTION SCOOP CONFIGURATIONS

[All dimensions are in inches]

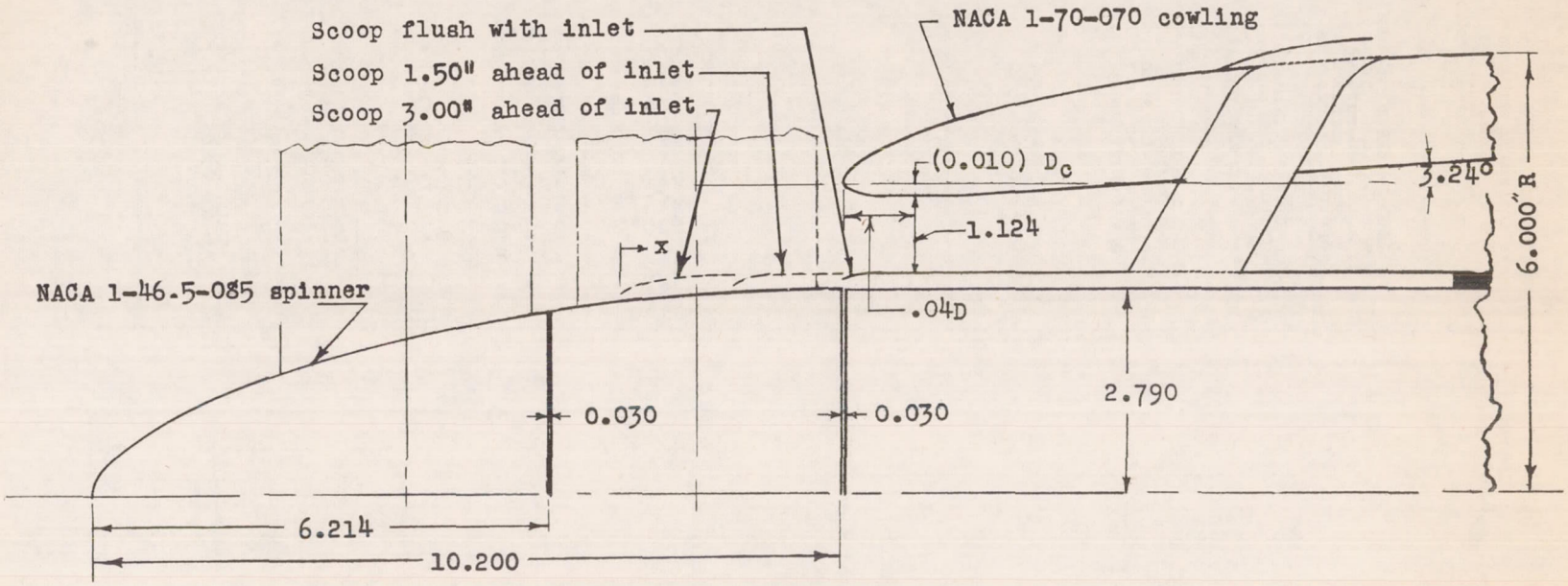

Scoop position relative to inlet									
3.00 ahead				1.50 ahead				flush	
X	R	X	R	X	R	X	R	X	R
0	2.76	1.00	2.96	0	2.87	0.50	2.98	0	2.91
.10	2.83	1.50	2.97	.10	2.92	1.00	2.99	.10	2.96
.20	2.86	2.00	2.98	.20	2.95	1.50	3.00	.30	2.995
.30	2.89	2.50	2.99	.30	2.96	cylindrical		.40	3.00
.40	2.91	3.00	3.00	.40	2.97	9.80	3.00	cylindrical	
.50	2.92	cylindrical						8.30	3.00
.75	2.95	11.30	3.00						

TABLE IV.- HIGH AND LOW AIRFOIL TYPE LANDS

[Airfoil land ordinates same as 24-percent-thick propeller shank ordinates. Blade root land gap is 0.010. All dimensions are in inches.]

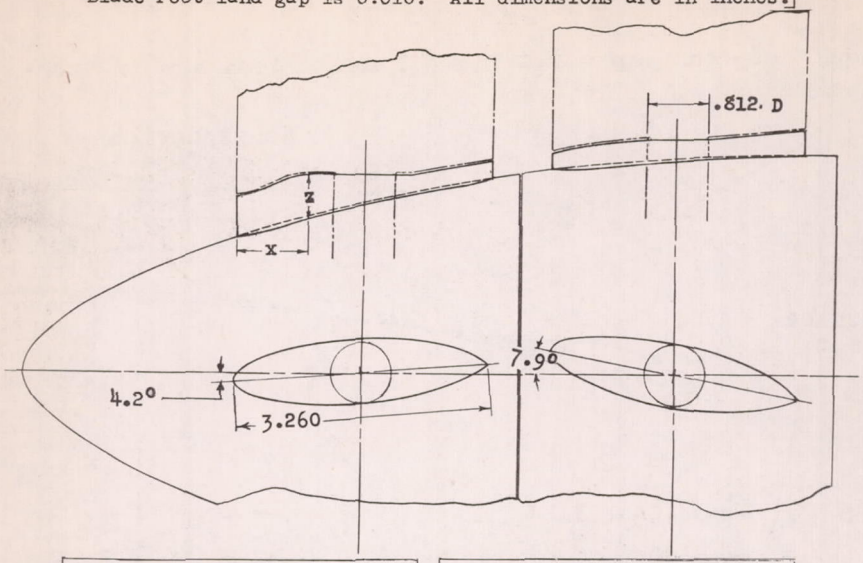

Front Land	
Station; x	Land Height; z
0	.535
.375	.520
.625	.565
.750	.565
.875	.555
1.005	.530
2.245	.240
2.255	.245

Rear Land	
Station; x	Land Height; z
0	.265
.63	.299
1.38	.300
2.13	.252
2.88	.295
3.26	.335

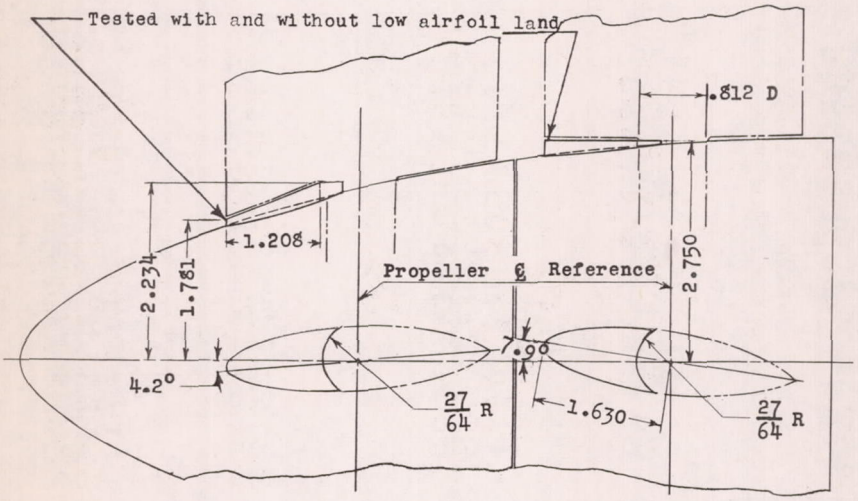

NACA

TABLE V.- LOW LAND WHICH COVERS BASE OF BLADE THROUGH 20° BLADE-ANGLE CHANGE

[Blade root-land gap = 0.010. All dimensions are in inches]

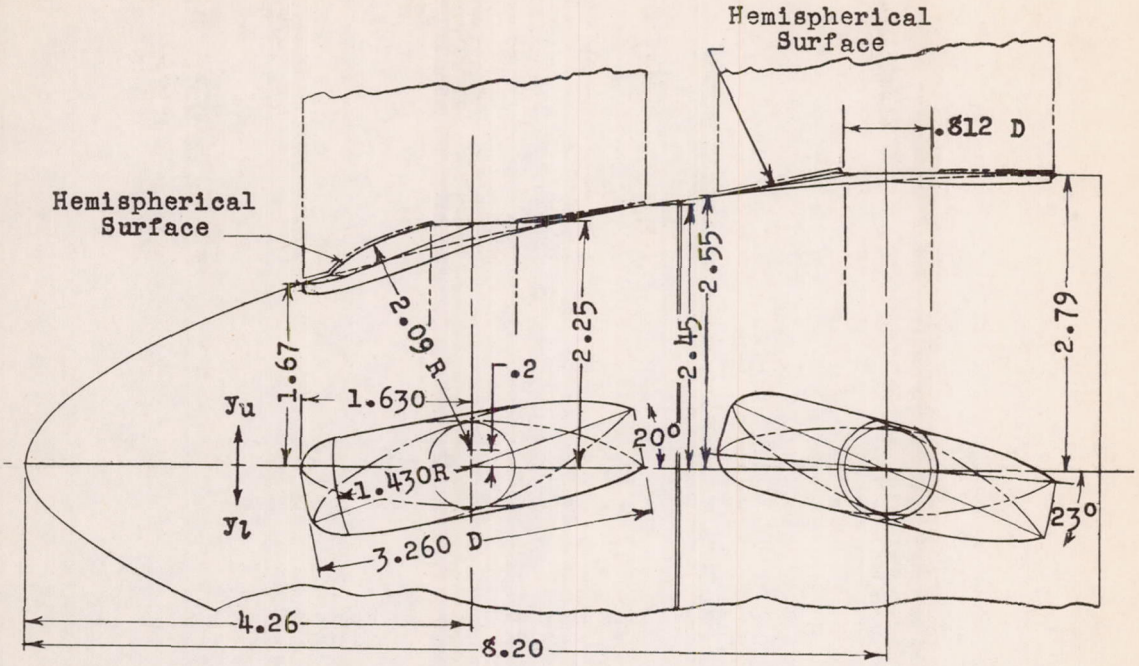

	Front Land		Rear Land	
Station; x	Upper; y_u	Lower; y_l	Upper; y_u	Lower; y_l
0	0	0	.080	.080
.020	.060	-.240	.260	.025
.040	.090	-.345	.360	-.005
.060	.110	-.430	.440	-.030
.100	.145	-.560	.560	-.070
.200	.190	-.650	.695	-.135
.300	.235	-.675	.720	-.180
.500	.295	-.670	.720	-.250
.700	.340	-.645	.690	-.300
1.000	.390	-.590	.620	-.320
1.630	.490	-.465	.465	-.505
2.200	.590	-.355	.330	-.625
2.500	.620	-.290	.250	-.660
2.800	.620	-.210	.145	-.660
3.000	.600	-.135	.060	-.650
3.160	.560	-.060	0	-.625
3.220	.350	-.030	-.045	-.420
3.260	0	0	-.080	-.080

NACA

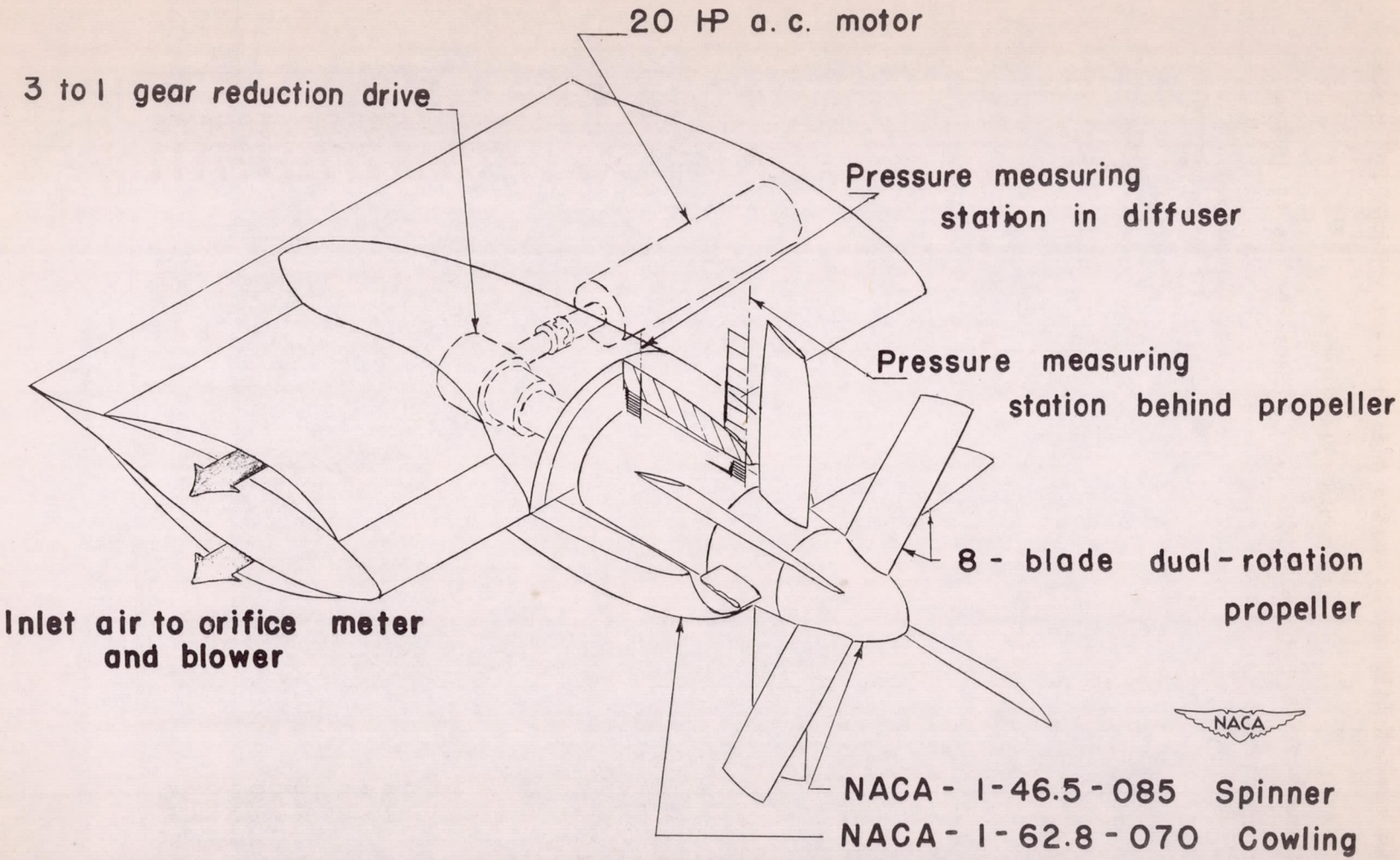

Figure 1.- General arrangement of model.

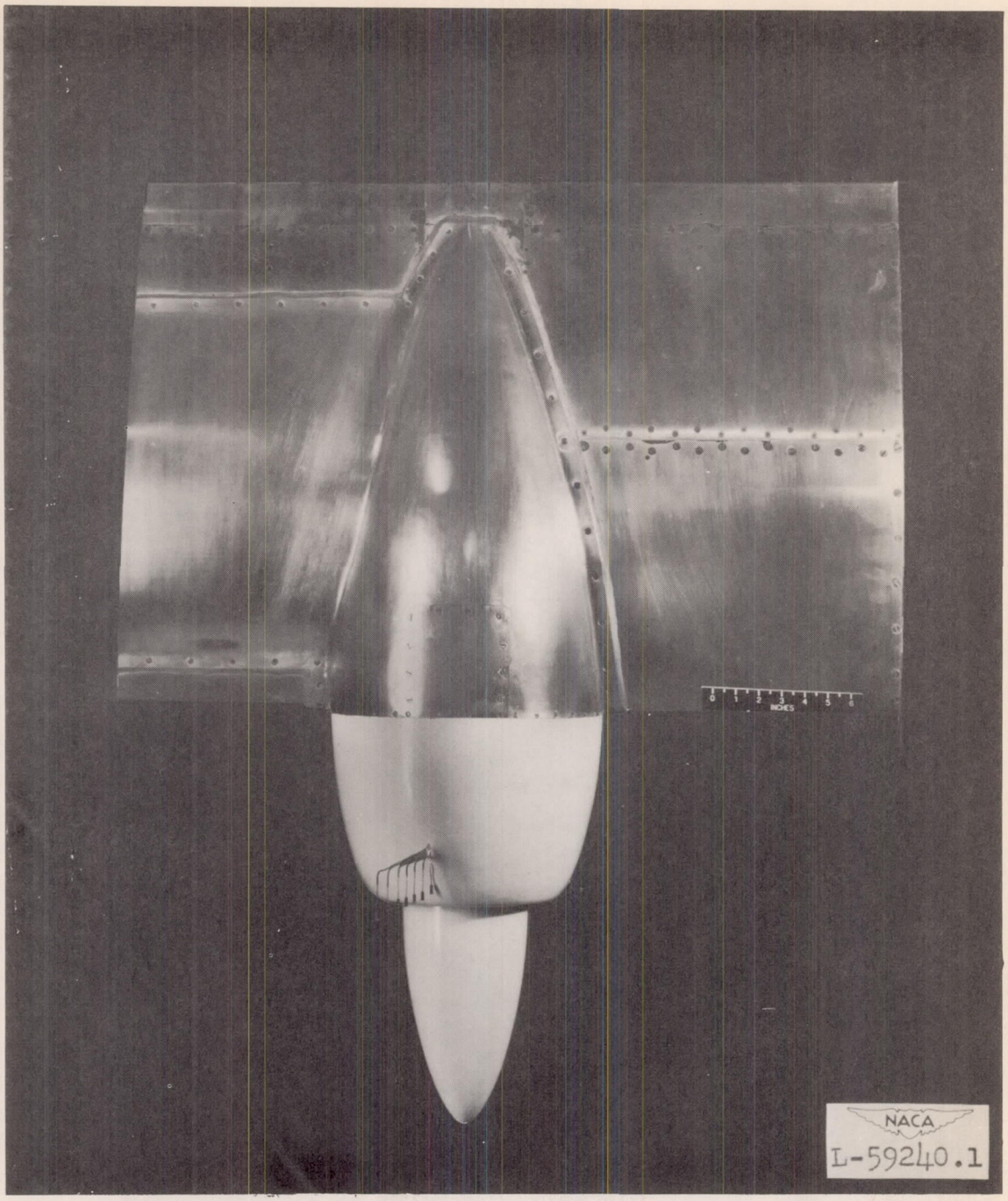

(a) Basic cowling-spinner combination, NACA 1-62.8-070 cowling with 1-46.5-085 spinner, plan view.

Figure 2.- Views of model.

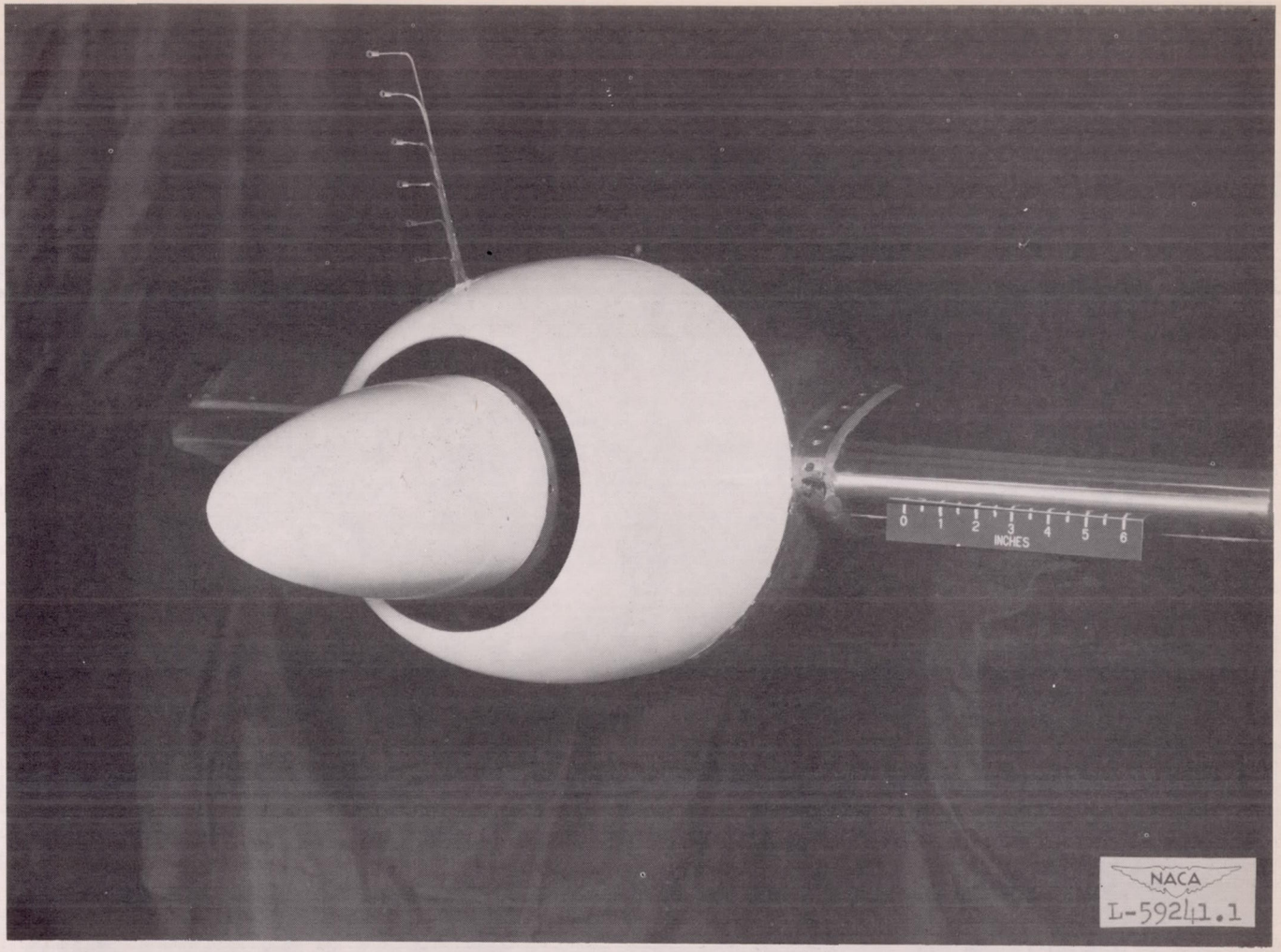

(b) Basic cowling-spinner combination, three-quarter front view.

Figure 2.- Continued.

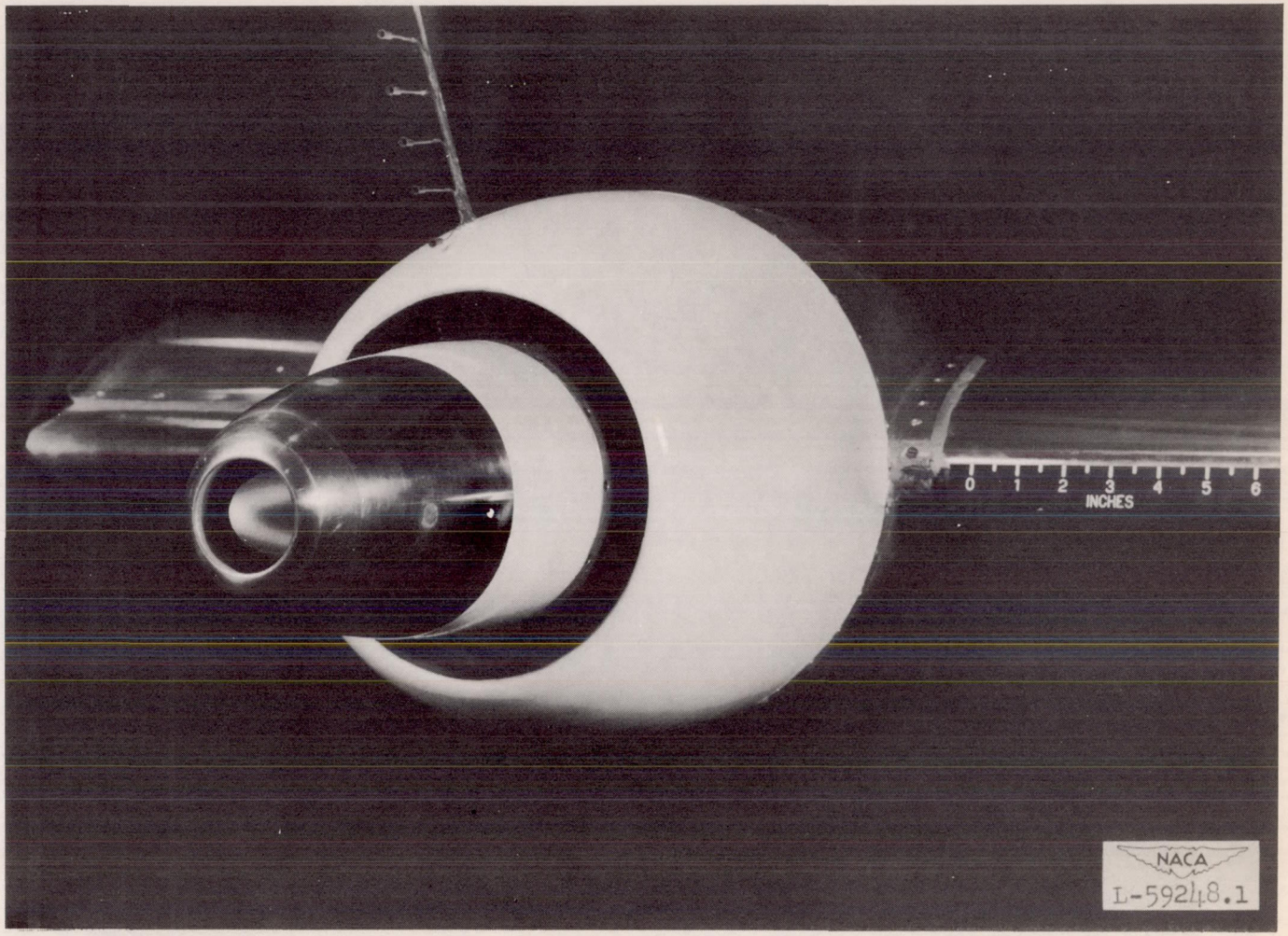

(c) Open-nose boundary-layer-control spinner.

Figure 2.- Continued.

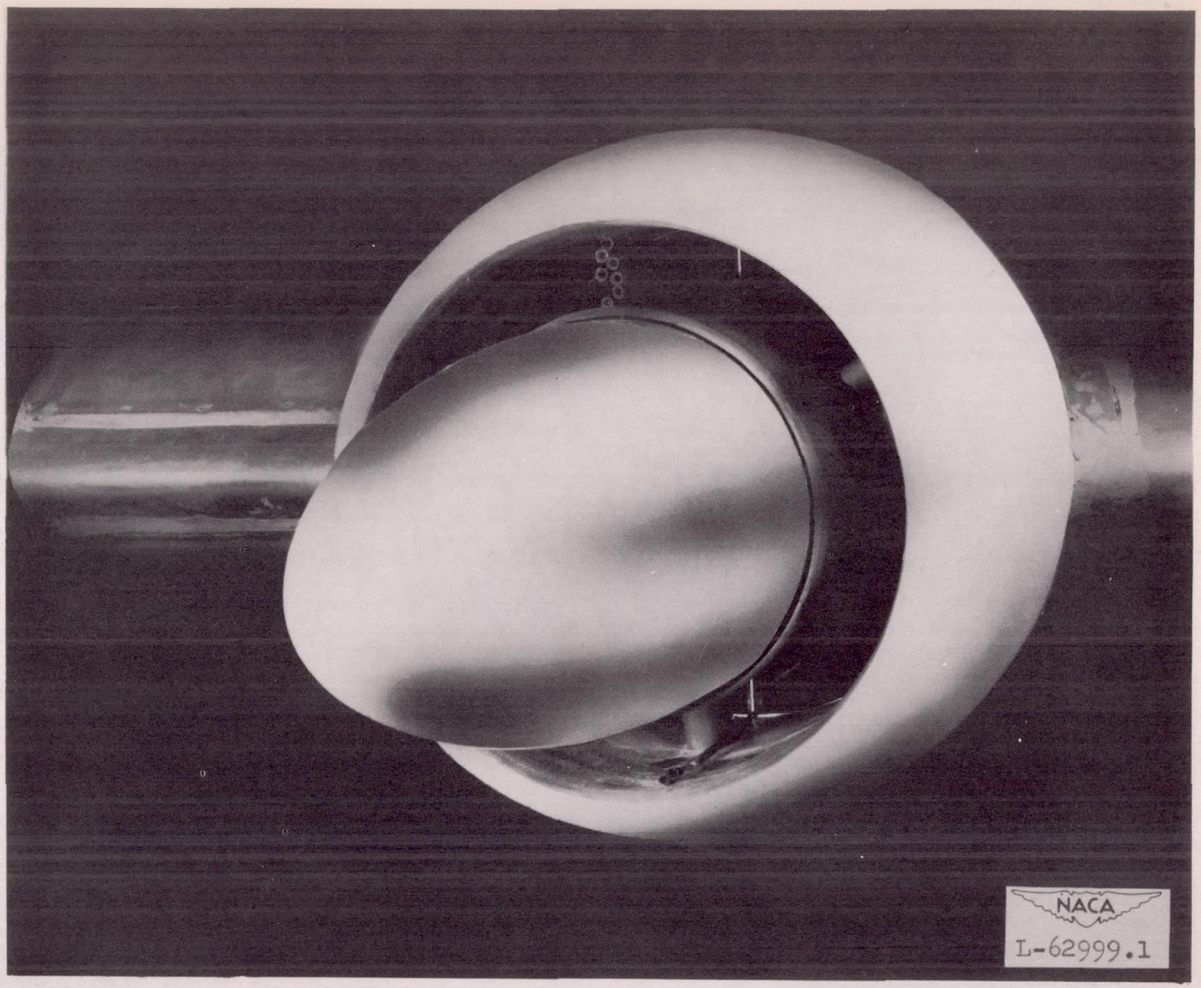

(d) Configuration with boundary-layer suction scoop at base of spinner, NACA 1-70-070 cowling with 1-46.5-085 spinner.

Figure 2.- Continued.

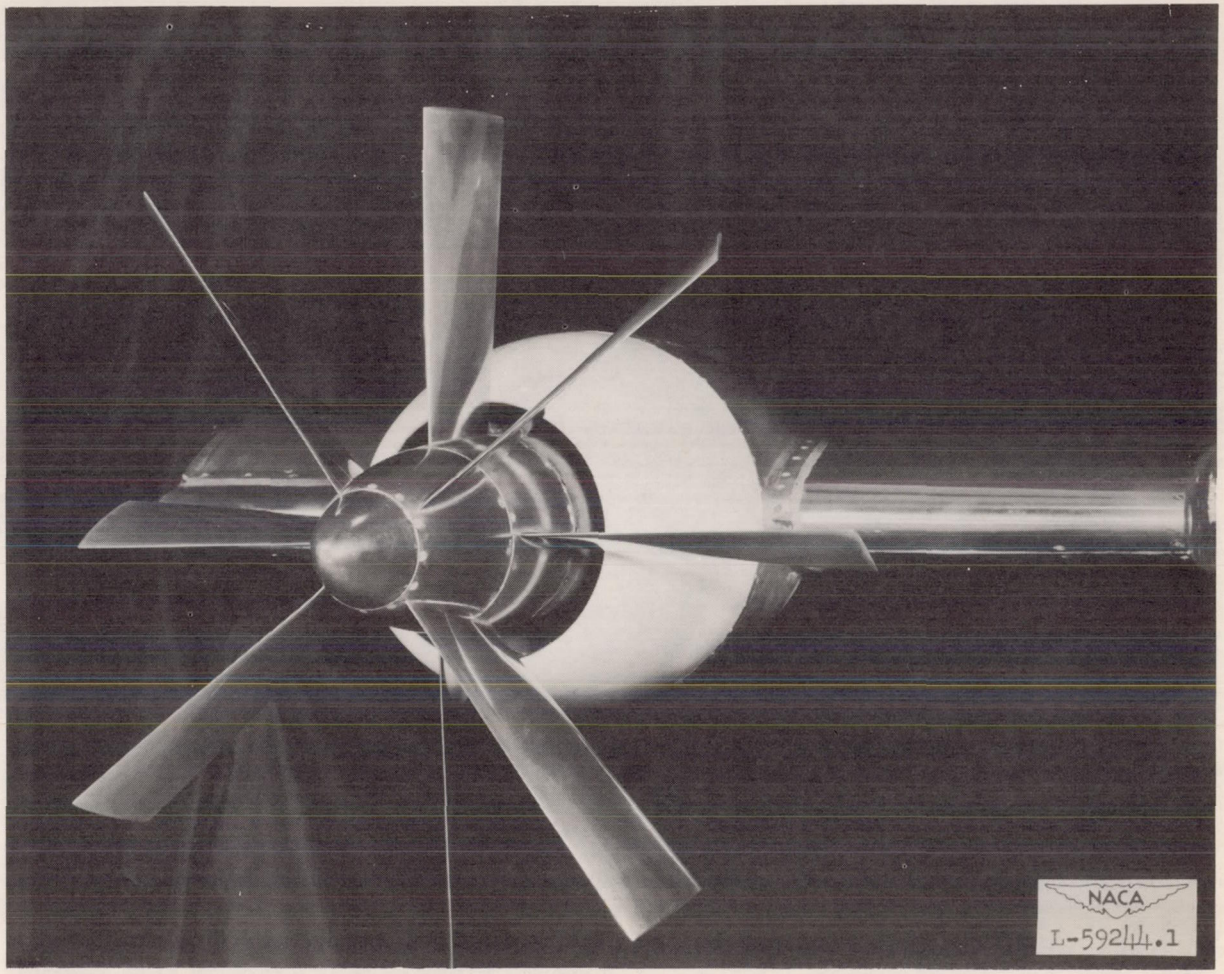

(e) 12-percent-thick shank propeller, ideal juncture, basic cowling-spinner combination.

Figure 2.- Continued.

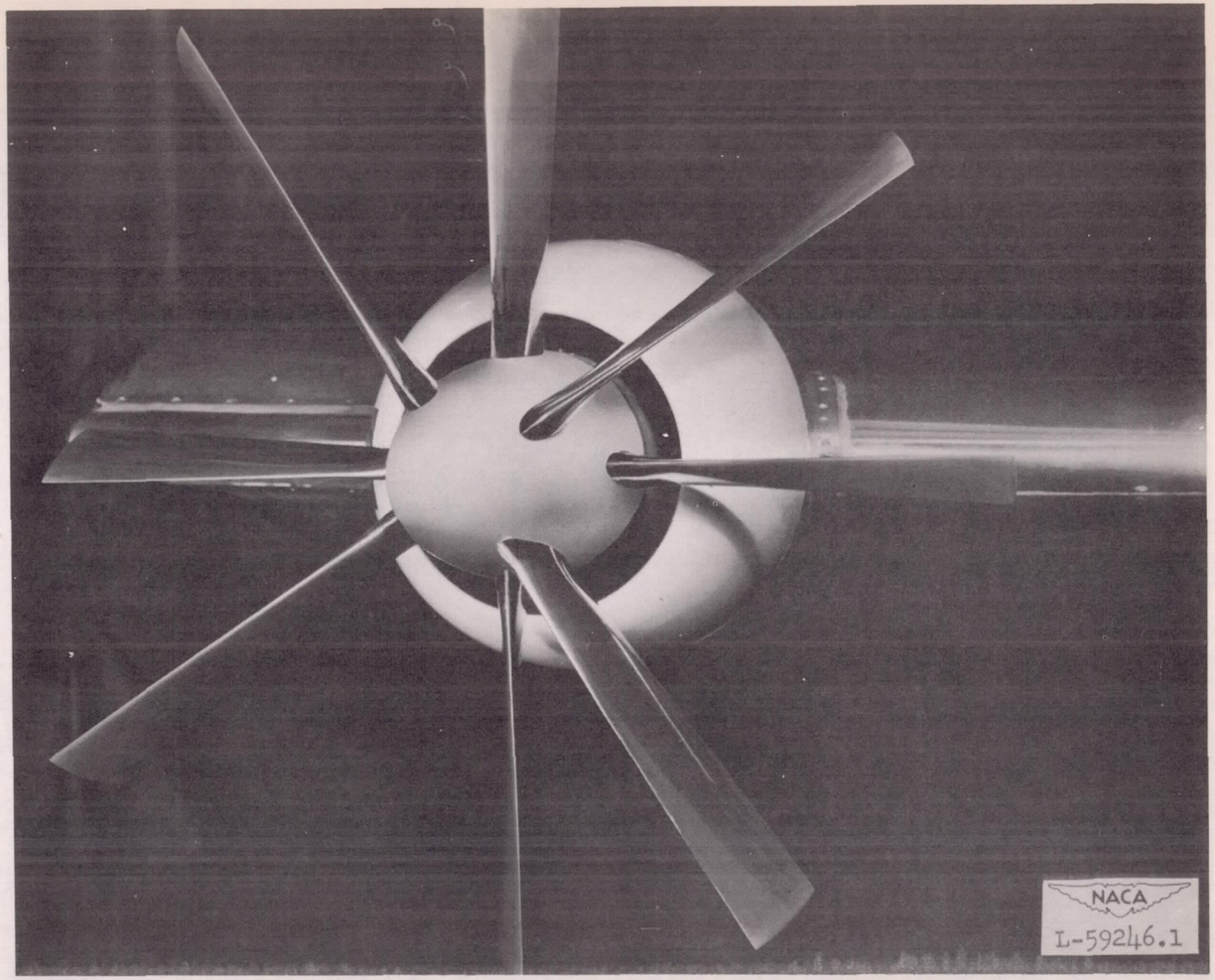

(f) 24-percent-thick shank propeller, ideal juncture, basic cowling-spinner combination.

Figure 2.- Continued.

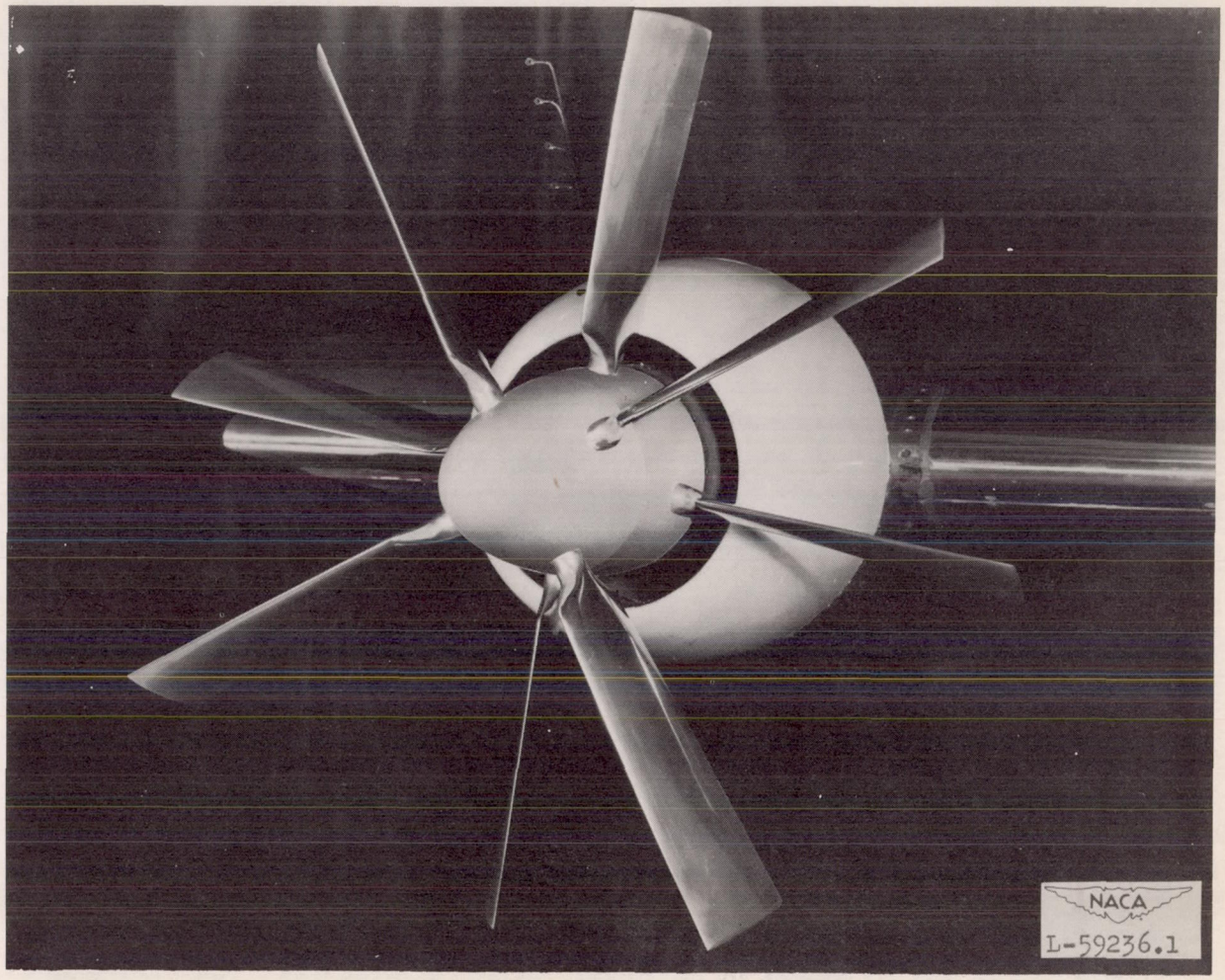

(g) Small round-shank propeller, ideal juncture, basic cowling-spinner combination.

Figure 2.- Continued.

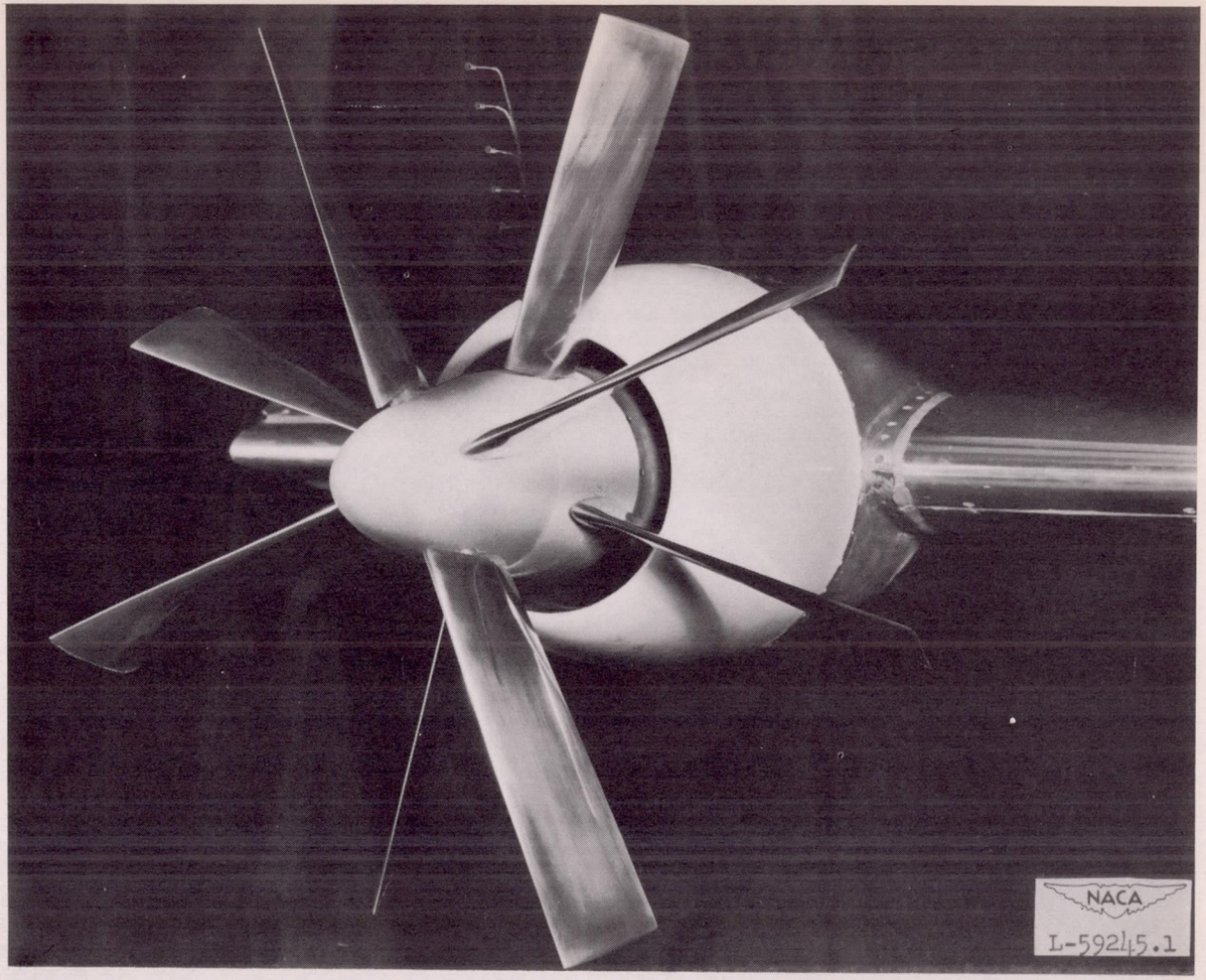

(h) 24-percent-thick shank propeller with minimum clearance gap to allow 120° blade rotation, basic cowling-spinner combination.

Figure 2.- Continued.

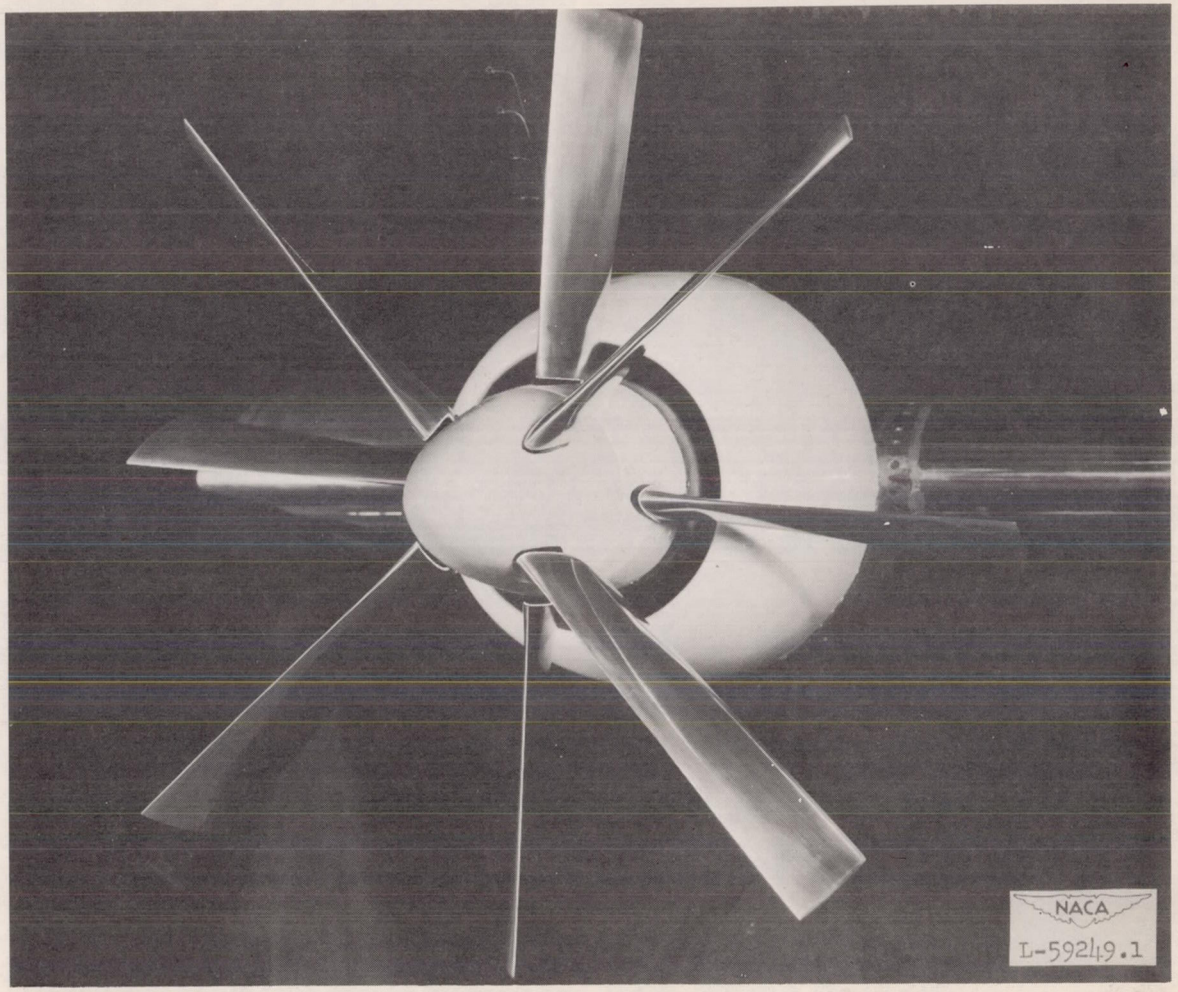

(i) 24-percent-thick shank propeller with low airfoil-land juncture, basic cowling-spinner combination.

Figure 2.- Continued.

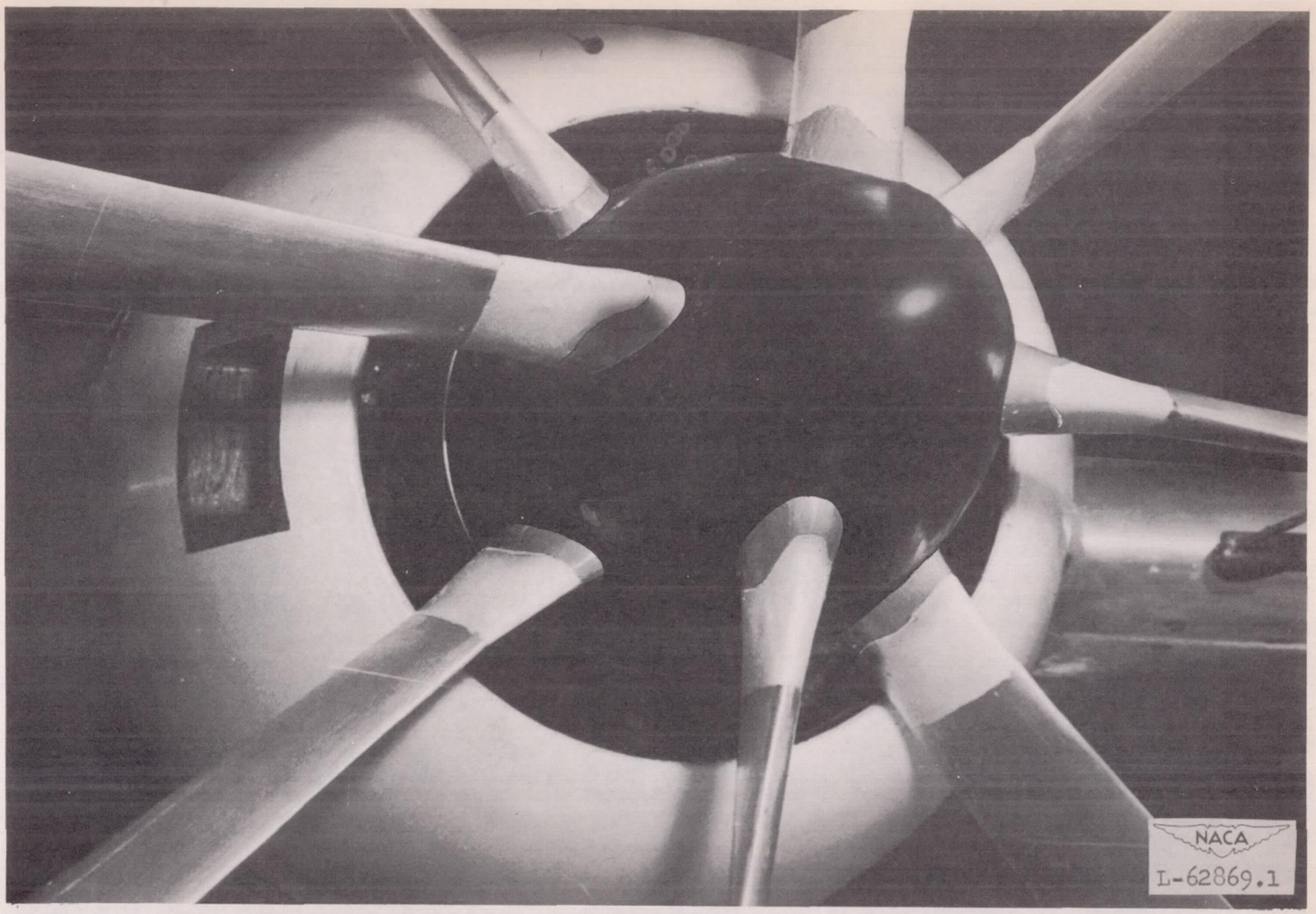

(j) 24-percent-thick shank propeller with high-land juncture, cruise blade angle, basic cowling-spinner combination.

Figure 2.- Continued.

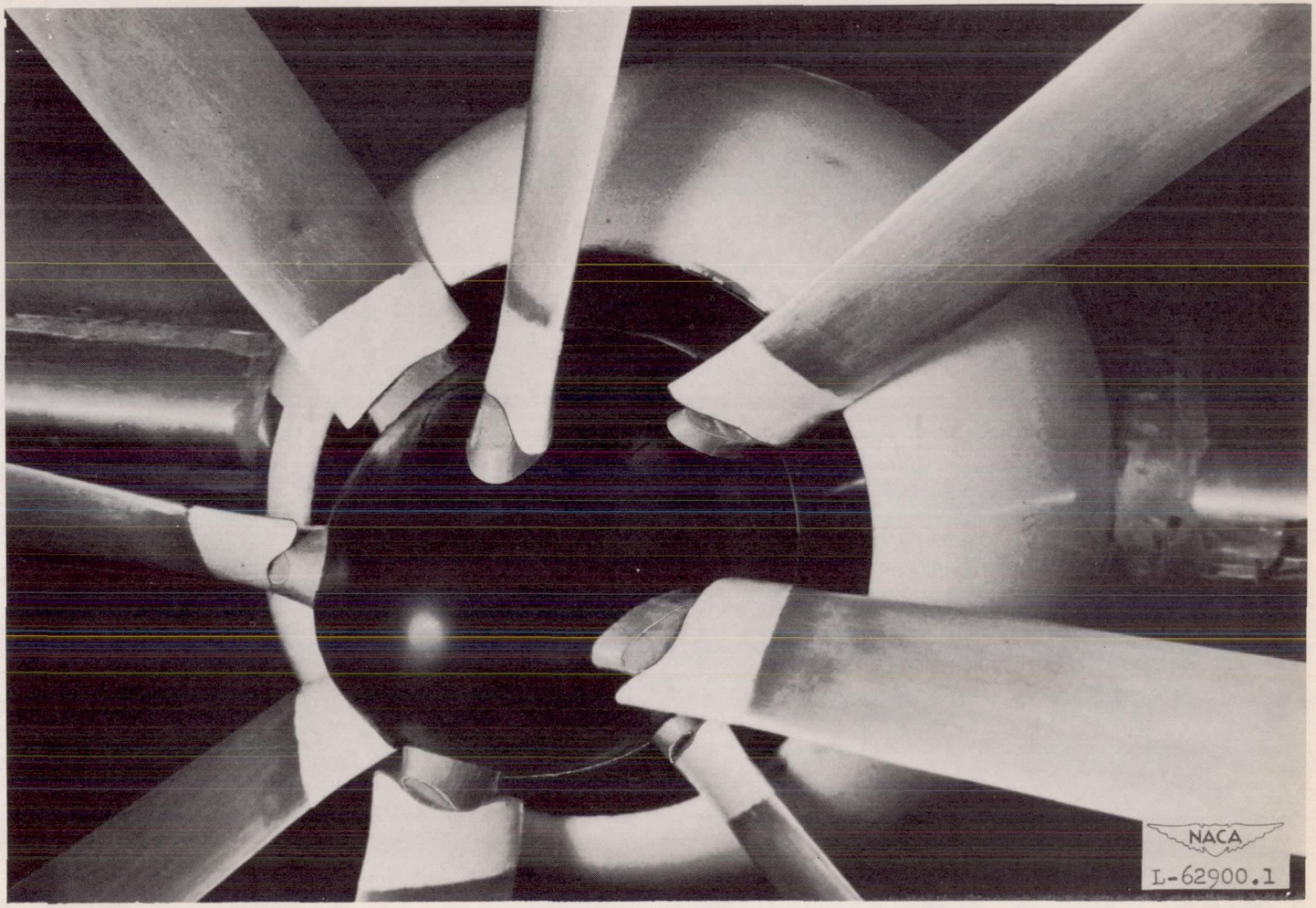

(k) 24-percent-thick shank propeller with high-land juncture, climb blade angle, basic cowling-spinner combination.

Figure 2.- Continued.

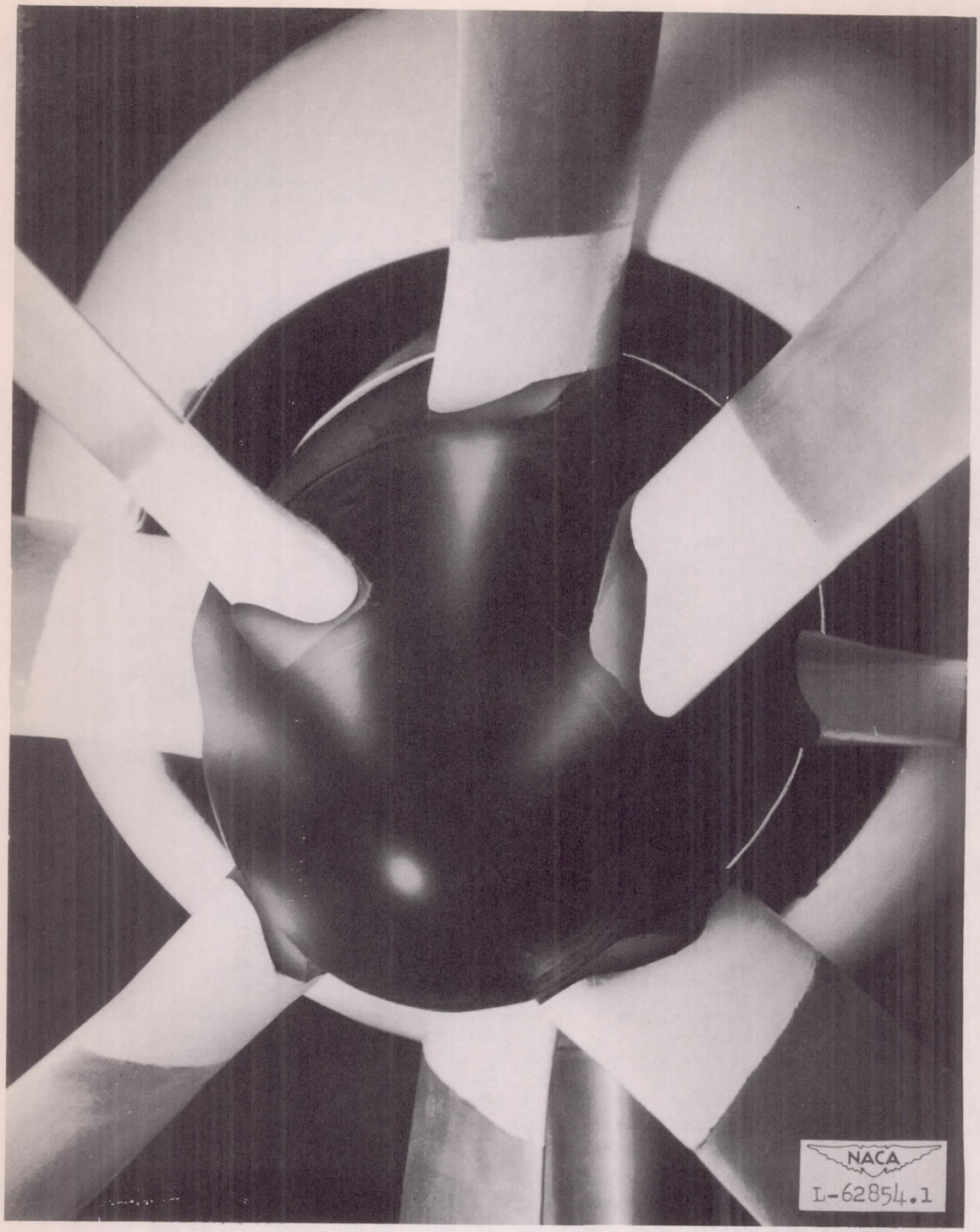

(*l*) 24-percent-thick shank propeller with land designed to cover base for 20° blade-angle change, climb blade angle.

Figure 2.- Concluded.

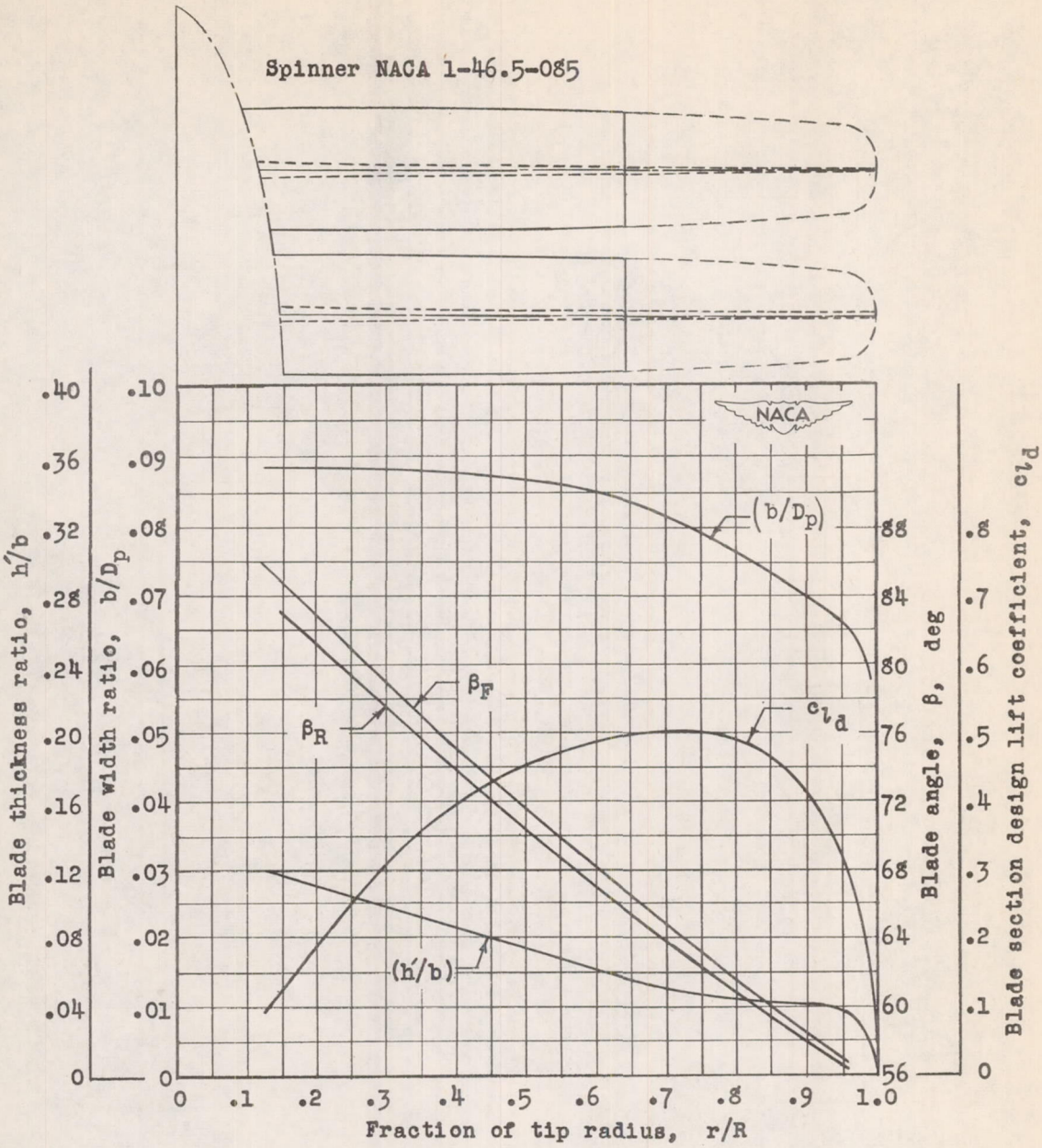

(a) Airfoil shank; 12 percent thick.

Figure 3.- Plan-form and blade-form curves for the 16-series, eight-blade, NACA 3.09-(5)(0.050)-04 dual-rotation propeller. Test propeller cut off at $\frac{r}{R} = 0.644$.

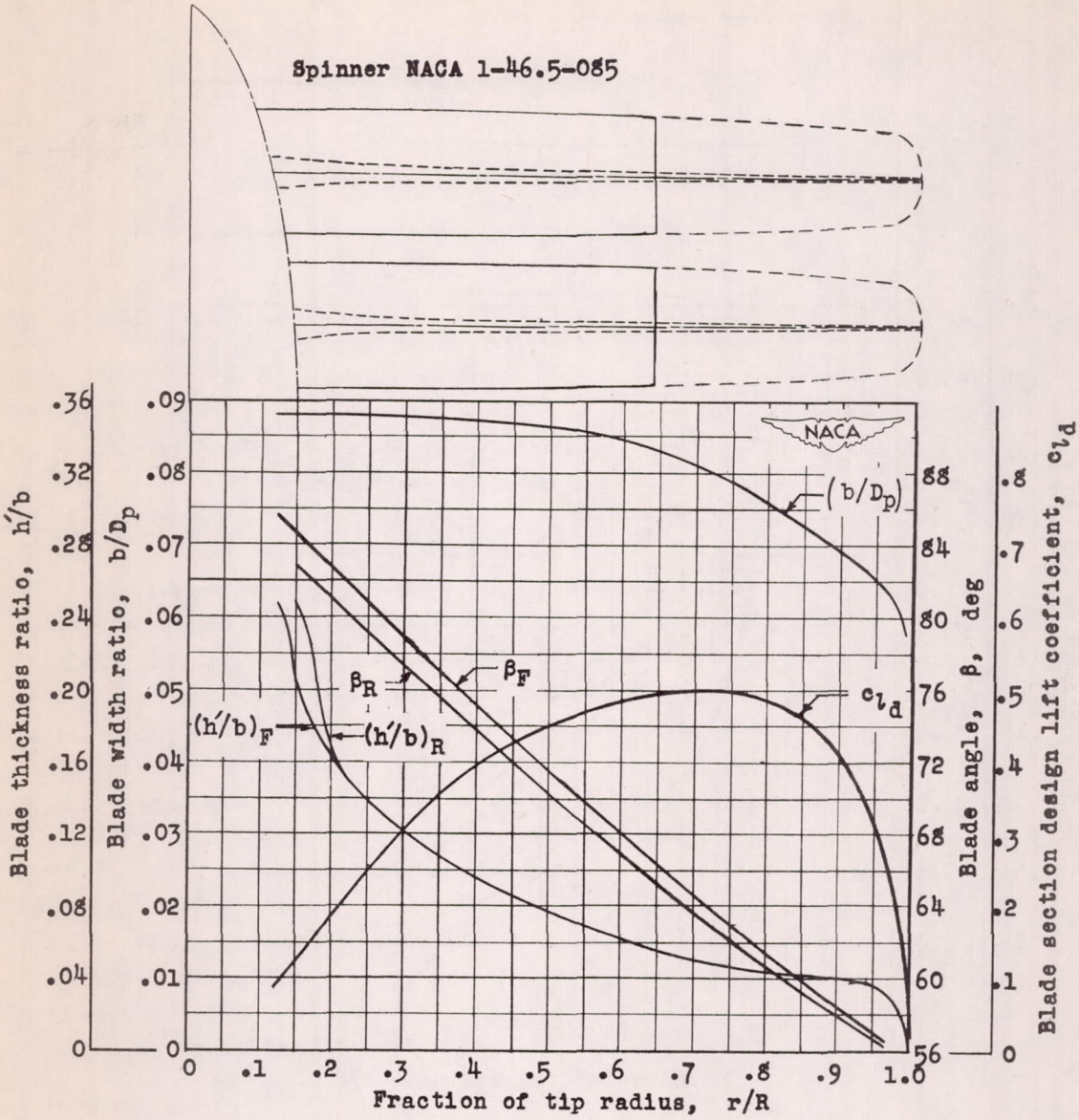

(b) Airfoil shank; 24 percent thick.

Figure 3.- Continued.

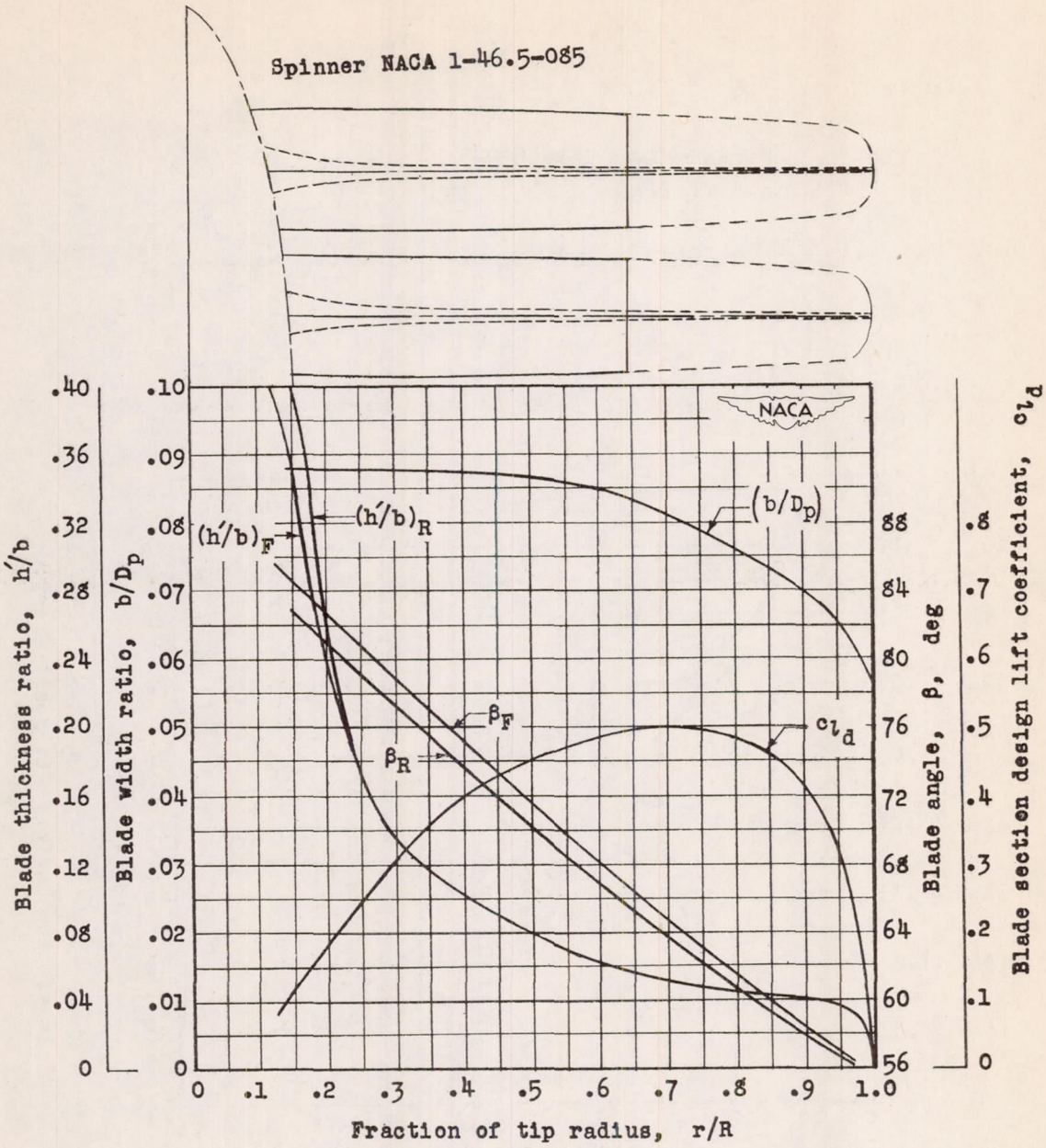

(c) Airfoil shank; 40 percent thick.

Figure 3.- Continued.

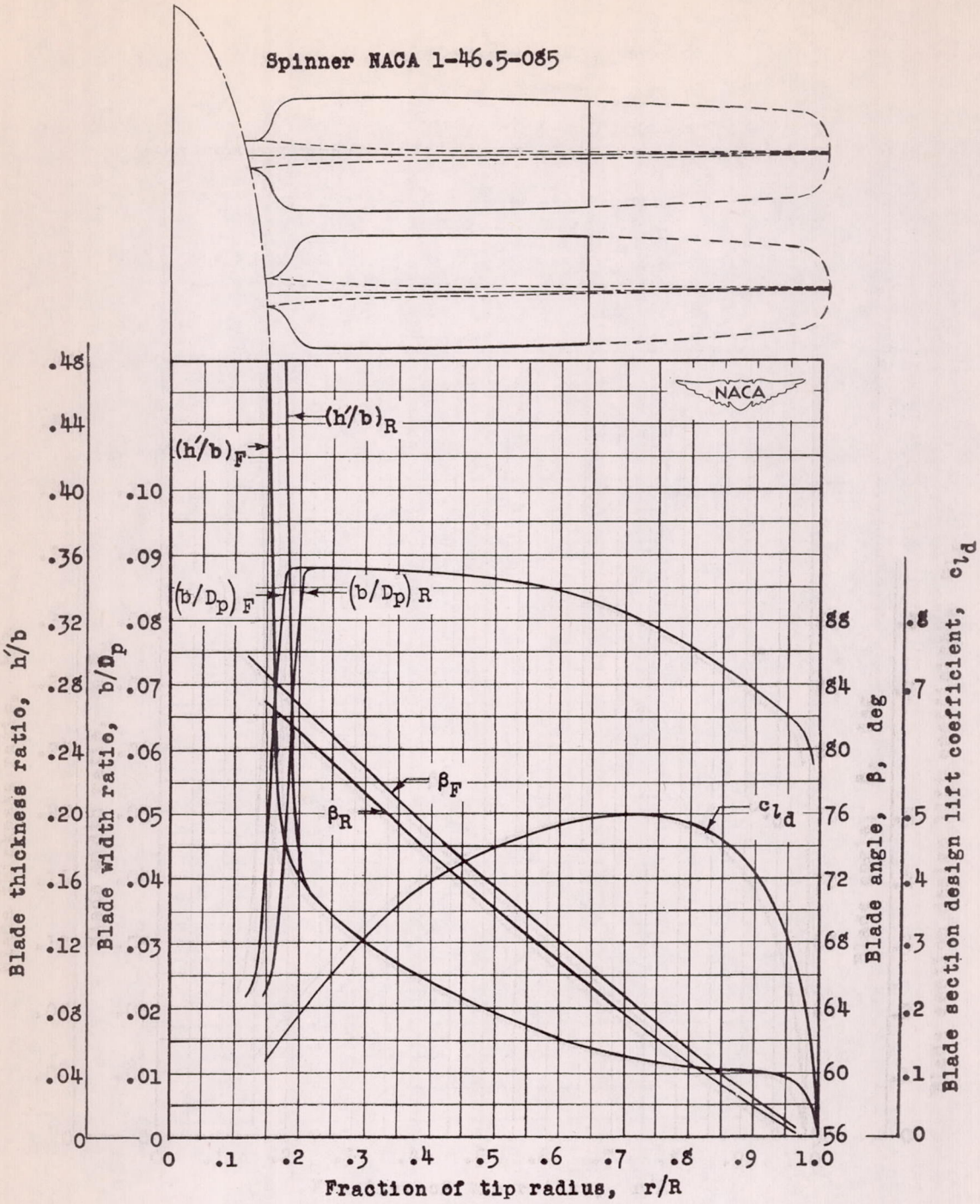

(d) Round shank; small.

Figure 3.- Continued.

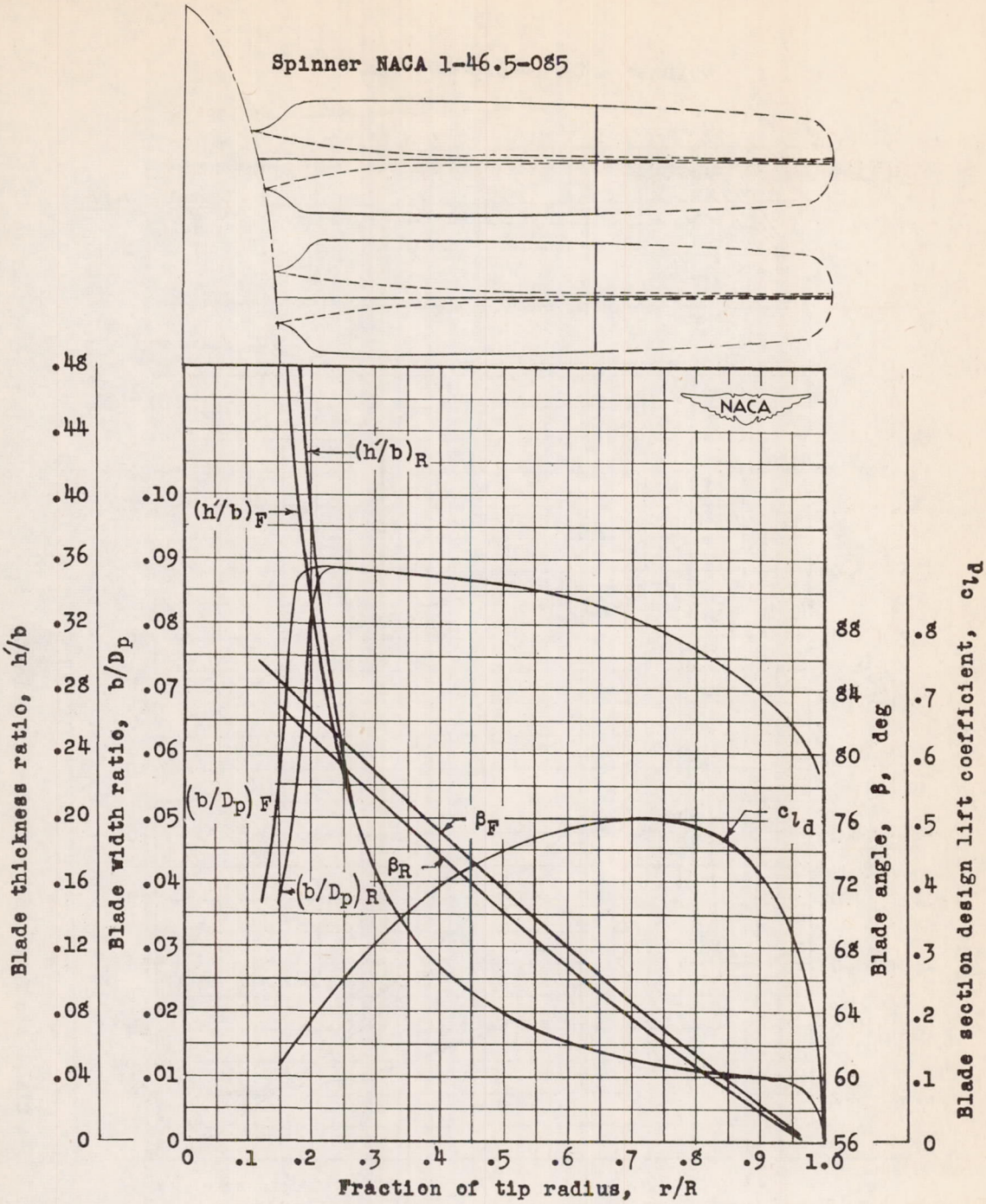

(e) Round shank; large.

Figure 3.- Concluded.

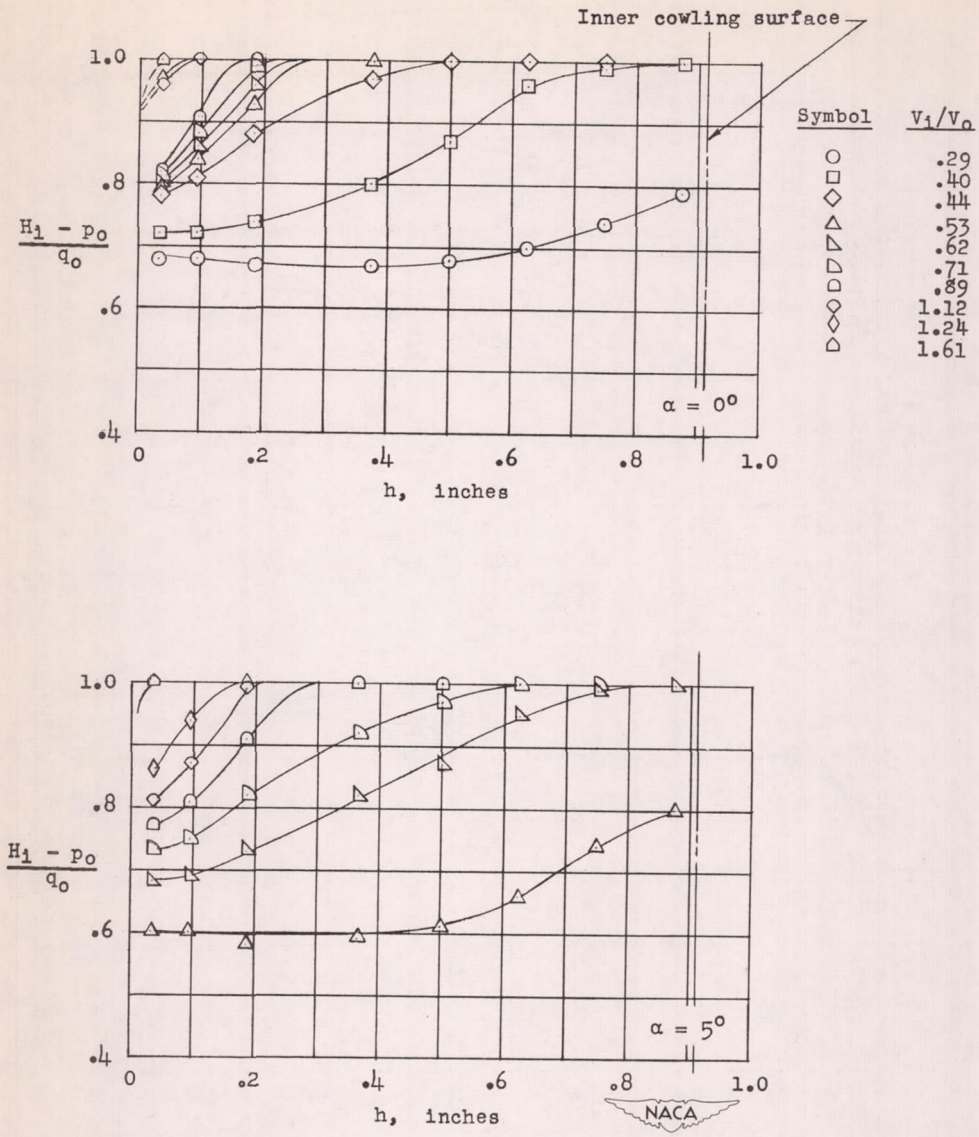

(a) Inlet.

Figure 4.- Total-pressure distribution at inlet and diffuser measuring stations, propeller removed.

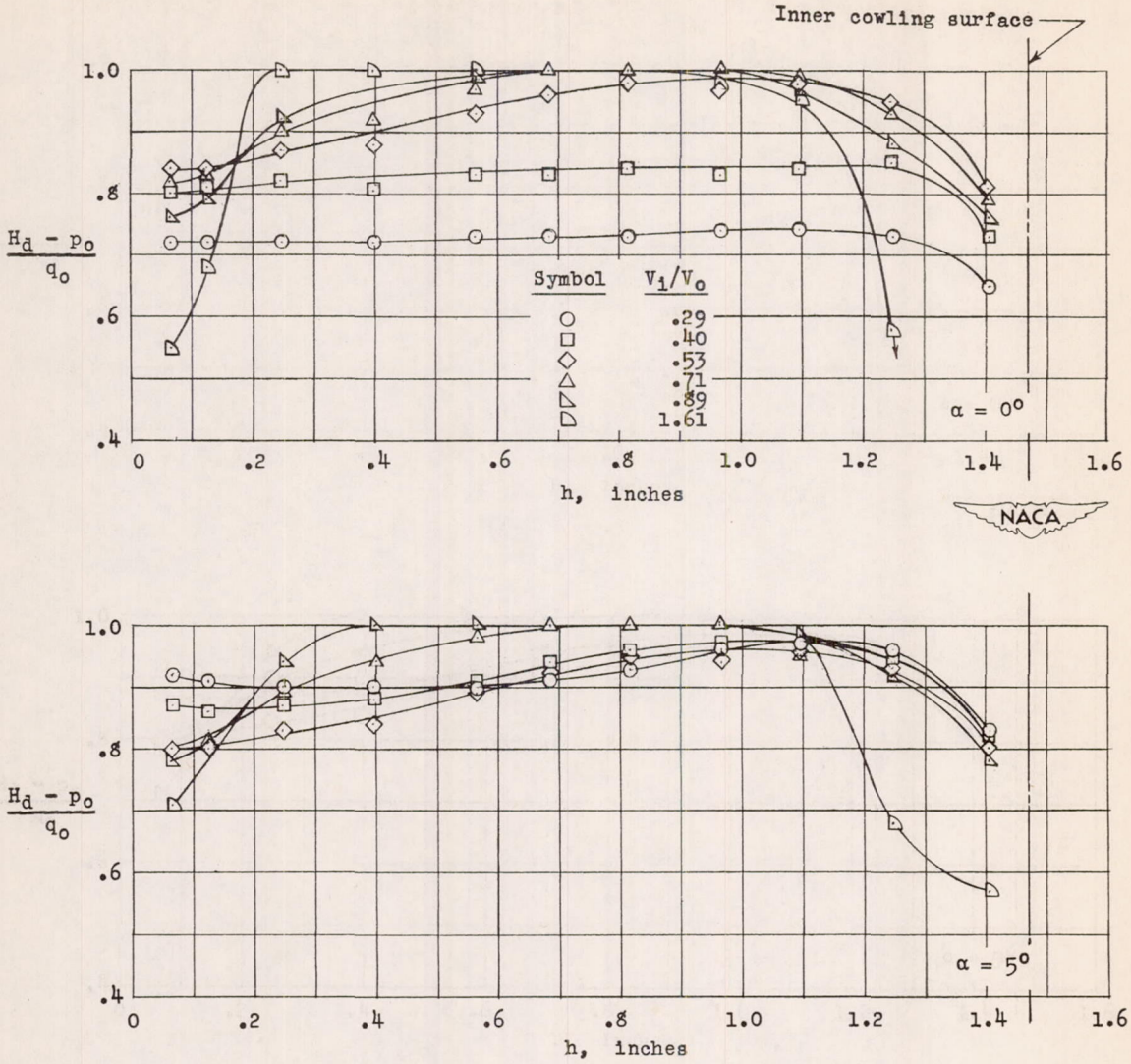

(b) Diffuser.

Figure 4.- Concluded.

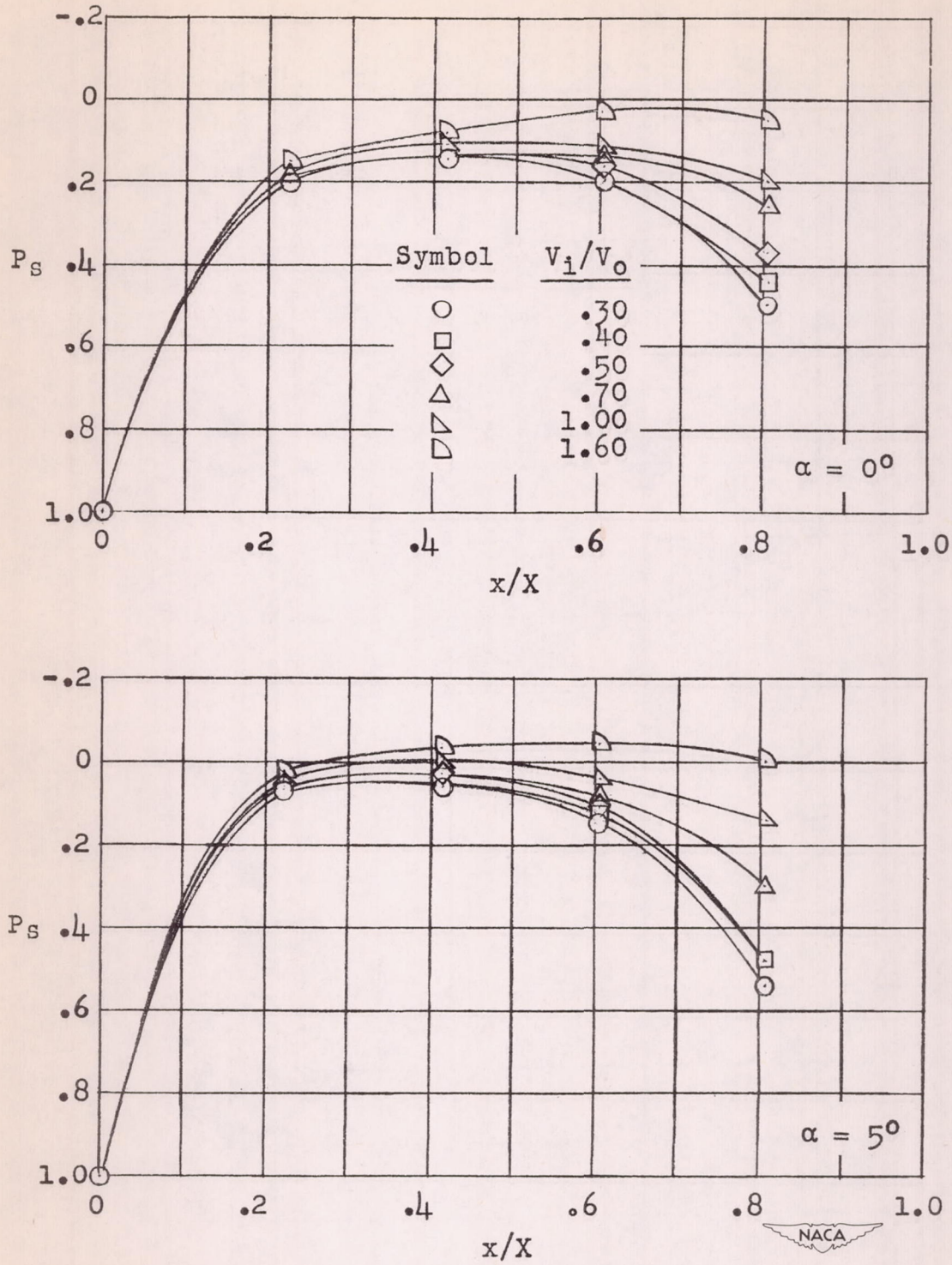

Figure 5.- Static-pressure distribution over top of basic spinner, propeller removed.

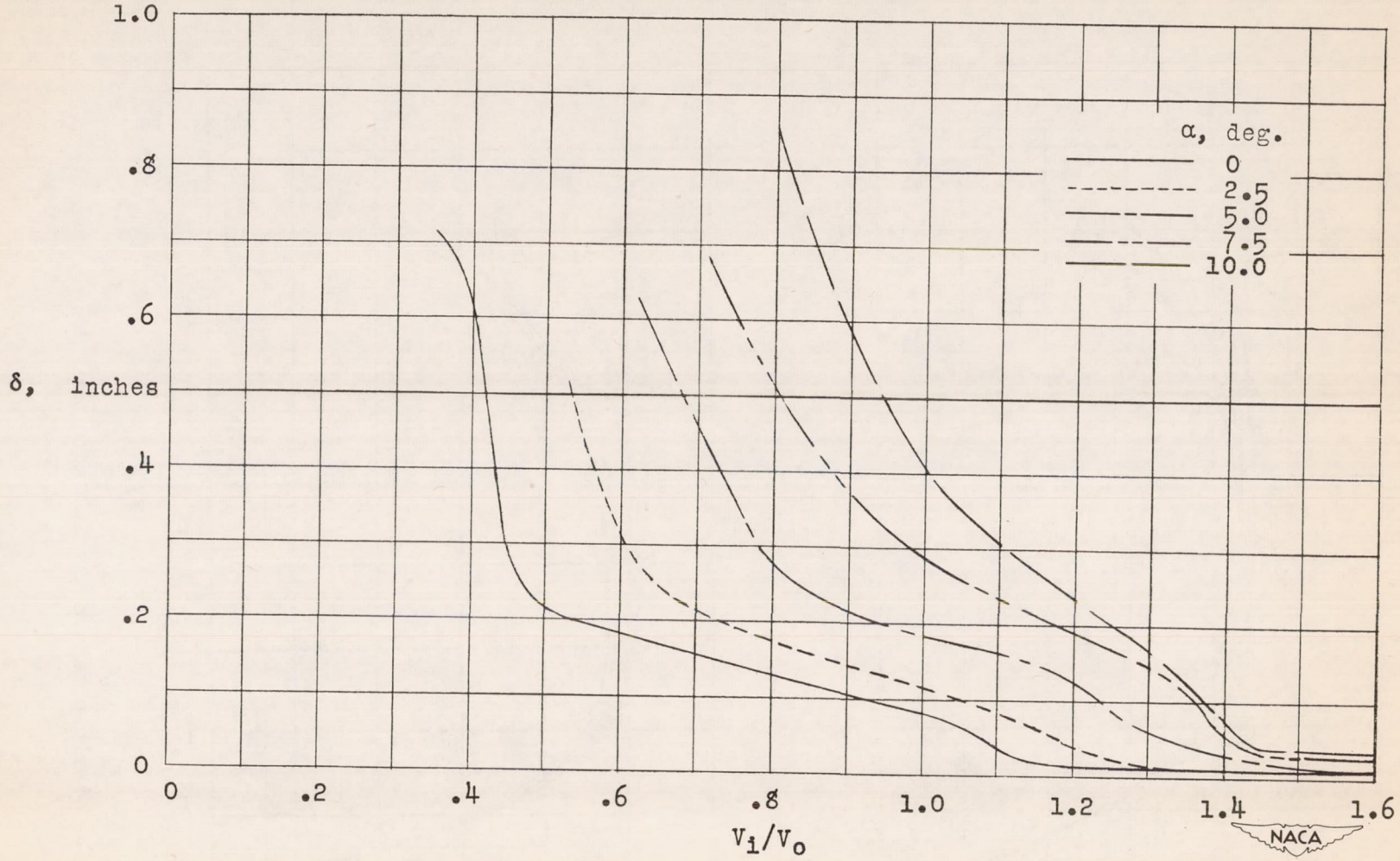

Figure 6.- Effect of inlet-velocity ratio and angle of attack on spinner boundary-layer thickness at top of inlet, propeller removed.

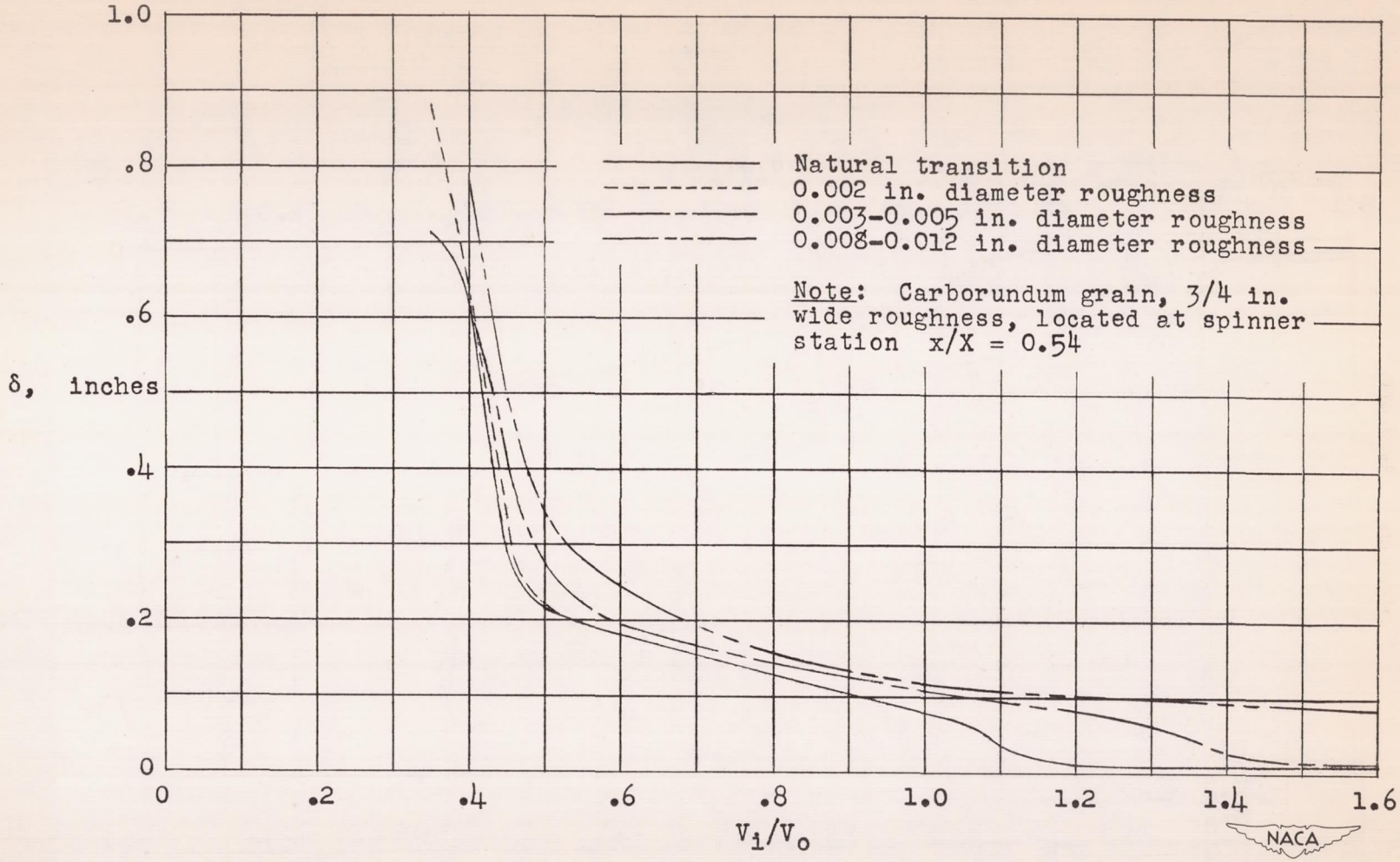

Figure 7.- Effect of roughness on spinner boundary-layer thickness at top of inlet, propeller removed; $\alpha = 0^{\circ}$.

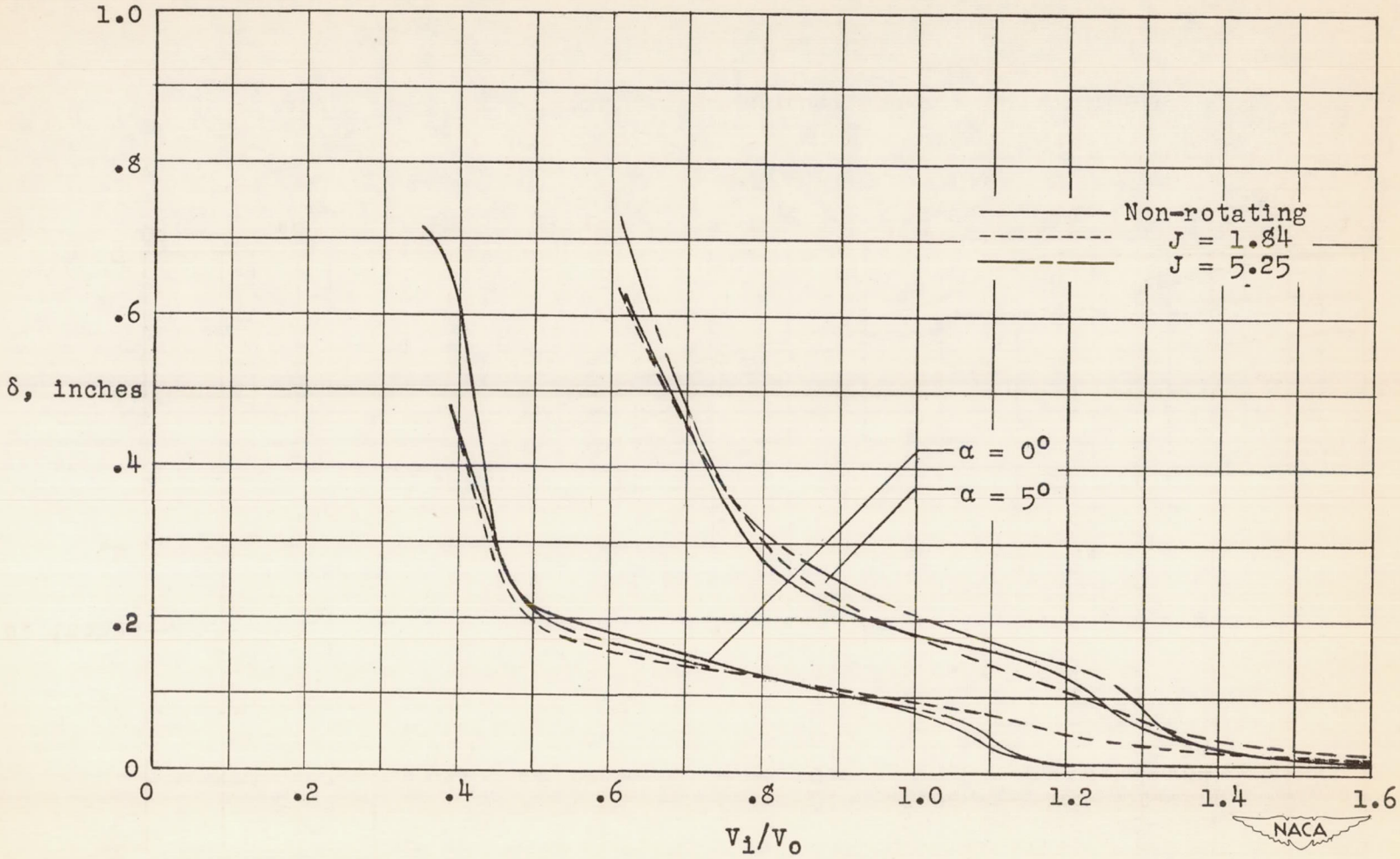

(a) Single-rotation spinner.

Figure 8.- Effect of spinner rotation on boundary-layer thickness at top of inlet, propeller removed.

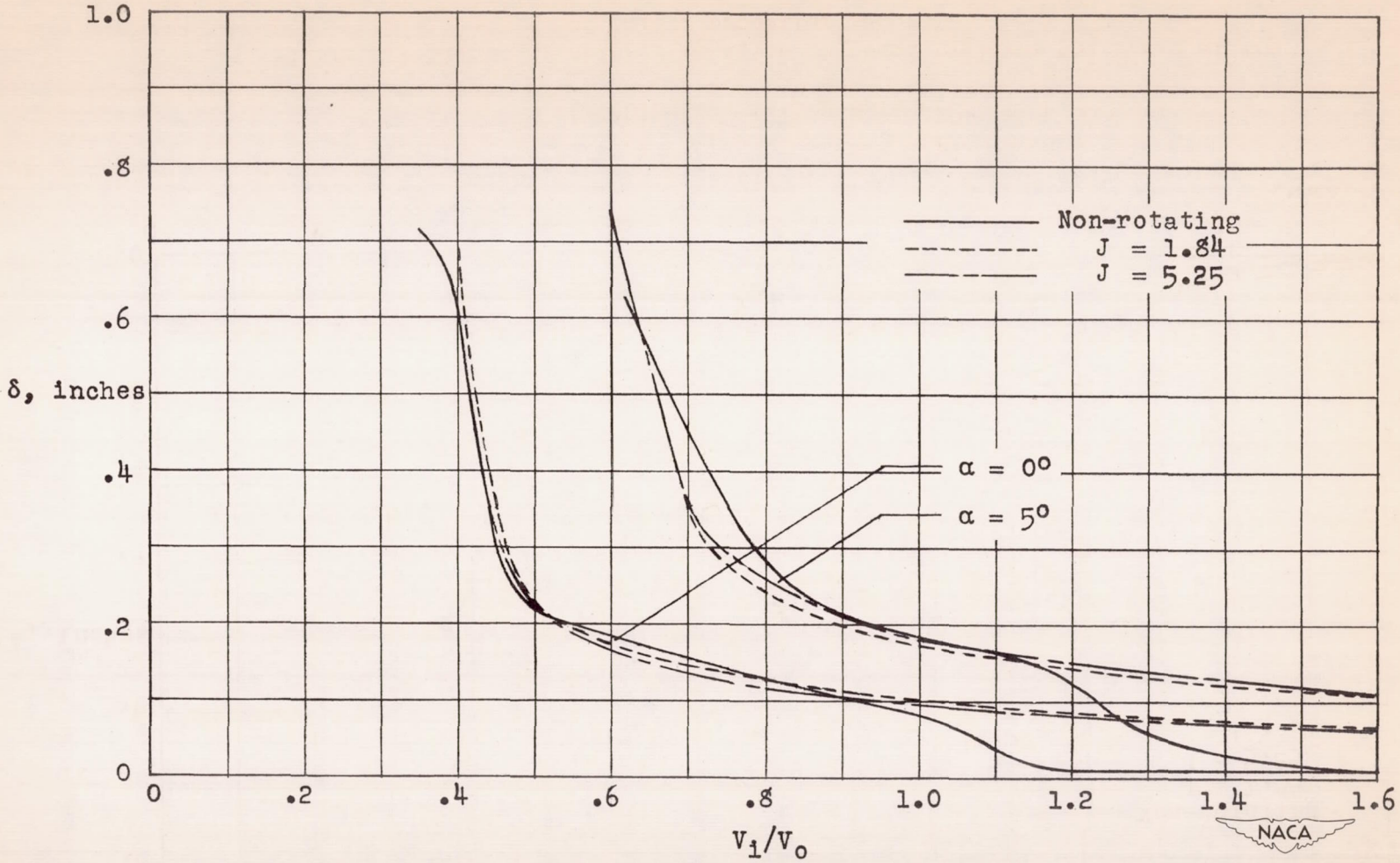

(b) Dual-rotation spinner.

Figure 8.- Concluded.

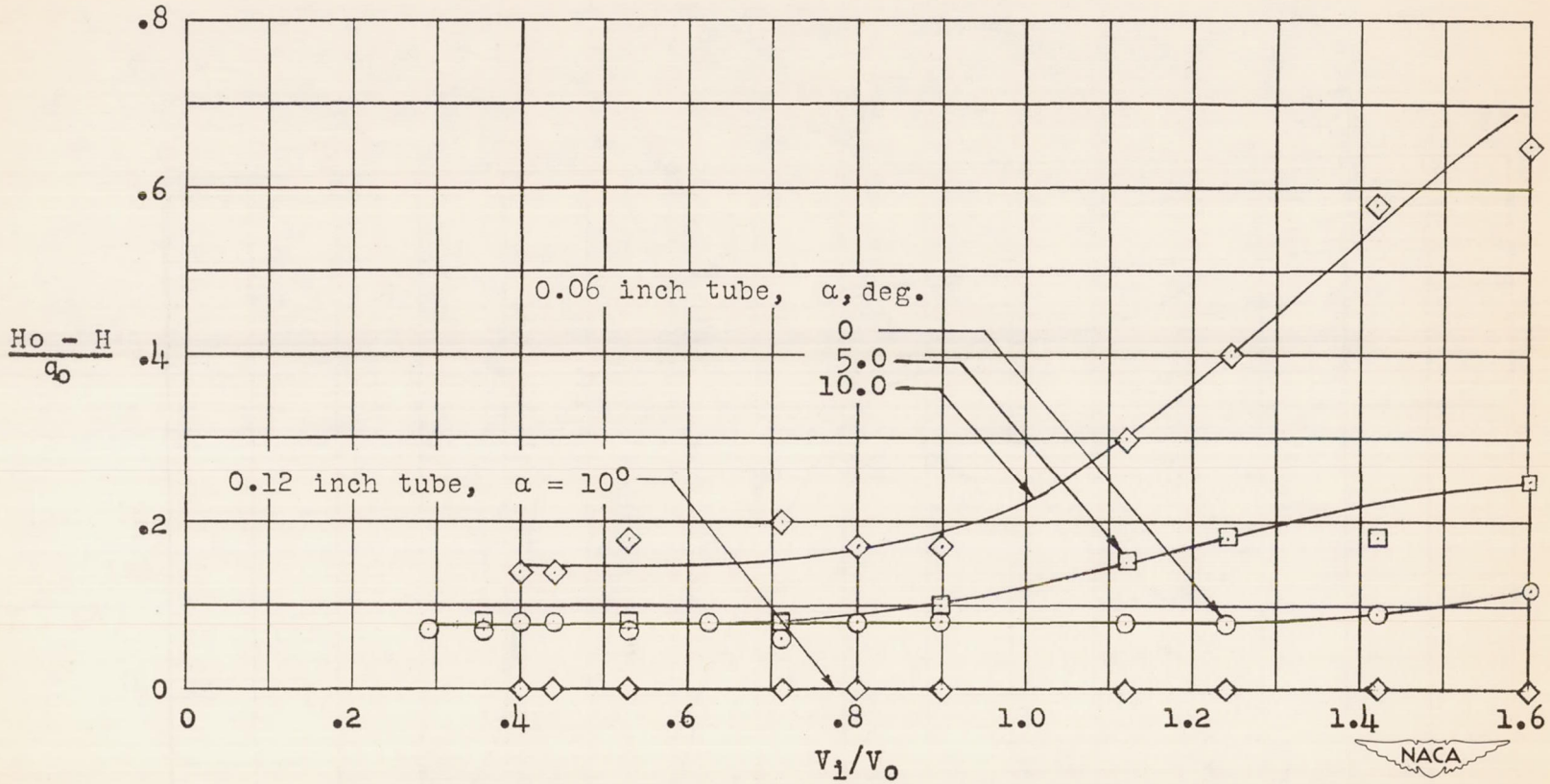

Figure 9.- Effect of inlet-velocity ratio on total-pressure loss coefficient measured by reference tubes 0.06 inch and 0.12 inch from lower inner cowling surface at inlet measuring station, propeller removed.

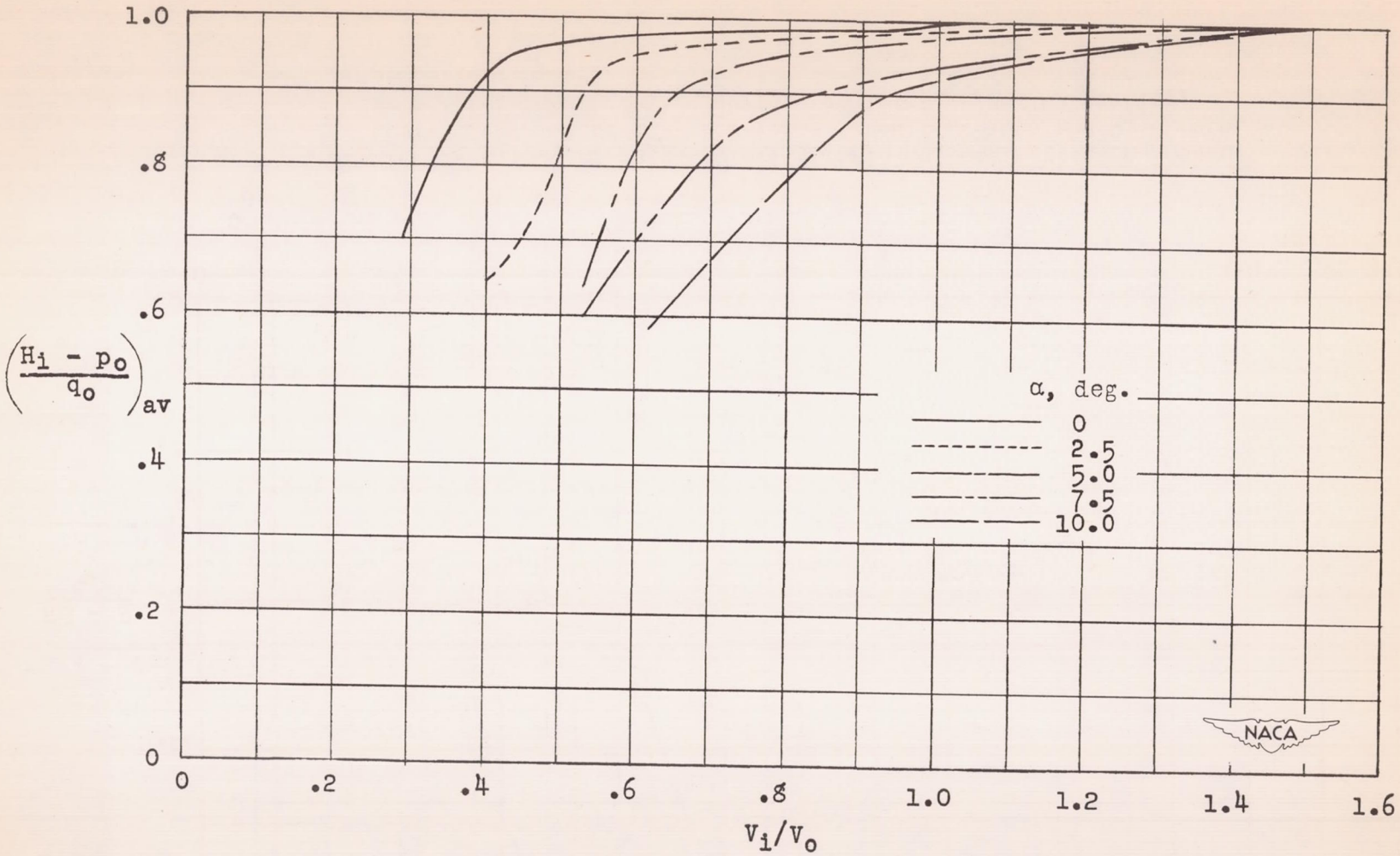

Figure 10.- Effect of inlet-velocity ratio and angle of attack on the average total pressure coefficient at top of inlet, propeller removed.

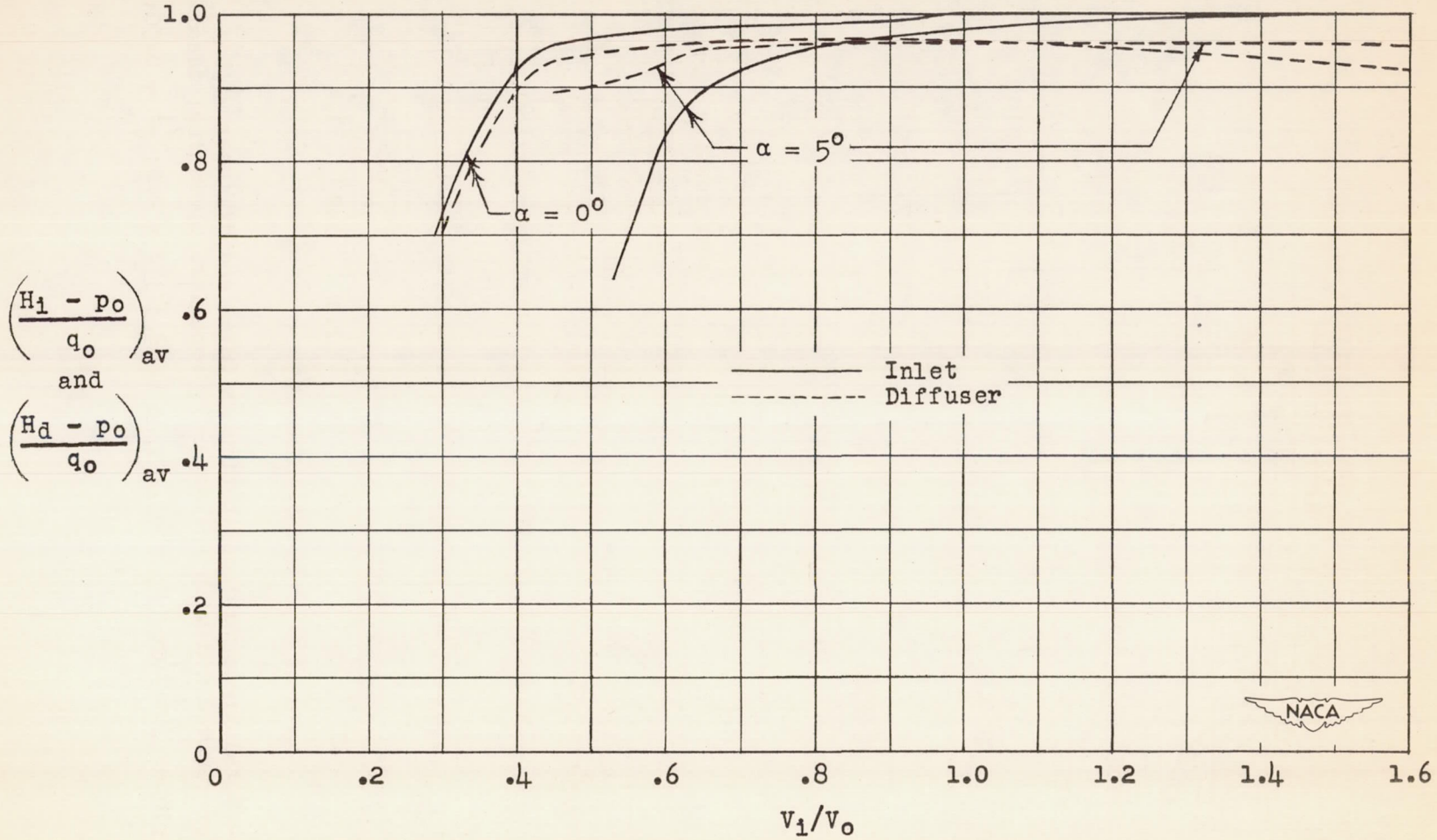

Figure 11.- Comparison of average total pressure coefficient at top of inlet and diffuser, propeller removed.

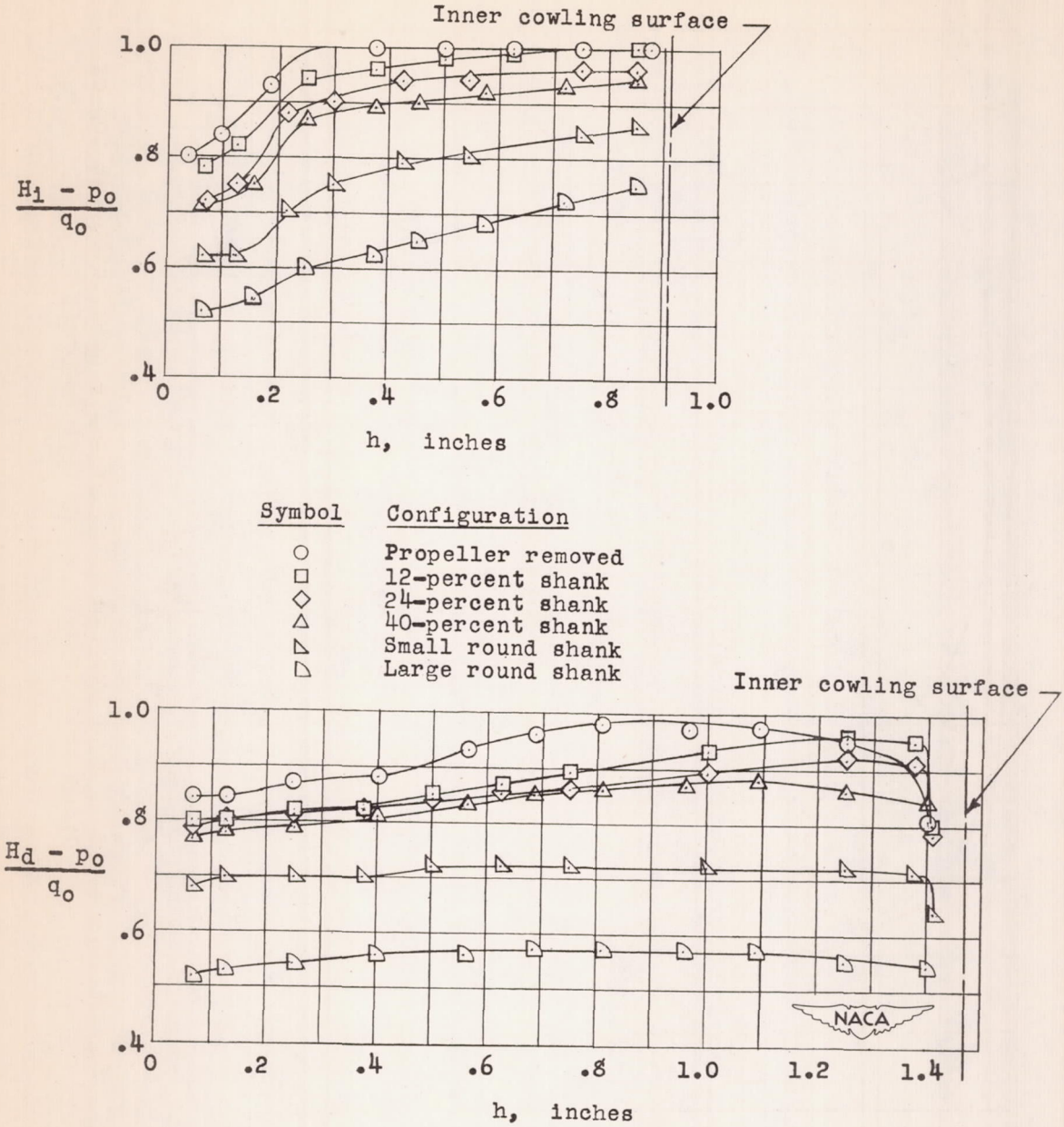

Figure 12.- Total pressure distribution at inlet and diffuser with propeller removed and with the several propellers operating; ideal shank-spinner juncture; $\beta_F = 63.1^\circ$; $\beta_R = 62.3^\circ$; $J = 4.2$; $\frac{V_i}{V_o} \approx 0.50$; $\alpha = 0^\circ$.

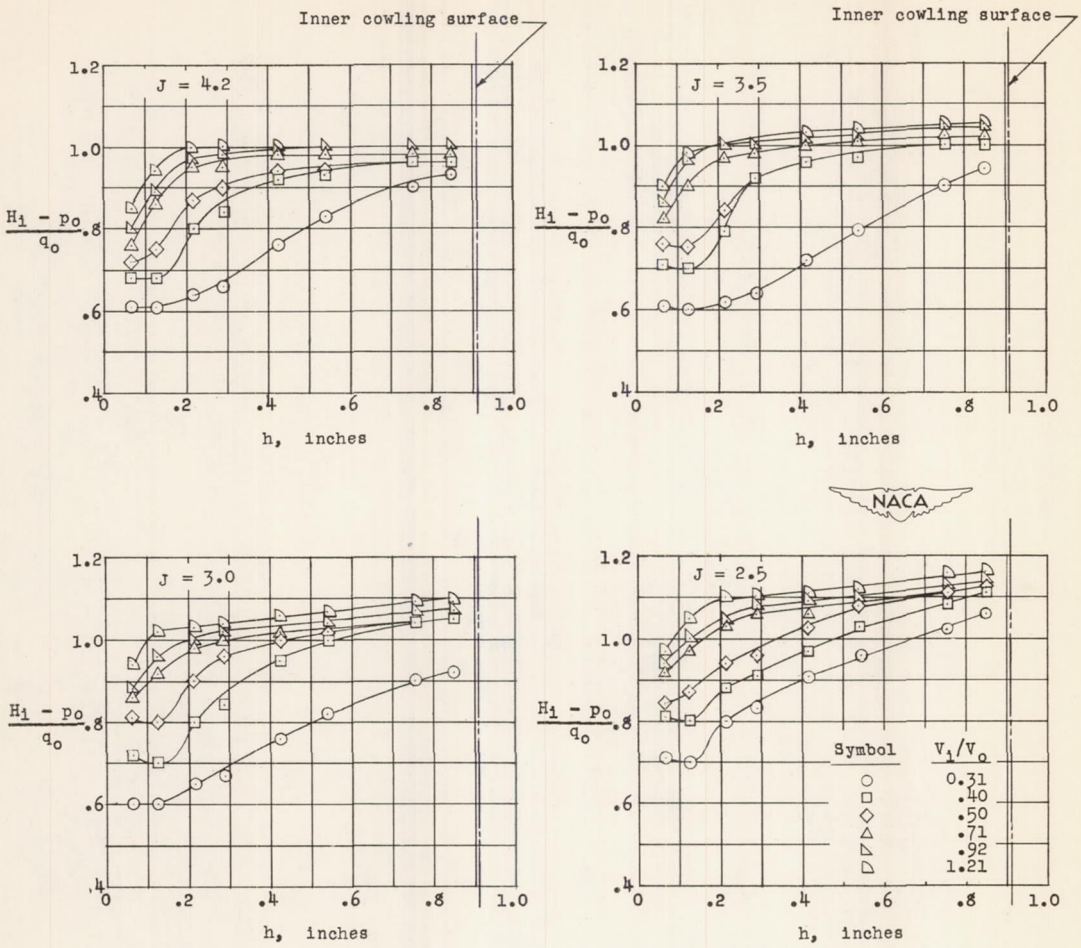

(a) Inlet, $\alpha = 0^{\circ}$.

Figure 13.- Effect of operation of the 24-percent-thick shank propeller on the total pressure distribution at top of the inlet and diffuser; ideal shank-spinner juncture; $\beta_F = 63.1^{\circ}$; $\beta_R = 62.3^{\circ}$.

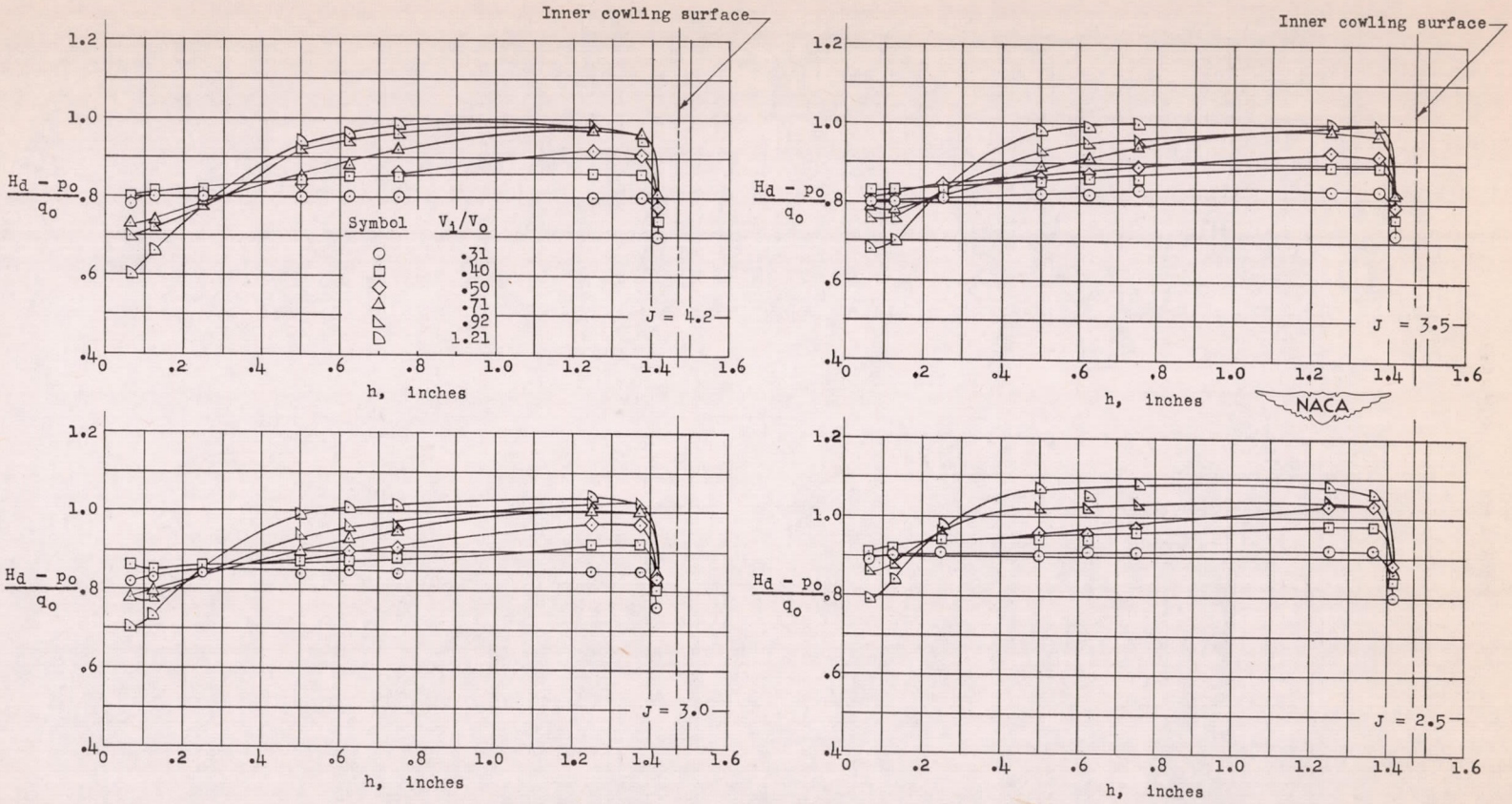

(b) Diffuser, $\alpha = 0^{\circ}$.

Figure 13.- Continued.

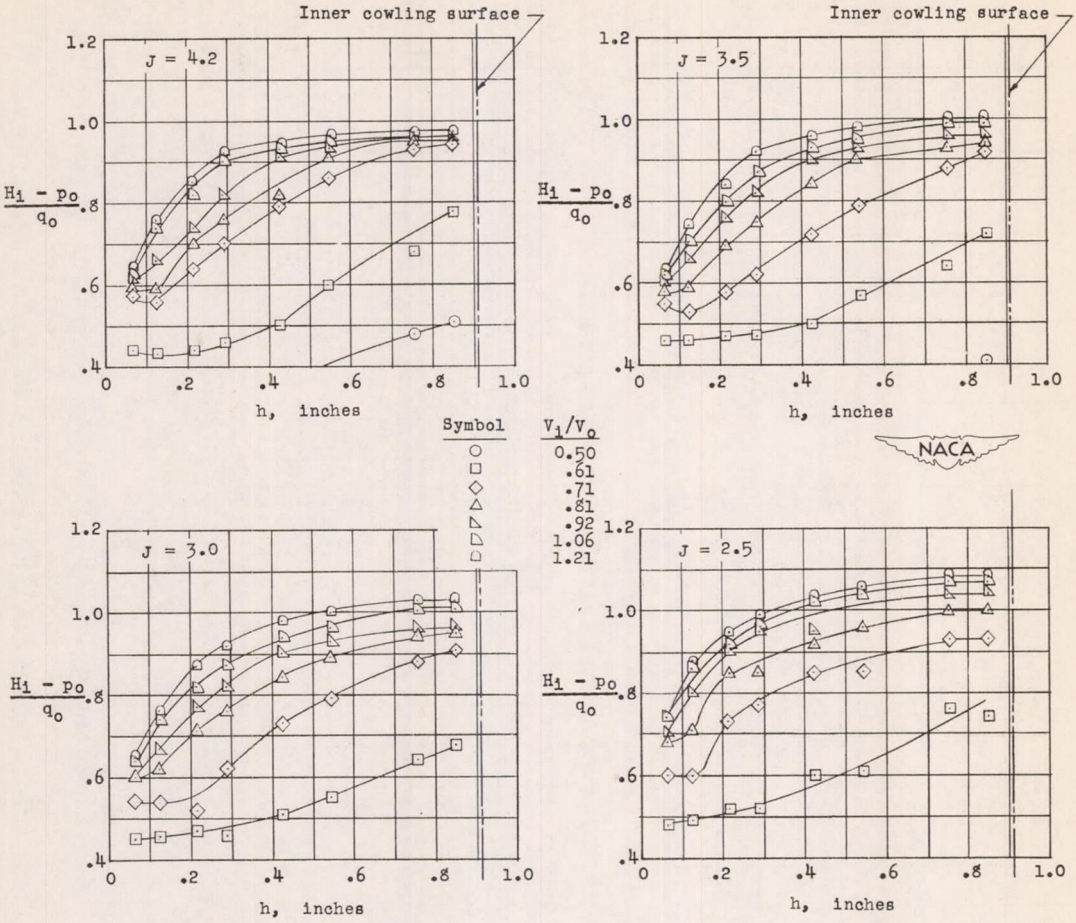

(c) Inlet, $\alpha = 5^{\circ}$.

Figure 13.- Concluded.

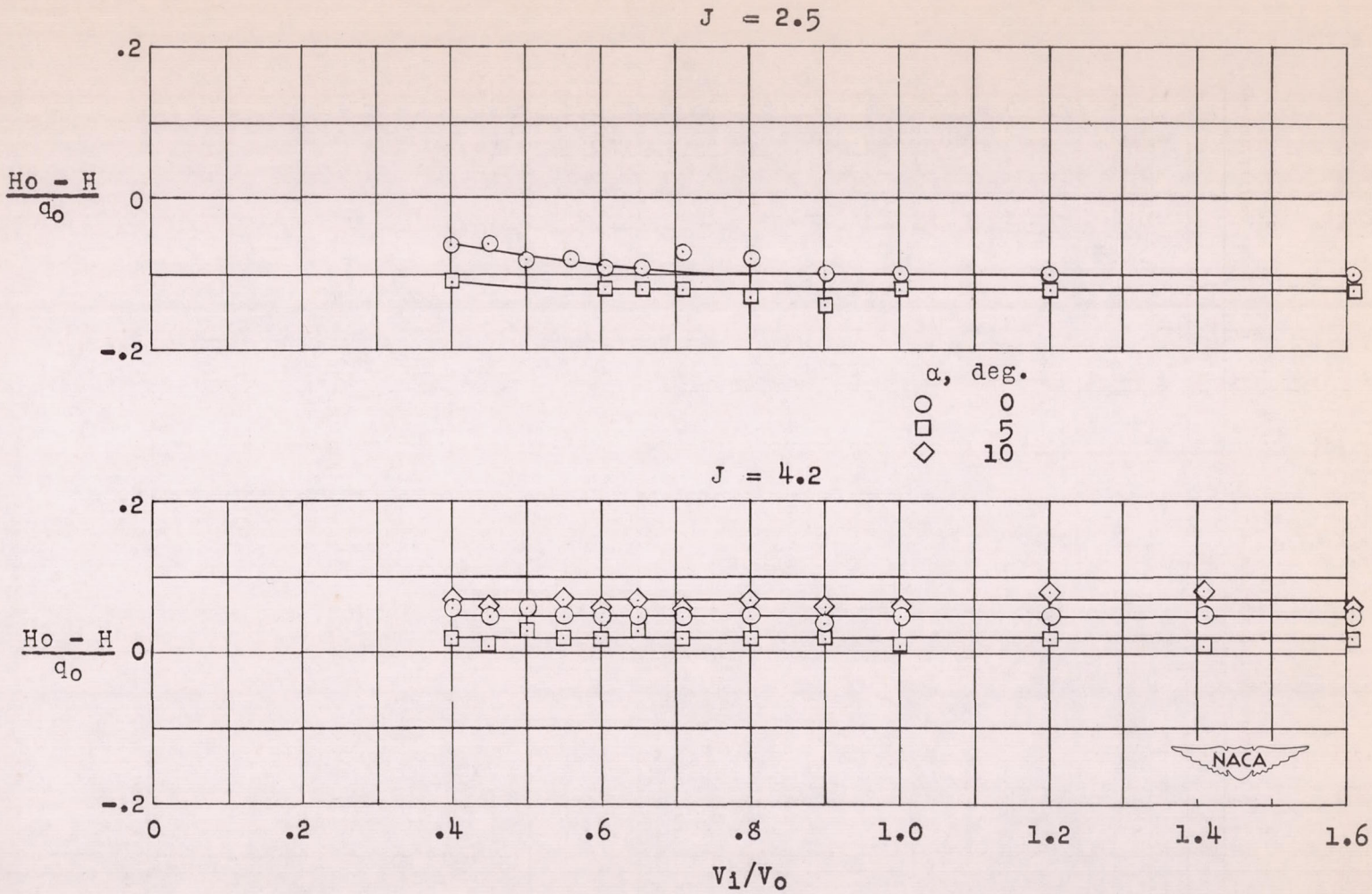

Figure 14.- Effect of inlet-velocity ratio and propeller operation on total-pressure loss coefficient measured by a reference tube 0.06 inch from lower-inner cowling surface at inlet measuring station. 24-percent-thick shank propeller; $\beta_F = 63.1$; $\beta_R = 62.3$.

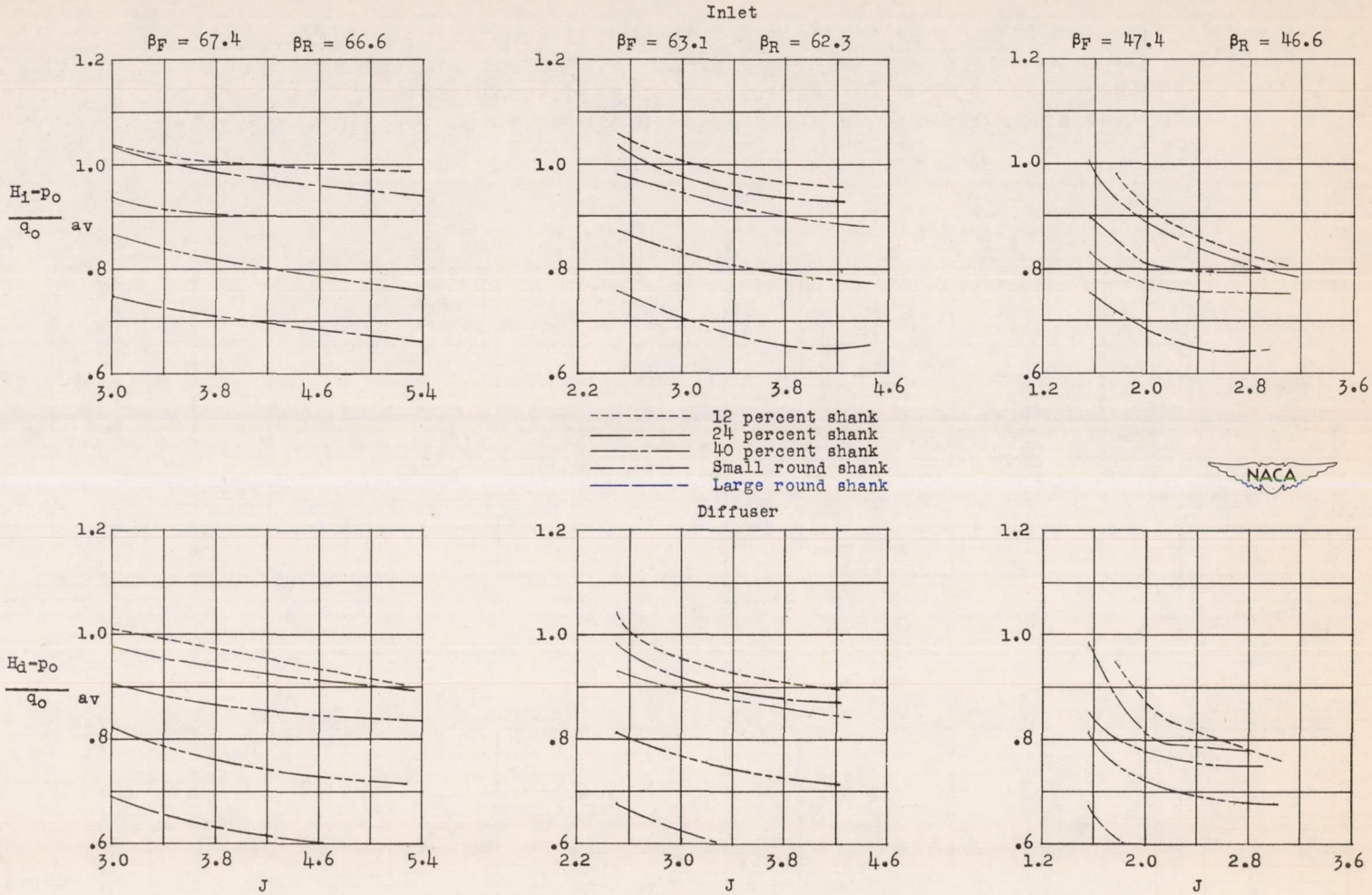

Figure 15.- Effect of variations in blade angle and advance ratio on the average total pressure coefficient at the inlet and diffuser. $\frac{V_i}{V_o} = 0.5$; $\alpha = 0^o$.

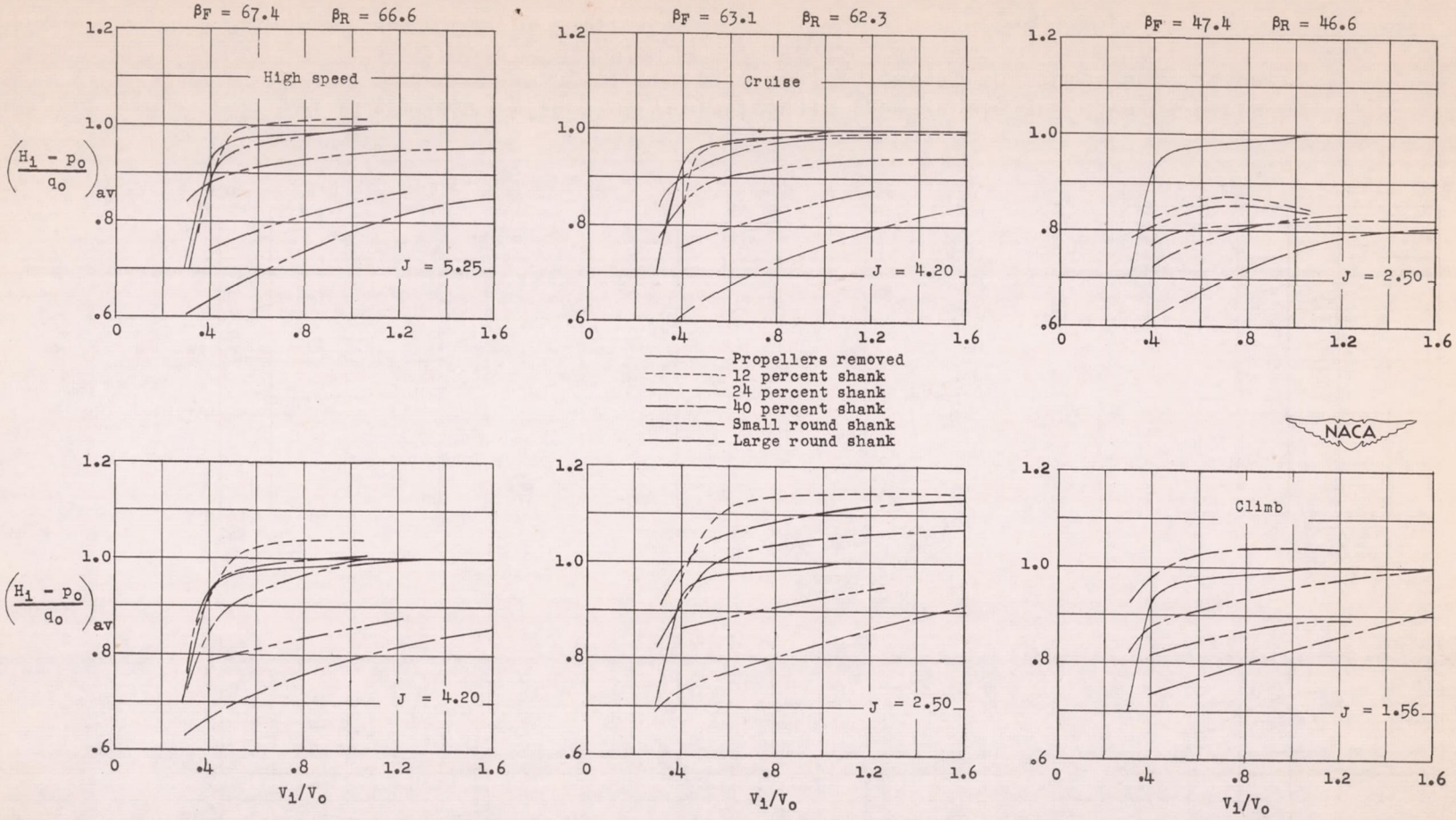

(a) Inlet.

Figure 16.- Average total pressure coefficient at inlet and diffuser as function of inlet-velocity ratio for several blade angles and values of advance ratio, $\alpha = 0^{\circ}$.

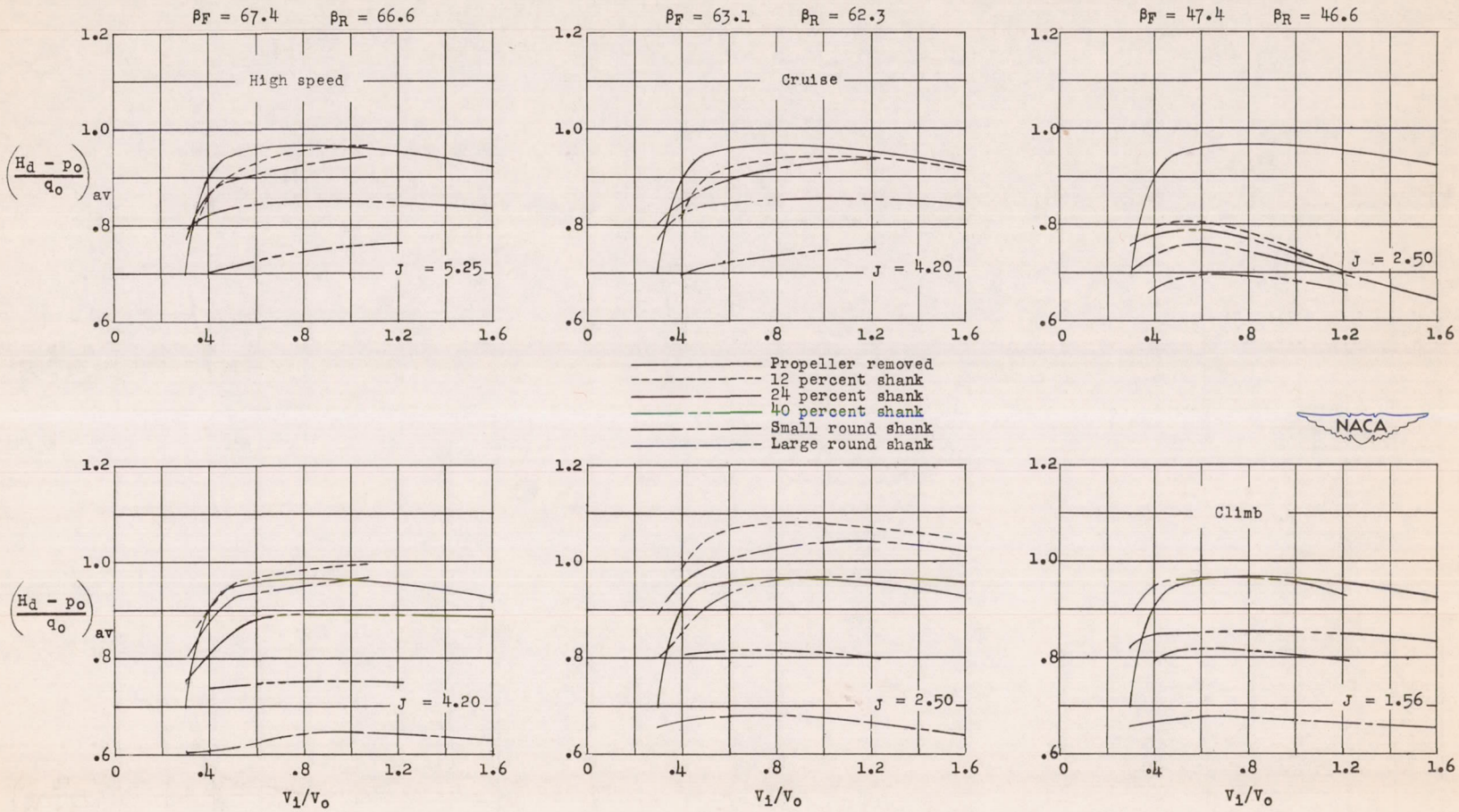

(b) Diffuser.

Figure 16.- Concluded.

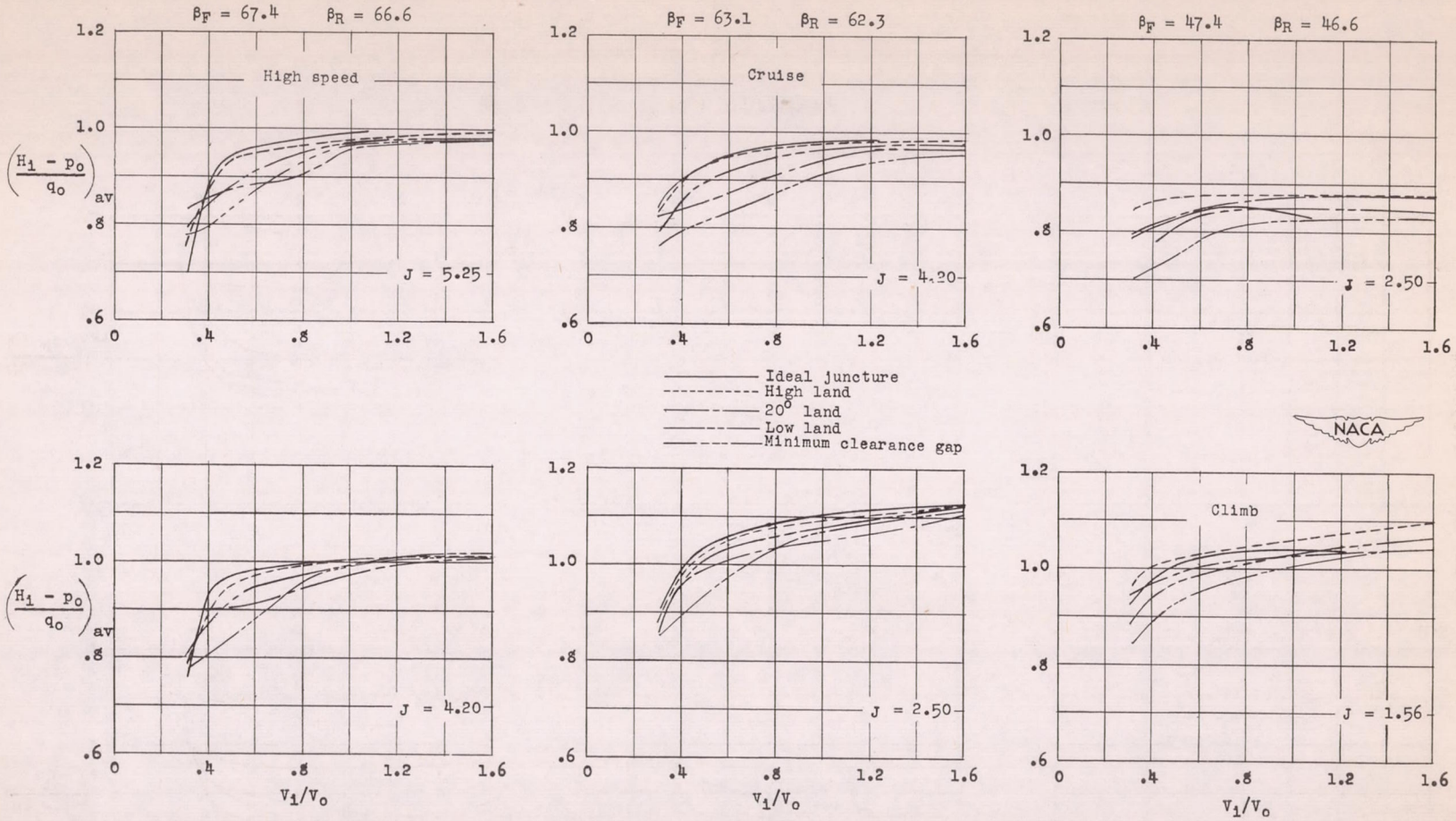

(a) Inlet.

Figure 17.- Comparison of the effect of the various propeller shank-spinner junctures on average total pressure coefficient at the inlet and diffuser. 24-percent-thick shank propeller; $\alpha = 0^{\circ}$.

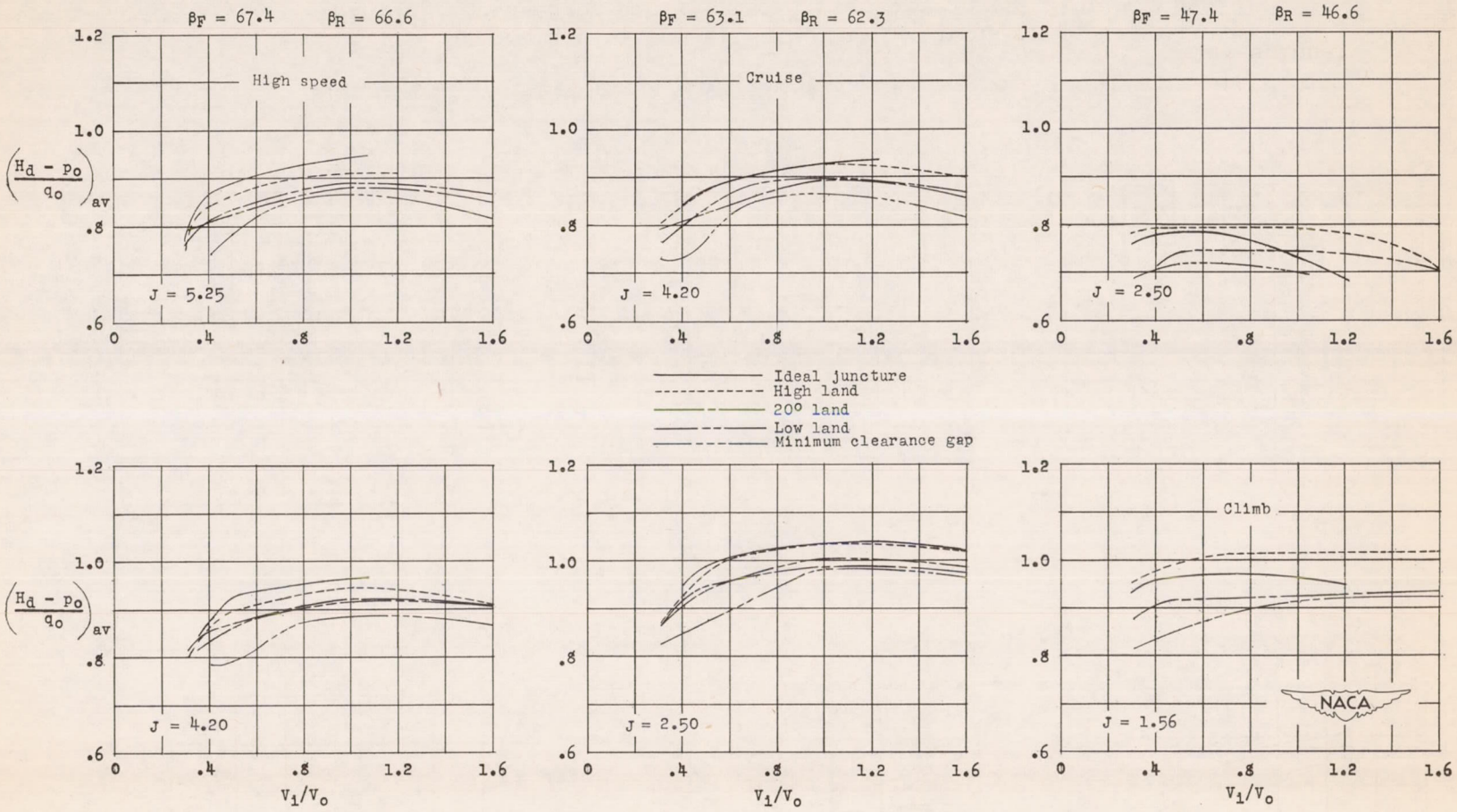

(b) Diffuser.

Figure 17.- Concluded.

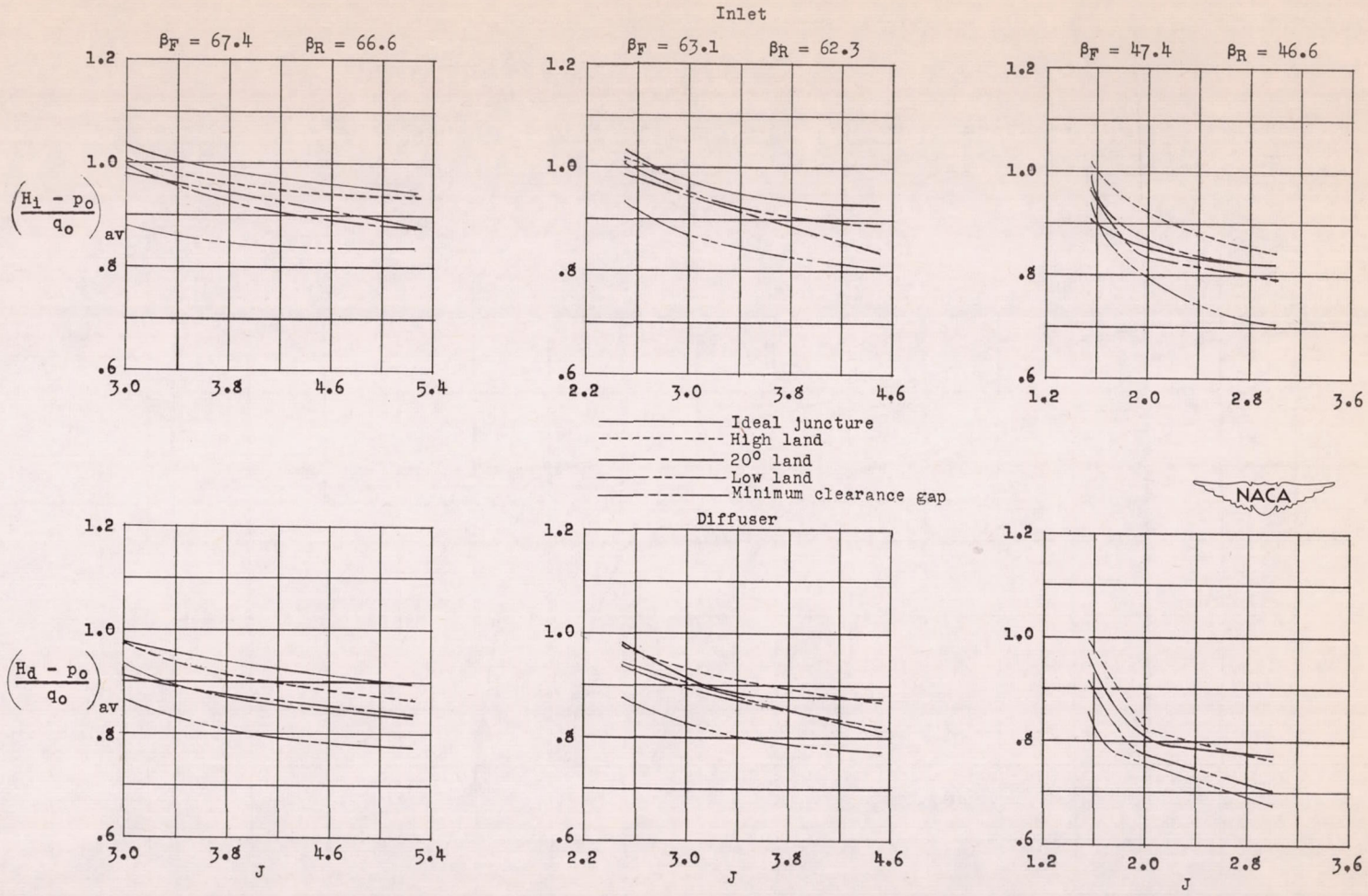

Figure 18.- Variation of inlet and diffuser average total pressure coefficient with advance ratio for the several propeller shank-spinner junctures. 24-percent-thick shank propeller; $\frac{V_i}{V_o} \approx 0.5$; $\alpha = 0^\circ$.

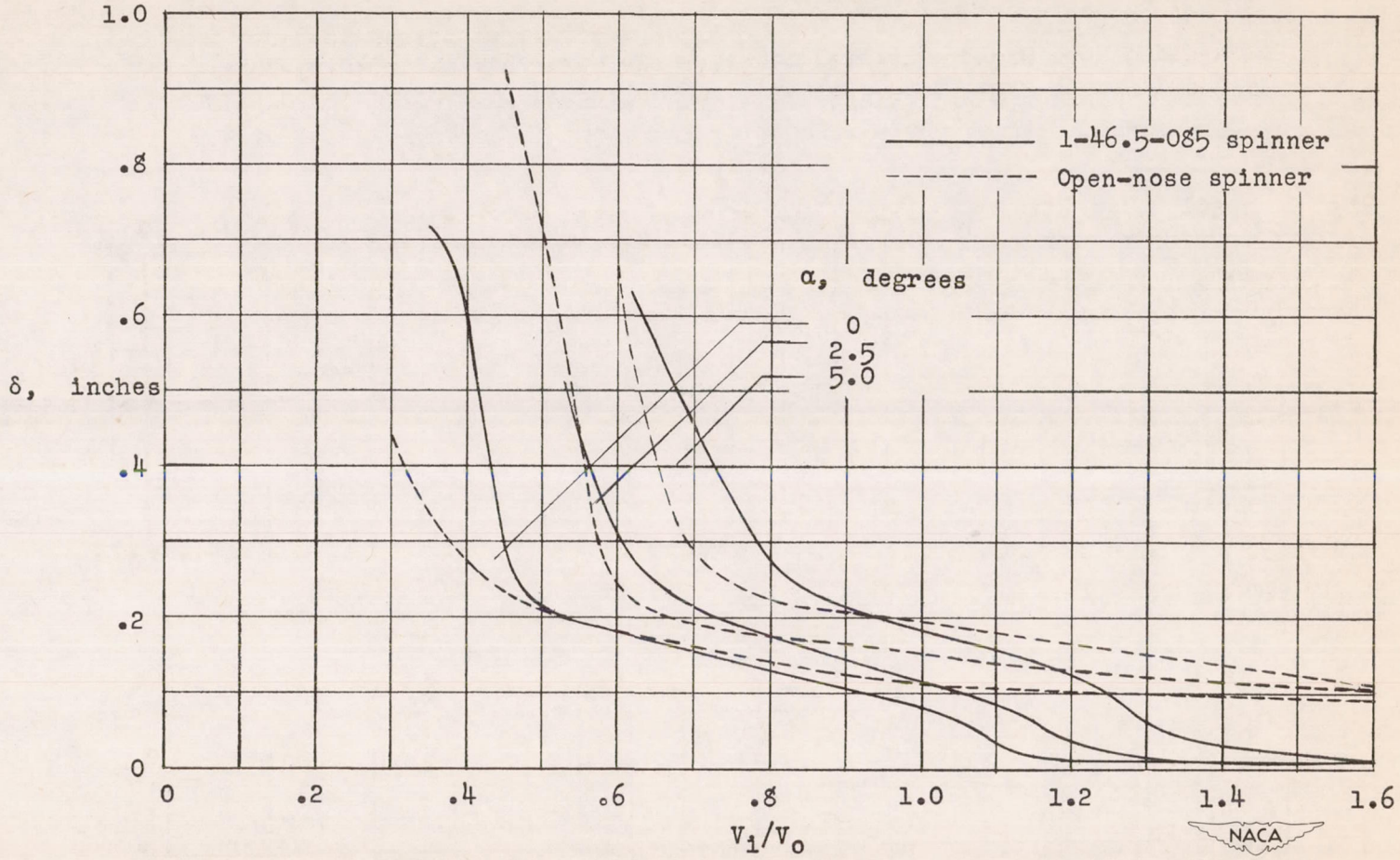

Figure 19.- Effect of blowing slot (open-nose-spinner configuration) on spinner boundary-layer thickness at top of inlet, propeller removed.

$\frac{Q_b}{Q_i} = 0.08$ at $\frac{V_i}{V_o} = 0.5$; $\left(\frac{V_i}{V_o}\right)_{\text{open-nose spinner}} = 0.63$.

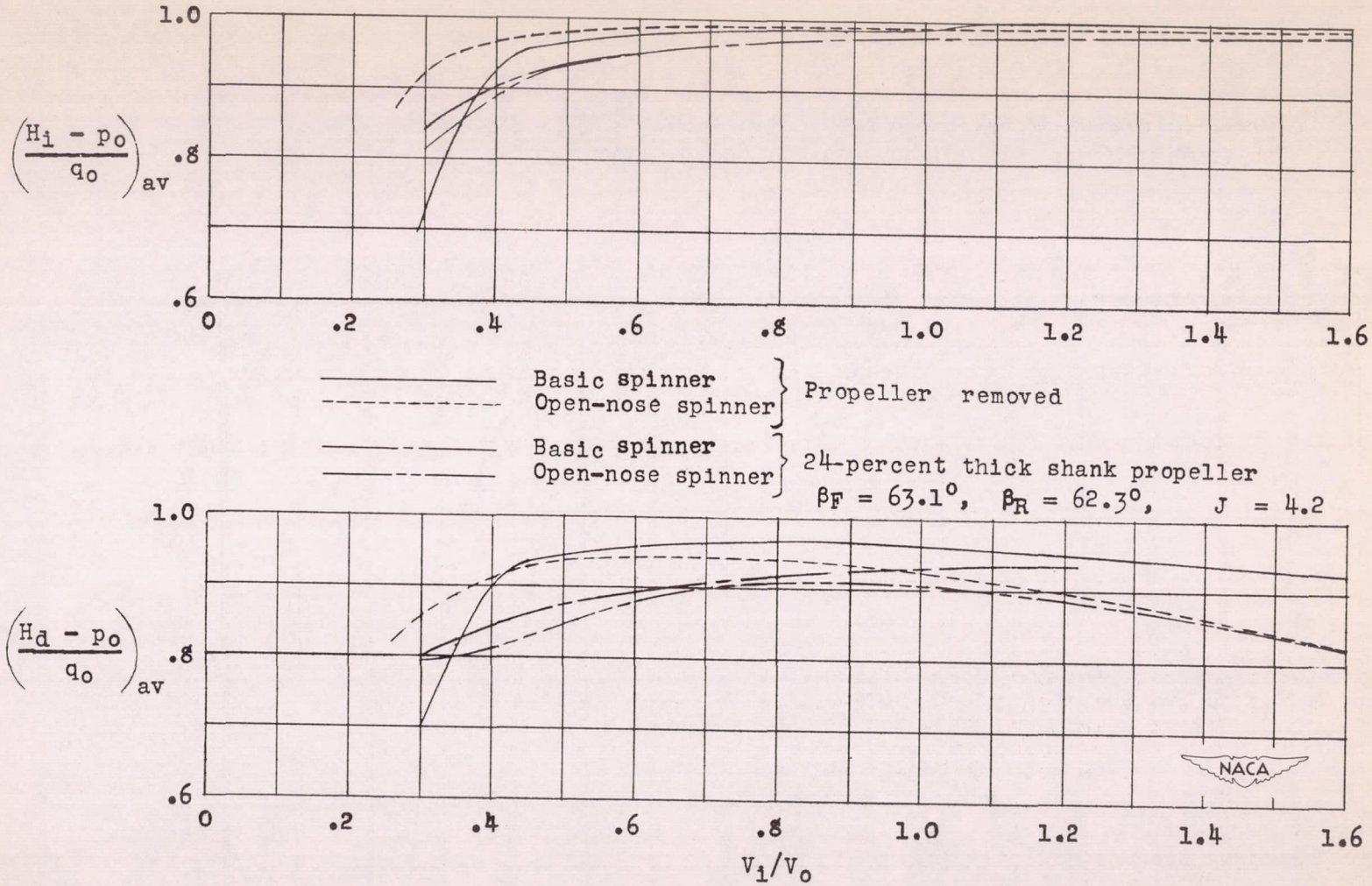

Figure 20.- Effect of propeller operation on the average total pressure coefficient at the inlet and diffuser for the blowing slot (open-nose-spinner configuration), $\alpha = 0^\circ$.

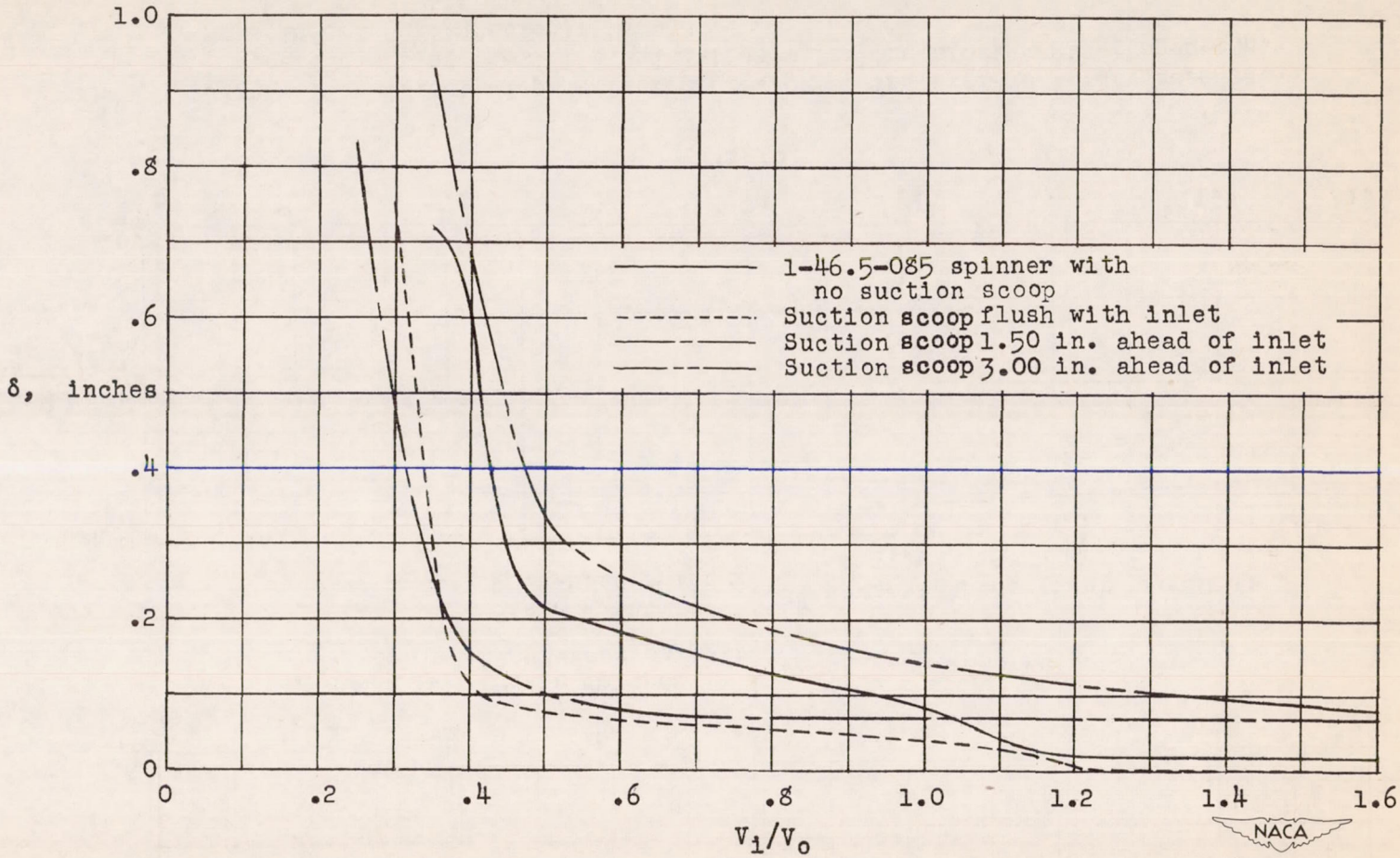

Figure 21.- Effect of suction scoop location on the spinner boundary-layer thickness at top of the inlet. NACA 1-70-070 cowling; propeller removed; $\alpha = 0^{\circ}$; $\frac{Q_b}{Q_i} = 0.09$ at $\frac{V_i}{V_o} = 0.5$.

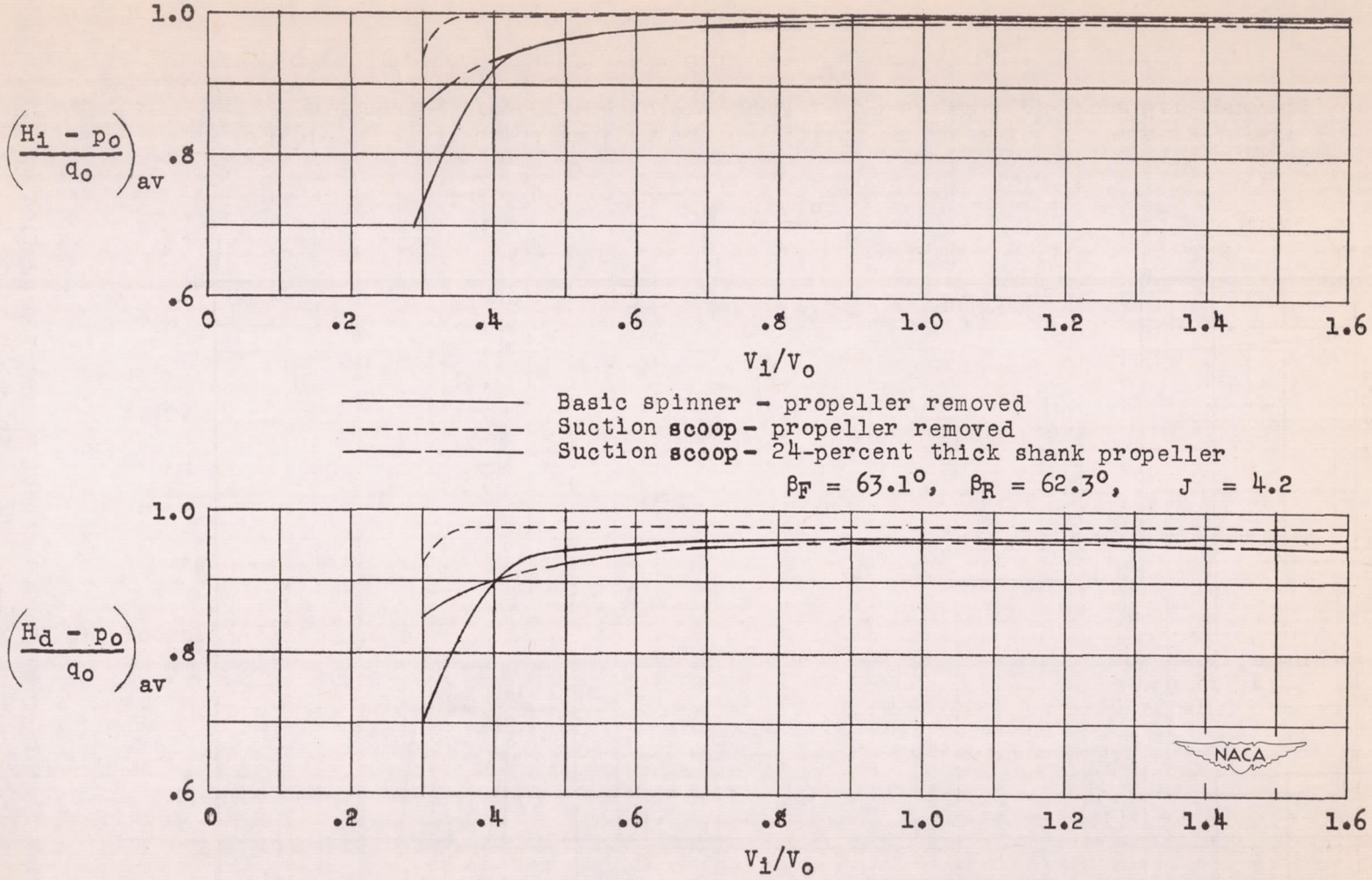

Figure 22.- Effect of propeller operation on the inlet and diffuser average total pressure coefficient for the flush suction scoop configuration. NACA 1-70-070 cowling; $\alpha = 0^\circ$.

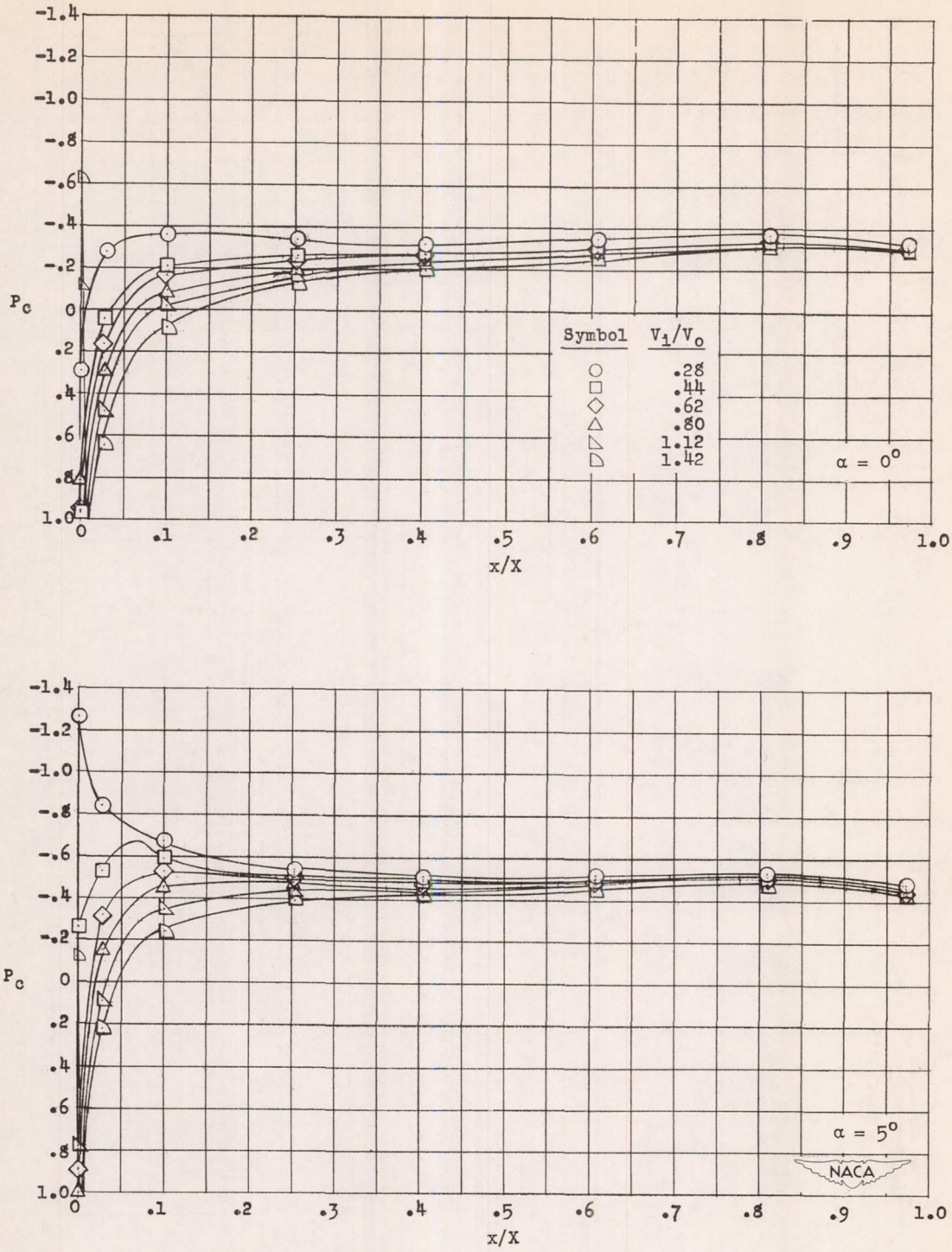

(a) Propeller removed.

Figure 23.- Static pressure distribution over top surface of NACA 1-62.8-070 cowling, NACA 1-46.5-085 spinner.

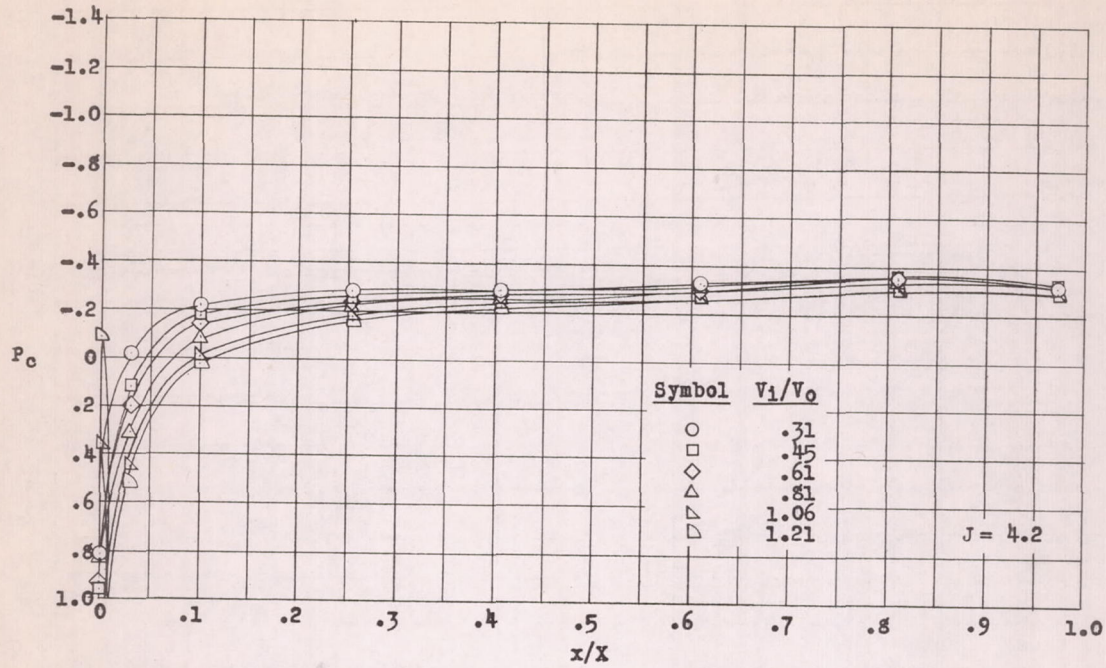

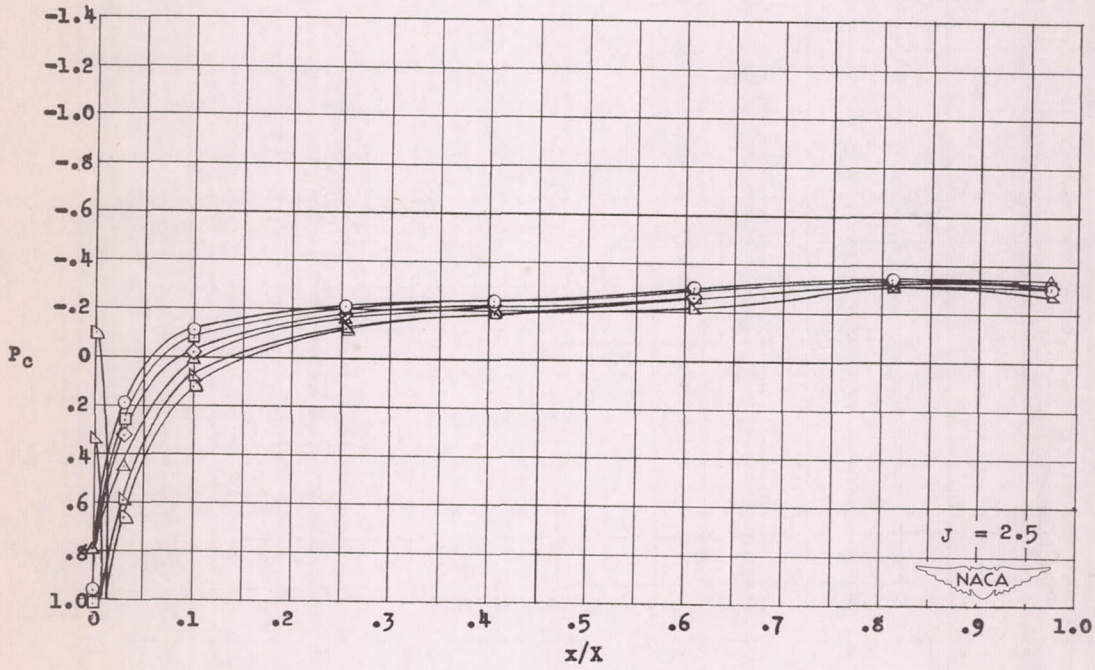

(b) 24-percent-thick shank propeller installed, $\beta_F = 63.1^\circ$, $\beta_R = 62.3^\circ$, $\alpha = 0^\circ$.

Figure 23.- Concluded.

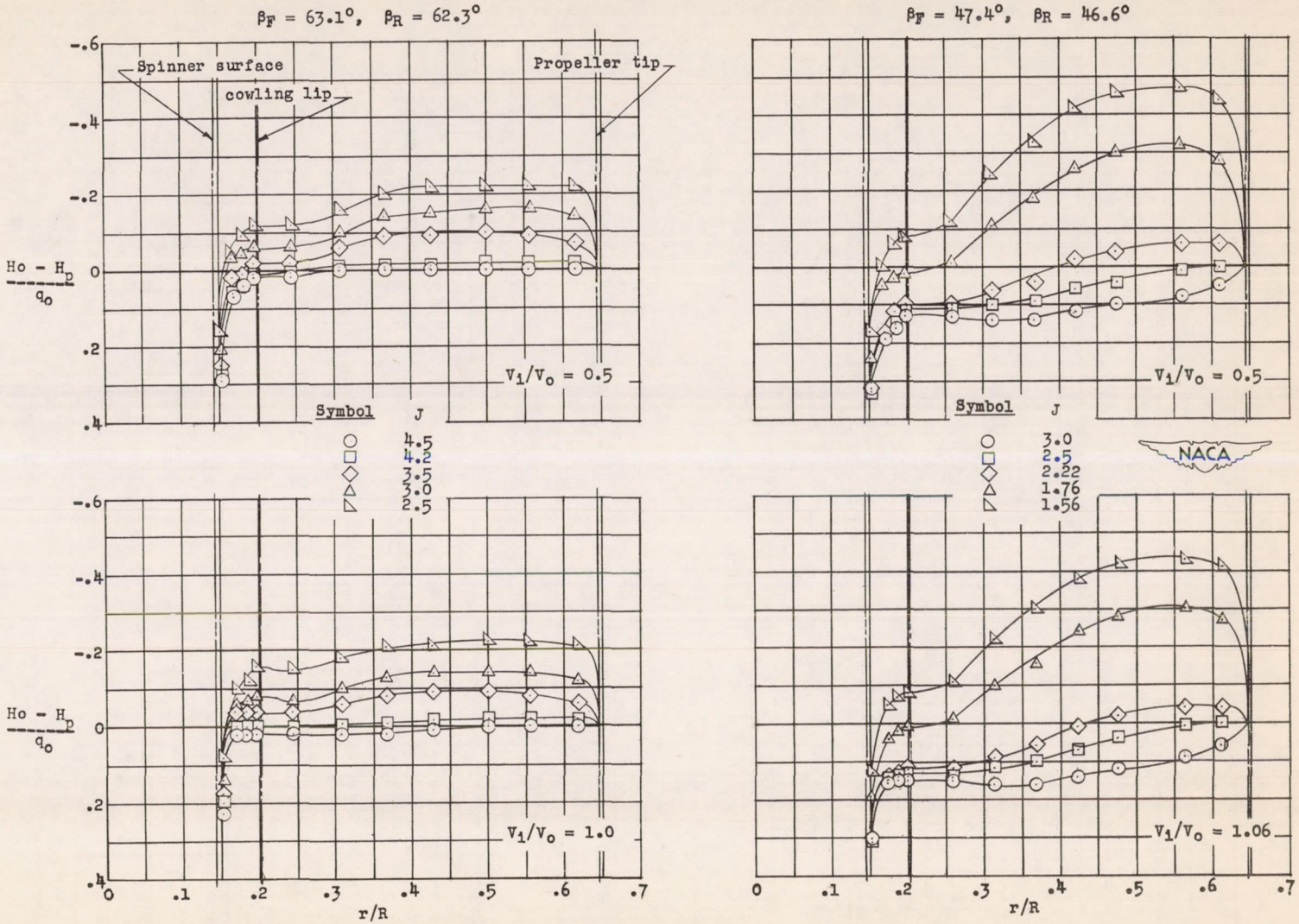

Figure 24.- Effect of advance ratio on the thrust loading of the 24-percent-thick shank propeller, $\alpha = 0^\circ$.

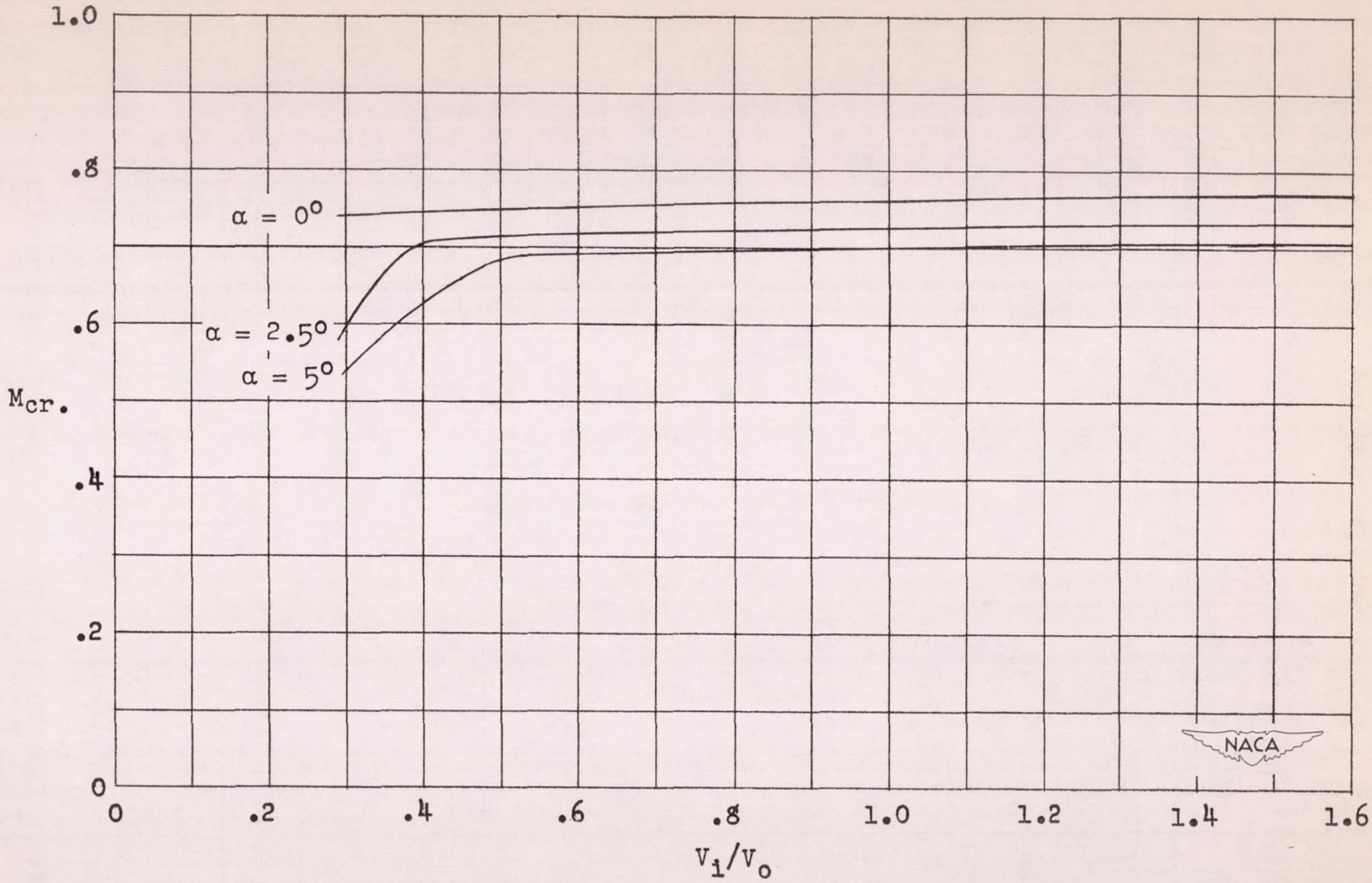

Figure 25.- Predicted critical Mach numbers for top surface of NACA 1-62.8-070 cowling with NACA 1-46.5-085 spinner installed, propeller removed.

NACA-Langley - 4-8-55 - 75